Supporting Information

1,5-Hydrogen Atom Transfer–Surzur-Tanner-rearrangement: A Radical Cascade Approach for the Synthesis of 1,6-Dioxaspiro[4.5]decane and 6,8-Dioxabicyclo[3.2.1]octane Scaffolds in Carbohydrate Systems

Elisa I. León,[a] Ángeles Martín,[a] Adrián S. Montes,[a,b] Inés Pérez-Martín,*[,a] María del Sol Rodríguez,[a] Ernesto Suárez*[,a]

[a] Síntesis de Productos Naturales, Instituto de Productos Naturales y Agrobiología del CSIC, Avda. Astrofísico Francisco Sánchez 3, 38206, La Laguna, Tenerife, Spain
[b] Doctoral and Postgraduate School, Universidad de La Laguna, Avda. Astrofísico Francisco Sánchez s/n, 38200 La Laguna, Tenerife, Spain

Table of Contents:

Table S1. Comparison between Experimental and Calculated Ring Coupling Constant of 3-*C*-(Glycopyranosyl)1-propoxyphthalimides.[a]

Compound	Conformation[b]	$^3J_{1,2}$ [Hz]	$^3J_{2,3}$ [Hz]	$^3J_{3,4}$ [Hz]	$^3J_{4,5}$ [Hz]
1	$^4C_1$ ($^3J_{calc.}$)	6.4	9.2	9.5	9.2
	$^1C_4$ ($^3J_{calc.}$)	0.9	2.5	2.8	1.2
	$^3J_{exp.}$[c]	5.5	9.0	7.8	n.o.
2	$^4C_1$ ($^3J_{calc.}$)	5.8	9.0	8.7	9.2
	$^1C_4$ ($^3J_{calc.}$)	1.2	2.6	3.6	1.6
	$^3J_{exp.}$	5.5	9.4	5.7	n.o.
3	$^4C_1$ ($^3J_{calc.}$)	8.8	9.3	9.0	9.2
	$^1C_4$ ($^3J_{calc.}$)	0.8	2.4	3.4	1.4
	$^3J_{exp.}$	9.5	9.5	n.o.	8.0
4	$^4C_1$ ($^3J_{calc.}$)	8.7	8.9	9.1	9.2
	$^1C_4$ ($^3J_{calc.}$)	0.9	2.9	3.8	1.5
	$^3J_{exp.}$	9.5	8.9	9.3	9.5
5	$^4C_1$ ($^3J_{calc.}$)	0.8	2.9	9.6	9.2
	$^1C_4$ ($^3J_{calc.}$)	8.8	2.5	3.3	1.4
	$^3J_{exp.}$	2.6	3.4	8.7	8.4
6	$^4C_1$ ($^3J_{calc.}$)	1.0	2.3	9.1	9.2
	$^1C_4$ ($^3J_{calc.}$)	8.7	2.6	3.3	1.5
	$^3J_{exp.}$	2.9	2.9	n.o.	n.o.
7	$^4C_1$ ($^3J_{calc}$)	0.4	2.6	9.5	9.2
	$^1C_4$ ($^3J_{calc}$)	6.1	3.0	3.4	1.3
	$^3J_{exp}$	1.0	3.3	9.3	9.8
8	$^4C_1$ ($^3J_{calc.}$)	0.1	2.2	9.1	9.1
	$^1C_4$ ($^3J_{calc.}$)	6.2	2.7	3.8	1.5
	$^3J_{exp.}$	< 1	1.9	n.o.	n.o.
9	$^4C_1$ ($^3J_{calc.}$)	0.3	3.0	2.6	5.3
	$^1C_4$ ($^3J_{calc.}$)	5.4	9.0	2.7	0.5
	$^3J_{exp.}$	3.0	5.9	3.2	4.5
10	$^4C_1$ ($^3J_{calc.}$)	0.5	2.4	2.6	5.2
	$^1C_4$ ($^3J_{calc.}$)	5.0	9.4	2.8	0.4
	$^3J_{exp.}$	3.3	6.3	3.1	4.1
11	$^4C_1$ ($^3J_{calc.}$)	1.2	1.7	4.1	10.0, 7.5
	$^1C_4$ ($^3J_{calc.}$)	4.9	7.7	4.4	1.6, 1.6
	$^3J_{exp.}$	2.0	3.3	5.2	7.9, 6.0
12	$^4C_1$ ($^3J_{calc.}$)	0.8	2.8	2.5	10.4, 6.3
	$^1C_4$ ($^3J_{calc.}$)	5.1	8.5	2.9	0.6, 2.2
	$^3J_{exp.}$	1.3	4.1	n.o.	n.o.

[a]Vicinal ring coupling constants ($^3J_{HCCH}$) were calculated from a generalization of the Karplus equation established by Haasnoot et al.[1] as implemented in Maestro version 9.0, Schrödinger, LLC, New York, NY, 2009.

[b]Minimized structure performed with AMBER* force field as implemented in MacroModel, version 9.9.013 with the GB/SA solvent model for $CHCl_3$, Schrödinger, LLC, New York, NY, 2009. The structures of compounds containing phosphorous were minimized with Chem3D 19.0.

[c]Experimental $^3J_{HH}$ extracted from simulated 1D ^{1}HNMR spectrum using the DAISY program as implemented in TOPSPIN, version 4.0.6, for Bruker.

Table S2. Comparison between Experimental and Calculated Ring Coupling Constant of *C*-(Glycopyranosyl)*N*-methoxyphthalimides.[a]

Compound	Conformation[b]	$^3J_{1,2}$ [Hz]	$^3J_{2,3}$ [Hz]	$^3J_{3,4}$ [Hz]	$^3J_{4,5}$ [Hz]	*d* O1'–H5 [Å][c]
16	$^4C_1$ ($^3J_{calc.}$)	5.8	9.1	9.4	9.2	2.425
	$^1C_4$ ($^3J_{calc.}$)	0.3	2.6	2.4	0.9	5.653
	$^3J_{exp.}$[d]	4.6	7.1	6.5	6.8	
17	$^4C_1$ ($^3J_{calc.}$)	6.6	8.2	8.6	9.1	2.411
	$^1C_4$ ($^3J_{calc.}$)	0.3	2.7	2.0	1.0	5.570
	$^3J_{exp.}$	5.3	7.4	7.0	7.0	
18	$^4C_1$ ($^3J_{calc.}$)	6.6	8.2	8.7	9.2	2.410
	$^1C_4$ ($^3J_{calc.}$)	0.2	2.8	2.5	1.0	5.565
	$^3J_{exp.}$	4.3	6.4	5.8	6.2	
19	$^4C_1$ ($^3J_{calc.}$)	6.5	8.2	8.5	9.1	2.280
	$^1C_4$ ($^3J_{calc.}$)	0.5	2.8	2.1	1.0	5.589
	$^3J_{exp.}$	4.7	7.3	7.3	7.9	
20	$^4C_1$ ($^3J_{calc.}$)	6.0	8.9	3.1	0.5	2.412
	$^1C_4$ ($^3J_{calc.}$)	0.1	3.2	2.9	5.8	5.644
	$^3J_{exp.}$	5.4	9.1	3.2	2.1	
21	$^4C_1$ ($^3J_{calc.}$)	6.1	9.0	2.1	-0.1	2.906
	$^1C_4$ ($^3J_{calc.}$)	-0.1	2.8	3.3	6.2	5.583
	$^3J_{exp.}$	5.6	8.2	2.9	2.7	
22	$^4C_1$ ($^3J_{calc.}$)	9.2	2.8	3.3	1.5	4.540
	$^1C_4$ ($^3J_{calc.}$)	2.0	3.7	5.4	6.2	3.013
	$^3J_{exp.}$	7.6	3.2	5.2	3.7	
23	$^4C_1$ ($^3J_{calc.}$)	0.2	3.1	3.1	5.7	4.674
	$^1C_4$ ($^3J_{calc.}$)	5.7	9.3	2.7	0.7	3.862
	$^3J_{exp.}$	5.9	9.3	3.4	2.0	
24	$^4C_1$ ($^3J_{calc}$)	0.3	2.6	2.7	5.3	4.541
	$^1C_4$ ($^3J_{calc}$)	5.6	9.3	2.7	0.1	3.031
	$^3J_{exp.}$	5.0	7.9	3.3	2.5	

[a]Vicinal ring coupling constants ($^3J_{HCCH}$) were calculated from a generalization of the Karplus equation established by Haasnoot et al.[1] as implemented in Maestro version 9.0, Schrödinger, LLC, New York, NY, 2009.
[b]Minimized structure performed with AMBER* force field as implemented in MacroModel, version 9.9.013 with the GB/SA solvent model for $CHCl_3$, Schrödinger, LLC, New York, NY, 2009. The structures of compounds containing phosphorous were minimized with Chem3D 19.0.
[c]The minimum distance O1'–H5 for each conformational isomer, was calculated performing a coordinate scan calculation of the O1'–C1'–C1–O1 dihedral from –180 to 180° in increments of 5°.
[d]Experimental $^3J_{HH}$ extracted from simulated 1D ^{1}HNMR spectrum using the DAISY program as implemented in TOPSPIN, version 4.0.6, for Bruker.

Table S3. Comparison between Experimental and Calculated Ring Coupling Constant of 10-Deoxy-1,6-dioxaspiro[4.5]decane Compounds.[a]

Compound	Conformation[b]	$^3J_{2a,3}$ [Hz]	$^3J_{2e,3}$ [Hz]	$^3J_{3,4}$ [Hz]	$^3J_{4,5}$ [Hz]	$^3J_{4,5a}$ [Hz]	$^3J_{4,5e}$ [Hz]
25	$^4C_1$ ($^3J_{calc.}$)	11.1	4.6	8.7	9.2	--	--
	$^1C_4$ ($^3J_{calc.}$)	2.7	3.0	3.2	1.5	--	--
	$^3J_{exp.}$[c]	11.5	5.1	8.9	9.9	--	--
31	$^4C_1$ ($^3J_{calc.}$)	2.4	3.3	2.8	5.2	--	--
	$^1C_4$ ($^3J_{calc.}$)	11.1	4.6	2.2	0.4	--	--
	$^3J_{exp.}$	12.1	4.5	2.7	1.7	--	--
37	$^4C_1$ ($^3J_{calc.}$)	3.2	2.5	4.1	--	10.2	7.1
	$^1C_4$ ($^3J_{calc.}$)	10.0	6.5	3.8	--	1.2	1.8
	$^3J_{exp.}$	8.7	6.3	5.5	--	2.4	1.0
38	$^4C_1$ ($^3J_{calc.}$)	2.5	3.0	3.1	--	10.3	6.7
	$^1C_4$ ($^3J_{calc.}$)	10.8	5.3	2.7	--	0.7	2.1
	$^3J_{exp.}$	11.7	5.3	3.5	--	2.3	1.6

[a]Vicinal ring coupling constants ($^3J_{HCCH}$) were calculated from a generalization of the Karplus equation established by Haasnoot et al.[1] as implemented in Maestro version 9.0, Schrödinger, LLC, New York, NY, 2009.
[b]Minimized structure performed with AMBER* force field as implemented in MacroModel, version 9.9.013 with the GB/SA solvent model for $CHCl_3$, Schrödinger, LLC, New York, NY, 2009. The structures of compounds containing phosphorous were minimized with Chem3D 19.0.
[c]Experimental $^3J_{HH}$ extracted from simulated 1D ^{1}HNMR spectrum using the DAISY program as implemented in TOPSPIN, version 4.0.6, for Bruker.

Table S4. Comparison between Experimental and Calculated Long-range ^4J_w Coupling Constants.

Compound	Conformation	Φ_1 [°][a]	Φ_2 [°][a]	^4J_W	$^4J_{calc.}$ [Hz][b]	$^4J_{exp.}$ [Hz][c]
31	$^1C_4$	176.2	–176.8	$^4J_{2a,4}$	1.3	1.3
[PhCH-^{2}H]**31**	$^1C_4$	173.8	–173.5	$^4J_{2a,4}$	1.3	1.0
45	$^4C_1$	–168.6	–160.2	$^4J_{2,1'a}$	1.1	1.1
46	$^1H_2$	164.1	161.9	$^4J_{2,4}$	1.1	1.5
47	$^1C_4$	170.4	–164.7	$^4J_{2,4}$	1.2	1.2
(5-^{2}H)**47**	$^1C_4$	170.4	–164.7	$^4J_{2,4}$	1.2	1.2
53	$^4C_1$	–171.8	–158.5	$^4J_{2,1'a}$	1.1	1.1

[a]Dihedral angles calculated over minimized structures using AMBER* force field as implemented in MacroModel, version 9.9.013 with the GB/SA solvent model for $CHCl_3$, Schrödinger, LLC, New York, NY, 2009.
[b]Long-range $^4J_{HH}$ were calculated from three-parameters equation ($^4J_{HH} = \cos^2 \Phi_1 + \cos^2 \Phi_2 - 0{,}7$) as established by Abraham et al.[2]
[c]All experimental $^4J_{HH}$ were extracted from simulated 1D ^{1}HNMR spectra using the DAISY program as implemented in TOPSPIN, version 4.0.6, for Bruker.

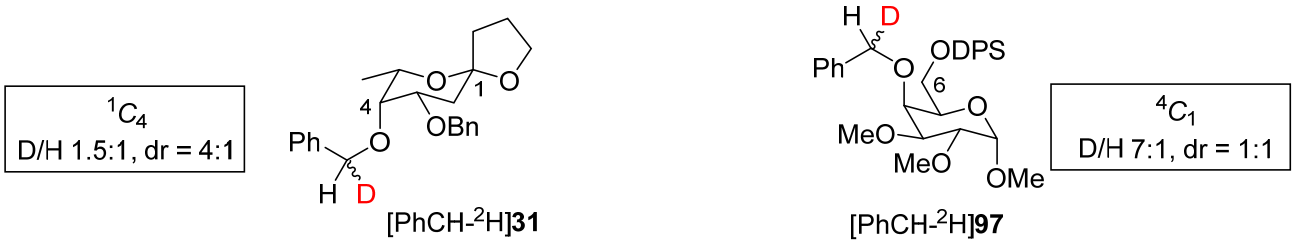

Table S5. Selected signals of ^{1}H NMR spectra of labelled [PhCH-^{2}H]**31** and [PhCH-^{2}H]**97**.

Compound	6-H [ppm] (rel. int.)		2-H_{ax} [ppm] (rel. int.)		3-H_{ax} [ppm] (rel. int.)		4-PhC*H*D-O [ppm] (rel. int.)	
	$CDCl_3$	C_6D_6	$CDCl_3$	C_6D_6	$CDCl_3$	C_6D_6	$CDCl_3$	C_6D_6
[PhCH-^{2}H]**31**	1.130 (d, 1.5H)[a] 1.133 (d, 0.3H) 1.135 (d, 1.2H)	1.276 (d, 1.5H)[a] 1.280 (d, 1.5H)	2.32 (dd, 1H)	2.494 (dd, 0.5H) 2.496 (dd, 0.5H)	3.929 (ddd, 0.5H) 3.931 (ddd, 0.5H)	4.02 (ddd, 1H)	4.71(br s, 0.1H) 4.72 (d, 0.4H) 4.93 (br s, 0.5H) 4.95 (d, 0.4H)	4.57 (br s, 0.1H) 4.59 (d, 0.4H) 5.02 (br s, 0.5H) 5.05 (d, 0.4H)
[PhCH-^{2}H]**97**	n. o.[b, c]	4.05 (dd, 0.5)[b] 4.06 (dd, 0.5) 4.107 (dd, 0.5) 4.105 (dd, 0.5)	n. o.[c]	n. o.[c]	3.56 (dd, 1H)	3.73 (dd, 1H)	4.589 (br s, 0.4H) 4.60 (d, 0.1H) 4.90 (br s, 0.4H) 4.91 (d, 0.1H)	4.58 (br s, 0.4H) 4.61 (d, 0.1H) 5.05 (br s, 0.4H) 5.07 (d, 0.1H)

[a]6-Me. [b]6-CH_2.[c]Not observed, overlapped with other signals.

Table S6. Selected signals of ^{13}C{H} NMR spectra of labelled [PhCH-^{2}H]**31** and [PhCH-^{2}H]**97**.

Compound	C4[ppm] (rel. int.)		4-PhC*H*D-O [ppm] (rel. int.)	
	$CDCl_3$	C_6D_6	$CDCl_3$	C_6D_6
[PhCH-^{2}H]**31**	74.97 (0.5) 75.02 (0.1) 75.09 (0.4)	76.85 (0.5) 76.88 (0.1) 76.93 (0.4)	73.59 (t, J_{CD} = 22.1 Hz) (0.6) 74.18 (s) (0.4)	74.85 (t, J_{CD} = 22.1 Hz) (0.6) 75.26 (s) (0.4)
[PhCH-^{2}H]**97**	73.56 (0.44) 73.59 (0.44) 73.64 (0.12)	75.48 (0.44) 75.51 (0.44) 75.55 (0.12)	74.35 (t, J_{CD} = 22.1 Hz) (0.88) 74.73 (s) (0.12)	75.05 (t, J_{CD} = 21.1 Hz) (0.44) 75.08 (t, J_{CD} = 22.1 Hz) (0.44) 75.45 (s) (0.12)

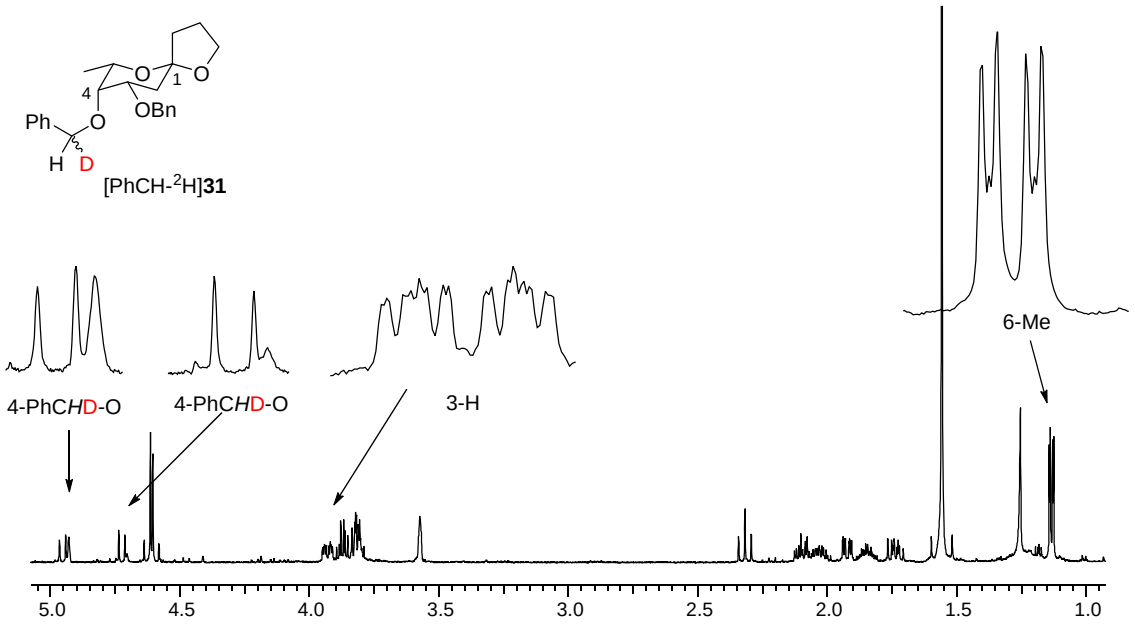

Figure S1. ^{1}H NMR (500 MHz, $CDCl_3$) of [PhCH-^{2}H]**31** (D/H 1.5:1, dr = 4:1) as a 1*R*/1*S* mixture (85:15), only major isomer shown.

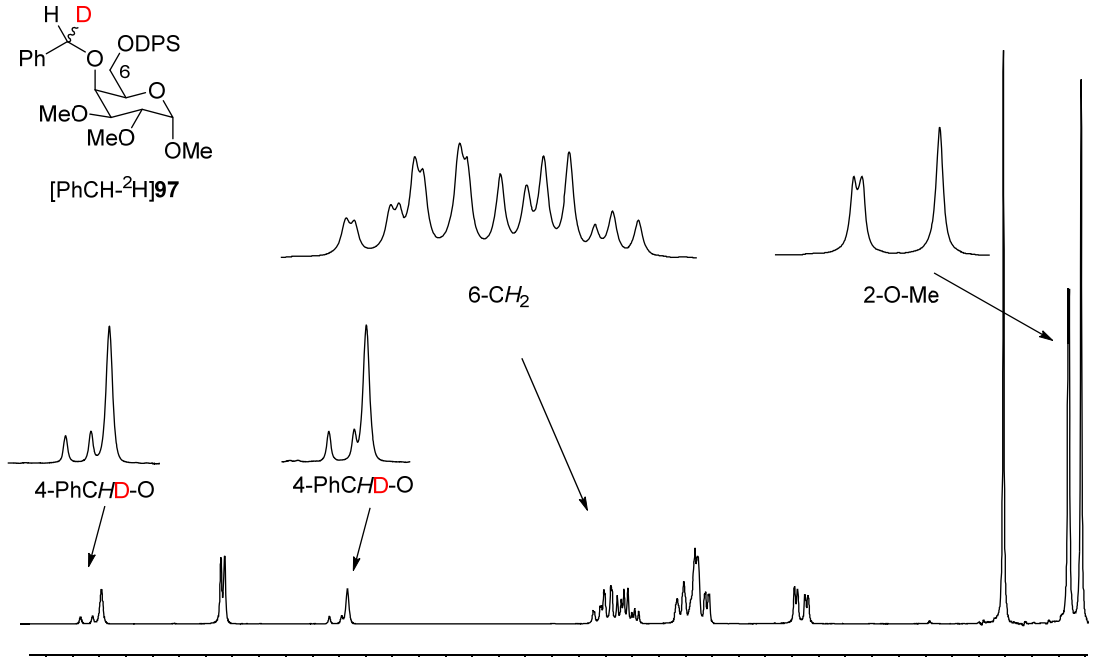

Figure S2. ^{1}H NMR (500 MHz, C_6D_6) of [PhCH-^{2}H]**97** (D/H 7:1, dr = 1:1).

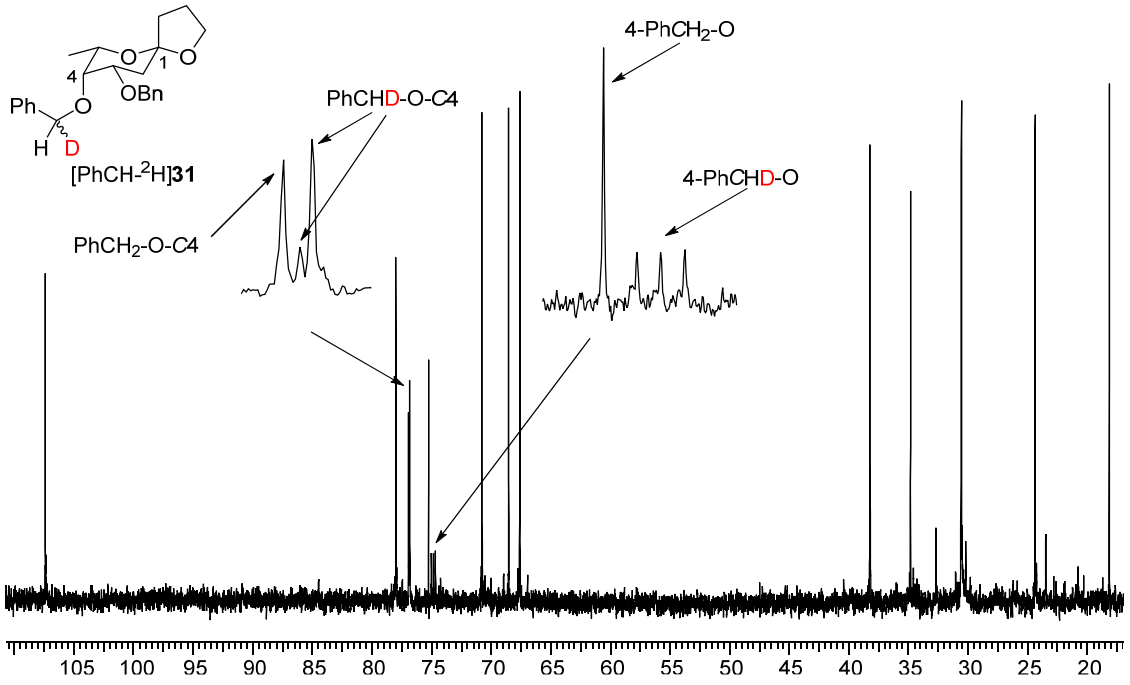

Figure S3. $^{13}C\{H\}$ NMR (125.7 MHz, C_6D_6) of [PhCH-^{2}H]**31** (D/H 1.5:1, dr = 4:1) as a 1*R*/1*S* mixture (85:15), only major isomer shown.

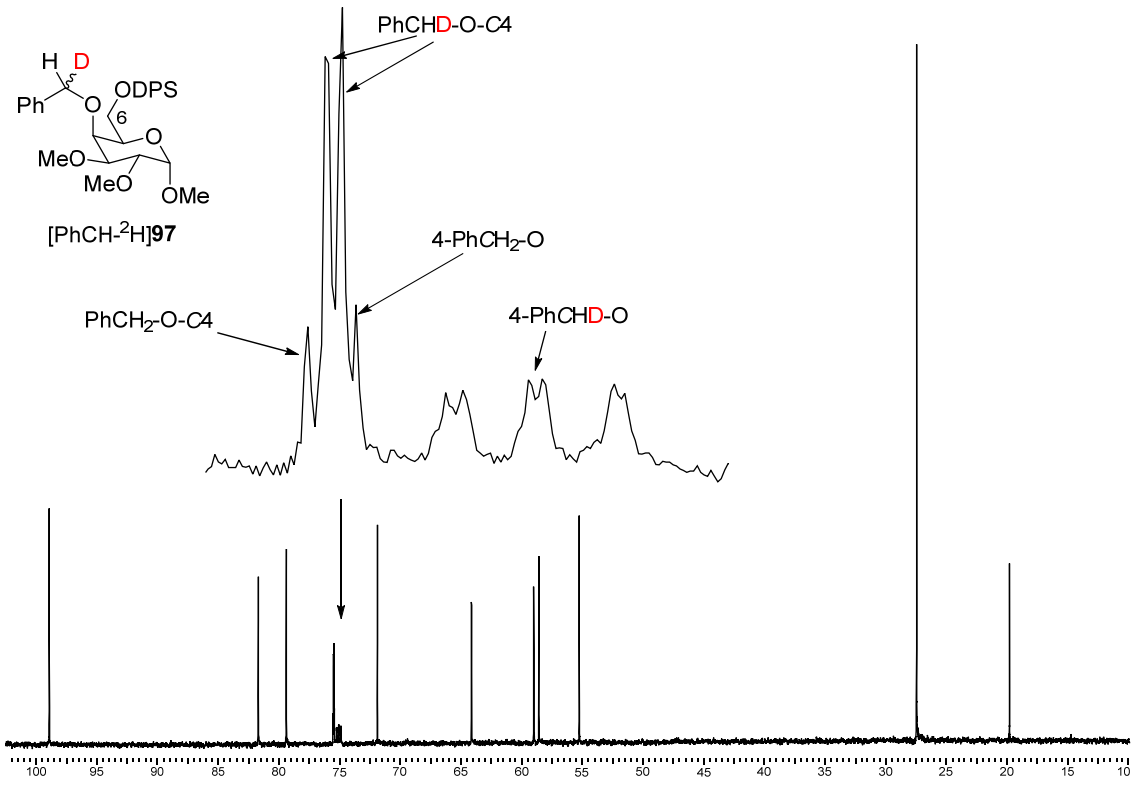

Figure S4. $^{13}C\{H\}$ NMR (125.7 MHz, C_6D_6) of [PhCH-^{2}H]**97** (D/H 7:1, dr = 1:1).

Table S7. Comparison between Experimental and Calculated Ring Coupling Constant of 4-Deoxy-6,8-dioxabicyclo[3.2.1]octane Compounds.[a]

Compound	Conformation	$^3J_{1,2}$ [Hz]	$^3J_{2,3}$ [Hz]	$^3J_{3,4a}$ [Hz]	$^3J_{3,4e}$ [Hz]	$^3J_{1,1'a}$ [Hz]	$^3J_{1,1'b}$ [Hz]
45	$^4C_1$ (Calc.)[b]	3.6	7.5	10.2	6.3	6.1	1.1
	Exper.[c]	4.3	8.0	10.1	6.6	5.0	0.0
53	$^4C_1$ (Calc.)	4.2	6.7	9.5	6.8	6.4	1.7
	Exper.	3.9	7.8	10.0	6.5	5.1	0.0
[4-^{2}H]**55**	$^1C_4$ (Calc.)	3.4	7.6	10.2	6.2	6.3	1.3
	Exper.	4.7	8.2	n.o.	6-7	4.7	0.0
61	$^1C_4$ (Calc.)	2.6	3.2	10.3	6.1	6.3	1.2
	Exper.	2.8	4.1	11.1	6.0	5.8	0.9

[a]Vicinal ring coupling constants ($^3J_{HCCH}$) were calculated from a generalization of the Karplus equation established by Haasnoot et al.[1] as implemented in Maestro version 9.0, Schrödinger, LLC, New York, NY, 2009.
[b]Minimized structure performed with AMBER* force field as implemented in MacroModel, version 9.9.013 with the GB/SA solvent model for $CHCl_3$, Schrödinger, LLC, New York, NY, 2009. The structures of compounds containing phosphorous were minimized with Chem3D 19.0.
[c]Experimental $^3J_{HH}$ extracted from simulated 1D ^{1}HNMR spectrum using the DAISY program as implemented in TOPSPIN, version 4.0.6, for Bruker

Table S8. Comparison between Experimental and Calculated Ring Coupling Constant of 3-*C*-(α-D-ribofuranosyl)1-propoxyphthalimides.

Compound	Conformation[a]	$^3J_{H,H}$	$^3J_{1,2}$ [Hz]	$^3J_{2,3}$ [Hz]	$^3J_{3,4}$ [Hz]
13	$^3T_2$ [27%, $P_N = 2^o$, $\varphi_m = 13^o$]	$^3J_{calc.}$	5.69	6.49	3.86
	$^3T_2$ [73%, $P_S = 354^o$, $\varphi_m = 48^o$]	$^3J_{calc.}$	2.56	3.99	7.70
		$^3J_{avg.}$	3.40	4.66	6.67
		$^3J_{exp.}$[b]	3.40	4.66	6.67
14	$^3T_2$ [55%, $P_N = 358^o$, $\varphi_m = 57^o$]	$^3J_{calc.}$	2.06	3.05	8.72
	$^2T_3$ [45%, $P_S = 179^o$, $\varphi_m = 3^o$]	$^3J_{calc.}$	6.49	6.53	2.11
		$^3J_{avg.}$	4.06	4.62	5.74
		$^3J_{exp.}$[b]	4.06	4.62	5.74
15	$^3T_2$ [100%, $P_S = 9^o$, $\varphi_m = 52^o$]	$^3J_{calc.}$	3.05	3.61	8.84
	$^3T_2$ [0%, $P_S = 1^o$, $\varphi_m = 20^o$]	$^3J_{calc.}$	5.20	6.24	4.70
		$^3J_{avg.}$	3.05	3.61	8.84
		$^3J_{exp.}$[b]	2.88	3.88	9.06

[a]The conformation of the five-membered ring has been established by pseudorotational analysis and designed using the Altona-Sundaralingam phase angle (*P*) and puckering amplitude (φ_m).[3]
[b]Experimental $^3J_{HH}$ extracted from simulated 1D ^{1}HNMR spectrum using the DAISY program as implemented in TOPSPIN, version 4.0.6, for Bruker.

Table S9. Reactivity Differences between LGs in the 1,5-Hydrogen Atom Transfer–Surzur-Tanner-rearrangement Sequence for the Synthesis of 1,6-Dioxaspiro[4.5]decane and 6,8-Dioxabicyclo[3.2.1]octane Scaffolds.[a]

Compound	Sugar Ring	LG	Method	Product	Yield (%)
1	α-D-*gluco*	Ac	B	**25**	50
2		$PO(OPh)_2$	D	(2-^{2}H)**25**	62
3	β-D-*gluco*	Ac	D	(2-^{2}H)**25**	33
4		$PO(OPh)_2$	D	(2-^{2}H)**25**	55
5	α-D-*manno*	Ac	D	--	--
6		$PO(OPh)_2$	D	(2-^{2}H)**25**	52
7	β-D-*manno*	Ac	E	[2-^{2}H]**25**	50
8		$PO(OPh)_2$	E	[2-^{2}H]**25**	65
9	α-L-*fuco*	Ac	D	[PhCH-^{2}H]**31**	53
10		$PO(OPh)_2$	A	**31**	52
11	α,β-D-*arabino*	$PO(OPh)_2$	A	**37**	60
12	β-D-*arabino*	$PO(OPh)_2$	D	[2-^{2}H]**38**	63
13	α-D-*ribo*	Ac	E	[2-^{2}H]**39**	40
14		Tf	A	**39**	46
15		$PO(OPh)_2$	A	**42** + **43**	62
16	α-D-*gluco*	Ac	E	[4-^{2}H]**45**	39
17		$PO(OPh)_2$	D	[4-^{2}H]**45**	58
18		Ts	D	[4-^{2}H]**45**	58
19		$PO(OPh)_2$	A	**53**	30
20	α-D-*galacto*	Ac	G	**45**	21
21		$PO(OPh)_2$	E	[4-^{2}H]**45**	41
22	α-L-*rhamno*	$PO(OPh)_2$	E	[4-^{2}H]**61**	66
23	α-L-*fuco*	Ac	G	**55**	23
24		$PO(OPh)_2$	E	[4-^{2}H]**55**	41

[a]Reagents and Conditions: Method *A*: *n*-Bu_3SnH (1 equiv), AIBN (0.1 equiv), $PhCH_3$ (0.013 M), reflux. *Method B*: *n*-Bu_3SnH (1 equiv/h), AIBN (0.1 equiv), $PhCH_3$ (0.013 M), reflux. *Method D*: *n*-Bu_3SnD (1 equiv), AIBN (0.1 equiv), $PhCH_3$ (0.013 M), reflux. *Method E*: *n*-Bu_3SnD (1 equiv), BF_3•Et_2O (0.2 equiv), AIBN (0.1 equiv), $PhCH_3$ (0.013 M), reflux. *Method G*: Hantzsch ester (0.37 equiv/h), *fac*-Ir(ppy)$_3$ (0.01 equiv), THF (0.007M), rt, blue LED.

References

(1) Haasnoot, C. A. G.; de Leeuw, F. A. A. M.; Altona, C. The Relationship between Proton-Proton NMR Coupling Constants and Substituent Electronegativities-I. An Empirical Generalization of the Karplus Equation. *Tetrahedron* **1980**, *36*, 2783–2792. https://doi.org/10.1016/0040-4020(80)80155-4.

(2) Abraham, R. J.; Gottschalck, H.; Paulsen, H.; Thomas, W. A. The Proton Magnetic Resonance Spectra and Conformations of Cyclic Compounds. Part II. The p.m.r. Spectra of the Conduritols. *J. Chem. Soc.* **1965**, 6268–6277. https://doi.org/10.1039/jr9650006268.

(3) Program Matlab GUI as described in the following: (a) Hendrickx, P. M.; Martins, J. C. A User-Friendly Matlab Program and GUI for the Pseudorotation Analysis of Saturated Five-Membered Ring Systems Based on Scalar Coupling Constants. *Chem. Cent. J.* **2008**, *2*, 20. https://doi.org/10.1186/1752-153X-2-20. For a description of the pseudorotation concept, see: (b) Altona, C.; Sundaralingam, M. Conformational Analysis of the Sugar Ring in Nucleosides and Nucleotides. A New Description Using the Concept of Pseudorotation. *J. Am. Chem. Soc.* **1972**, *94*, 8205–8212. https://doi.org/10.1021/ja00778a043. (c) Houseknecht, J. B.; Altona, C.; Hadad, C. M.; Lowary, T. L. Conformational Analysis of Furanose Rings with PSEUROT: Parametrization for Rings Possessing the Arabino, Lyxo, Ribo, and Xylo Stereochemistry and Application to Arabinofuranosides. *J. Org. Chem.* **2002**, *67*, 4647–4651. https://doi.org/10.1021/jo025635q.

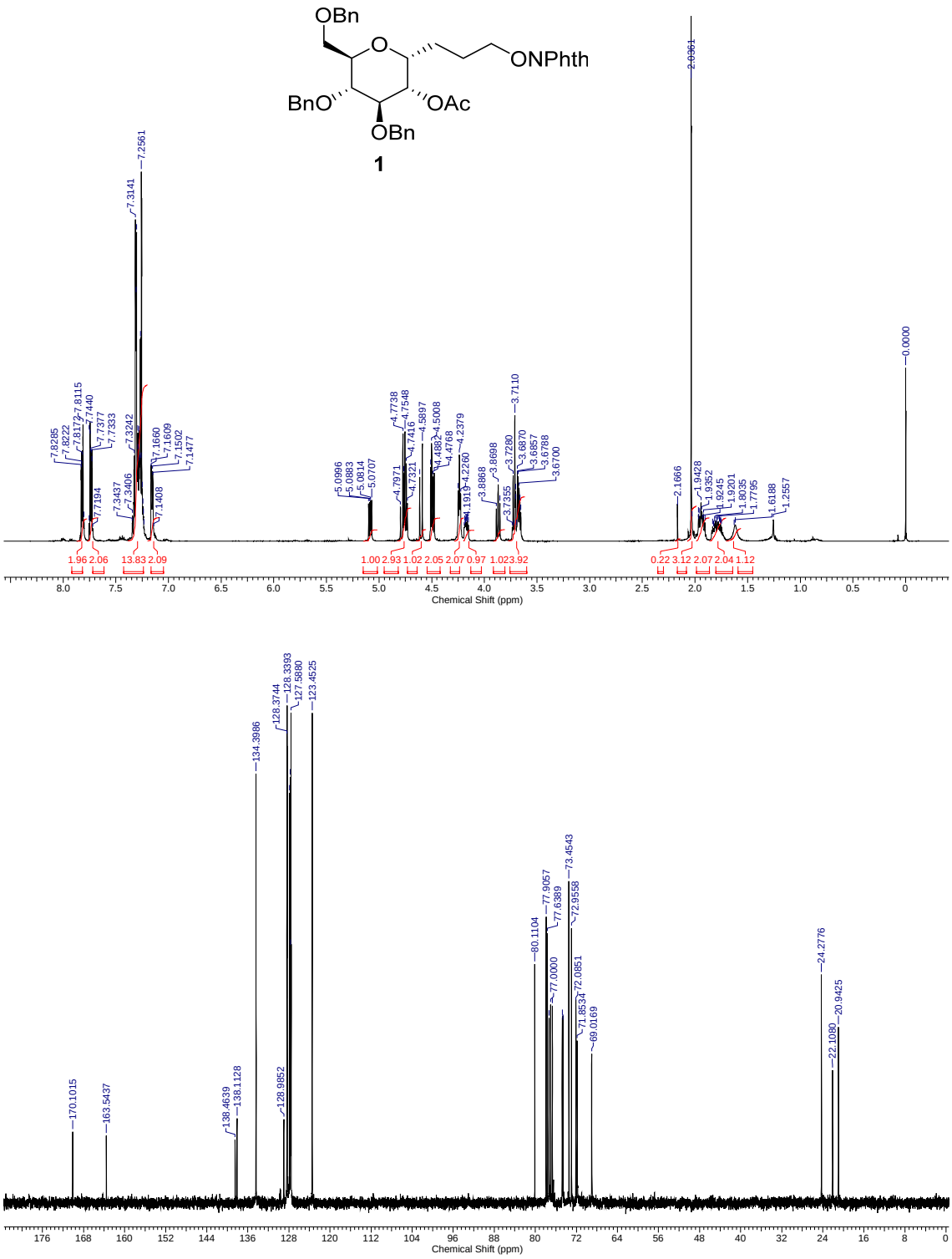

Fig. S5. ^{1}H NMR (500 MHz, $CDCl_3$) and $^{13}C\{H\}$ NMR (100.6 MHz, $CDCl_3$) of compound **1**.

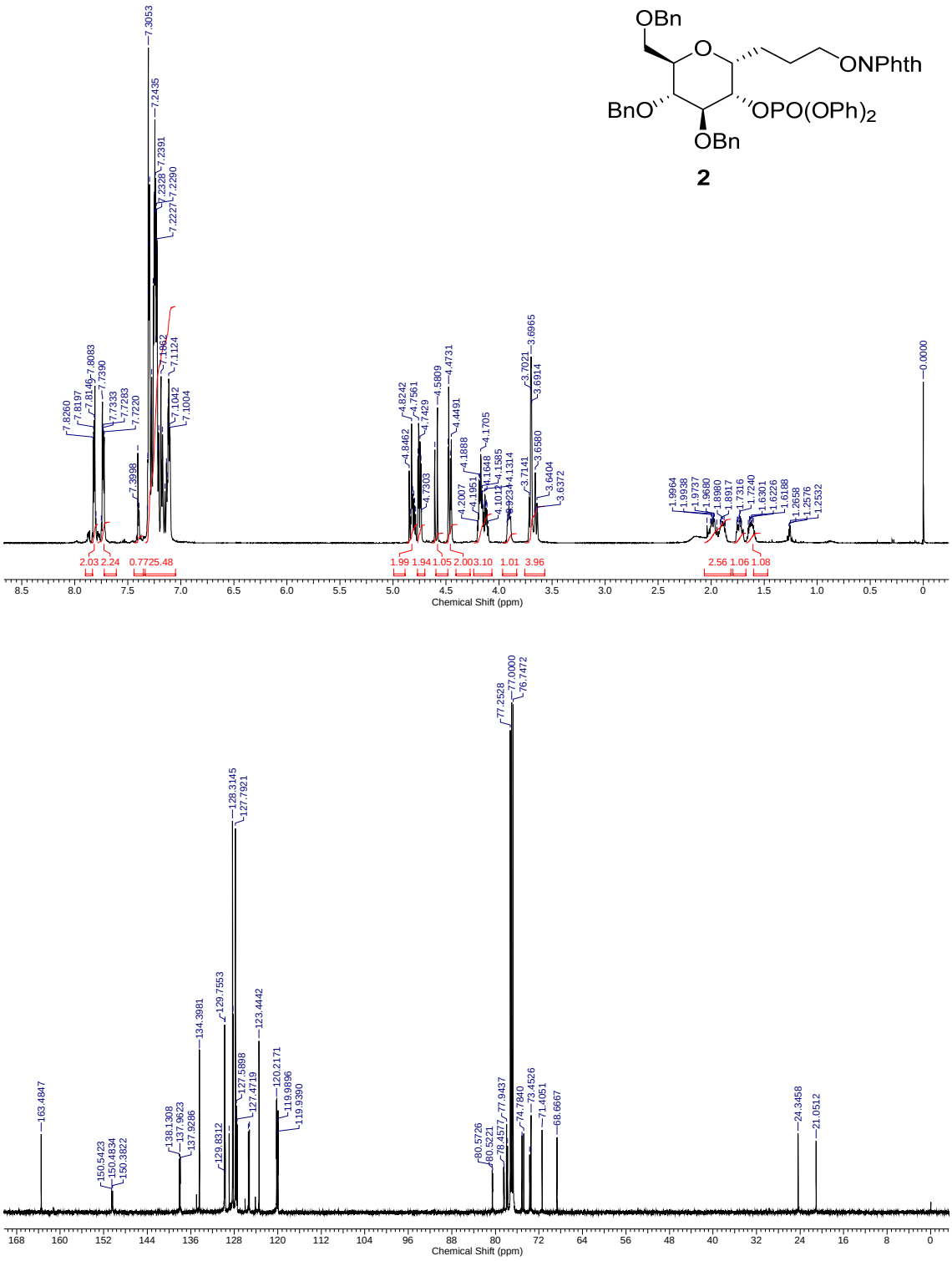

Fig. S6. ^{1}H NMR (500 MHz, $CDCl_3$) and $^{13}C\{H\}$ NMR (125.7 MHz, $CDCl_3$) of compound **2**.

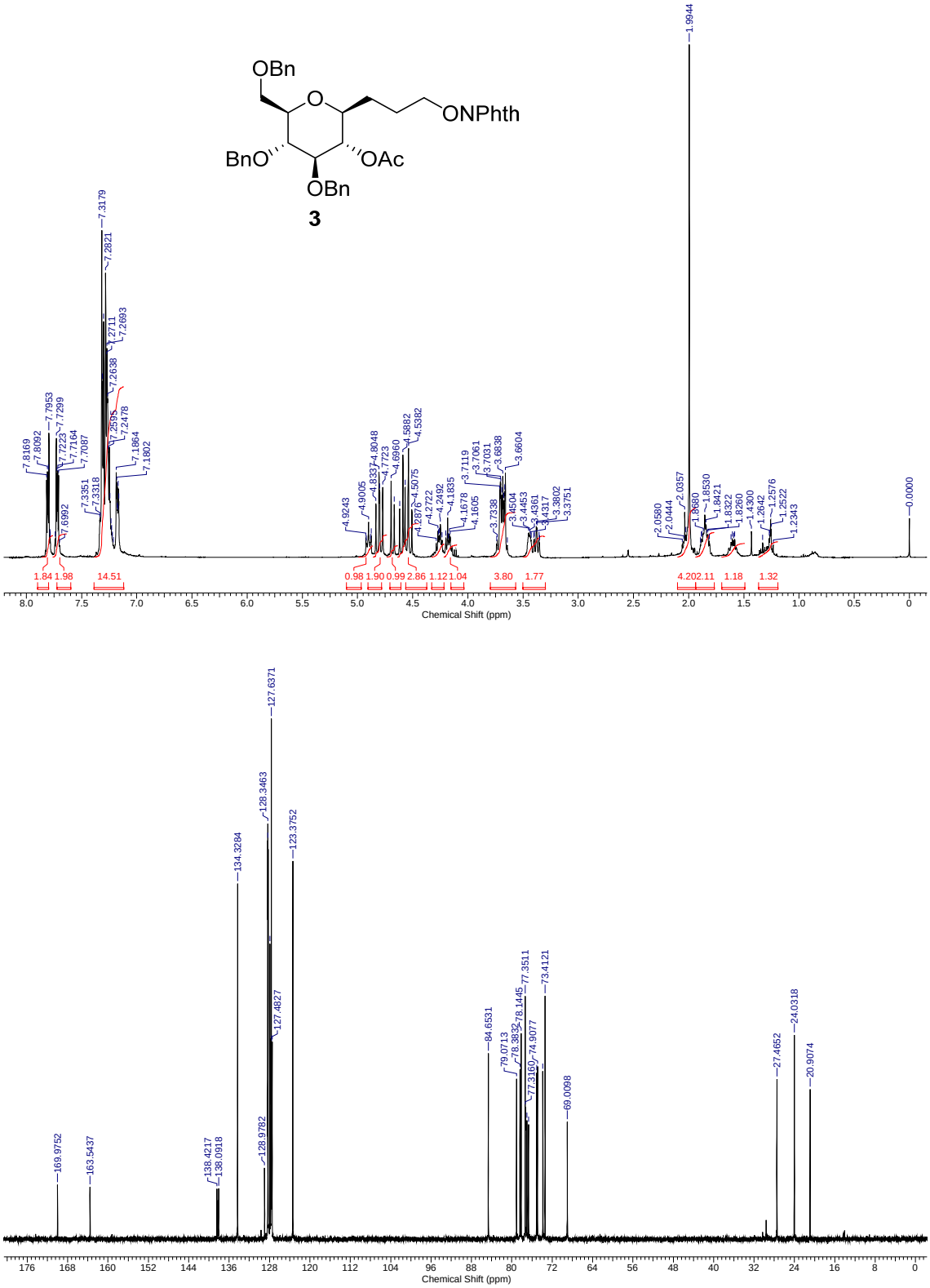

Fig. S7. ^{1}H NMR (400 MHz, $CDCl_3$) and $^{13}C\{H\}$ NMR (100.6 MHz, $CDCl_3$) of compound **3**.

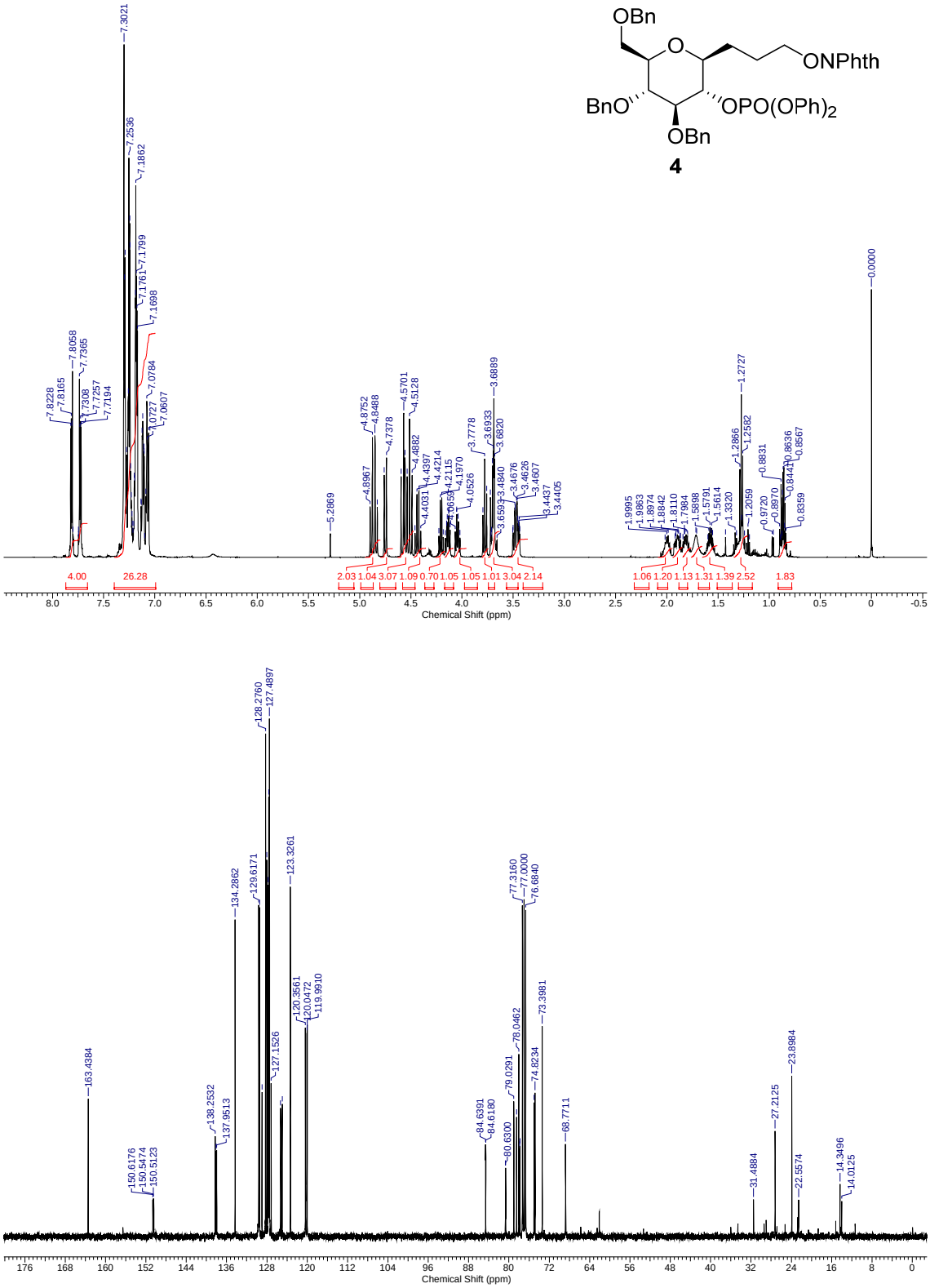

Fig. S8. ^{1}H NMR (500 MHz, $CDCl_3$) and $^{13}C\{H\}$ NMR (100.6 MHz, $CDCl_3$) of compound **4**.

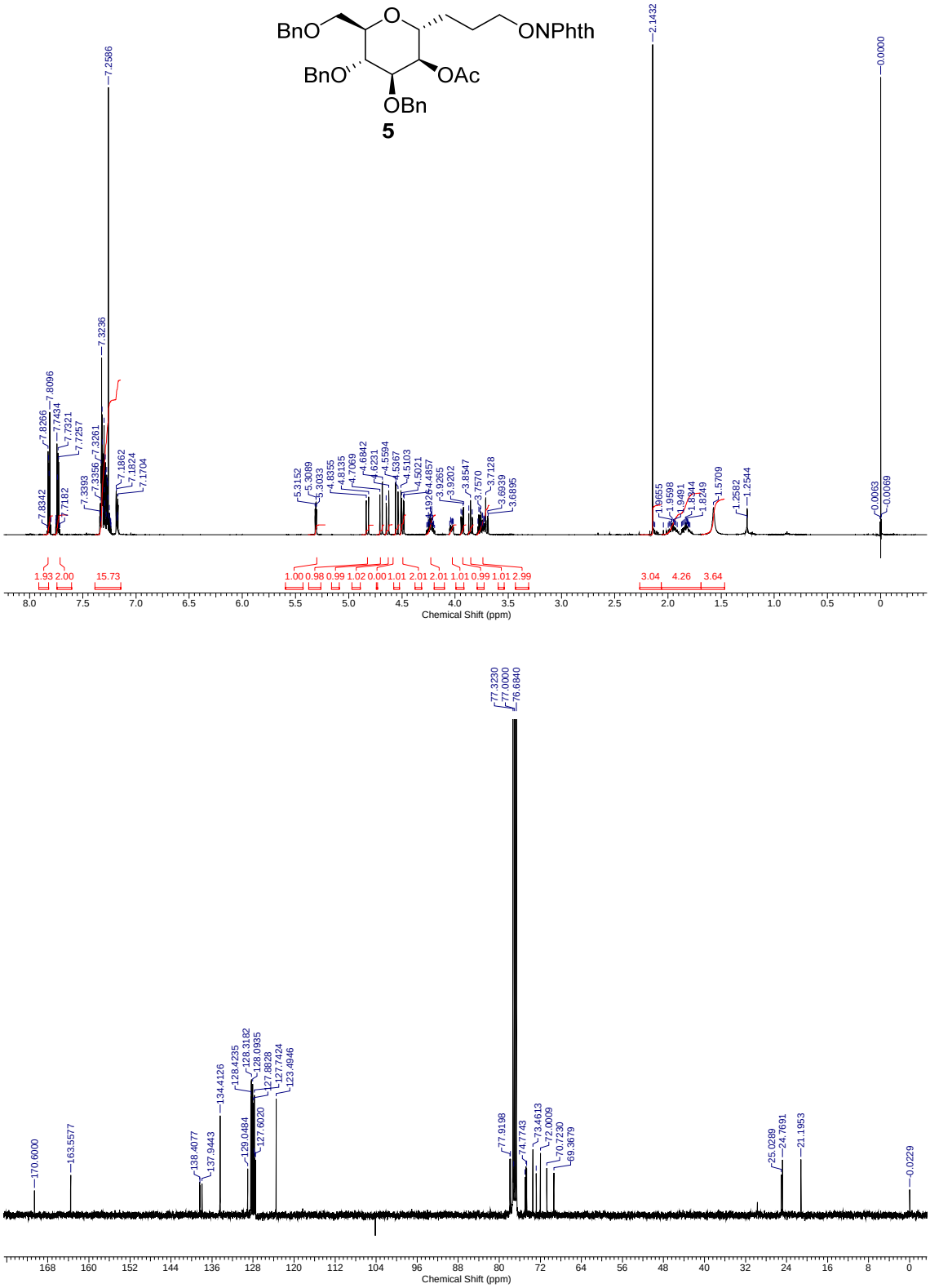

Fig. S9. ^{1}H NMR (500 MHz, $CDCl_3$) and $^{13}C\{H\}$ NMR (100.6 MHz, $CDCl_3$) of compound **5**.

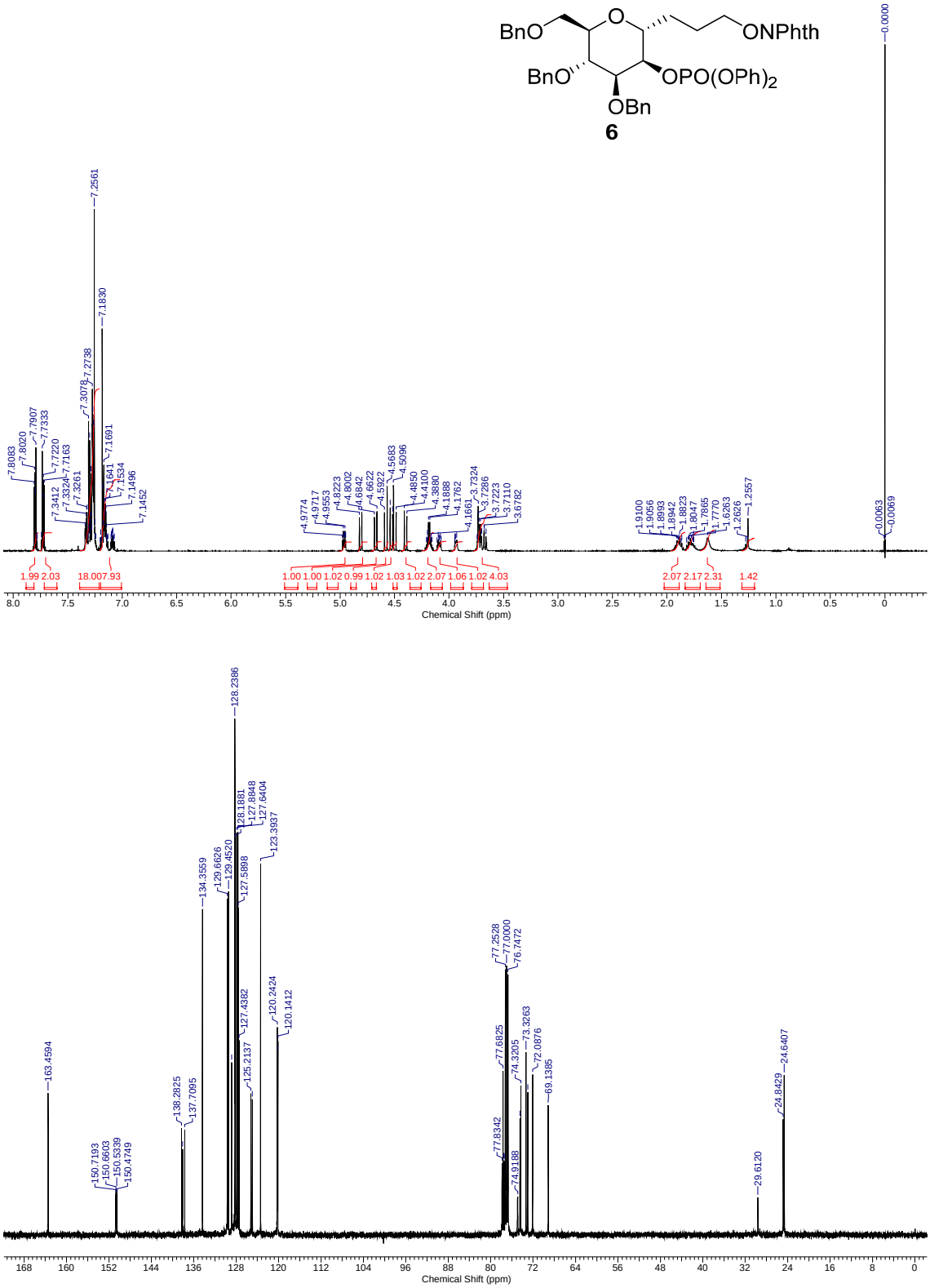

Fig. S10. ^{1}H NMR (500 MHz, $CDCl_3$) and $^{13}C\{H\}$ NMR (125.7 MHz, $CDCl_3$) of compound **6**.

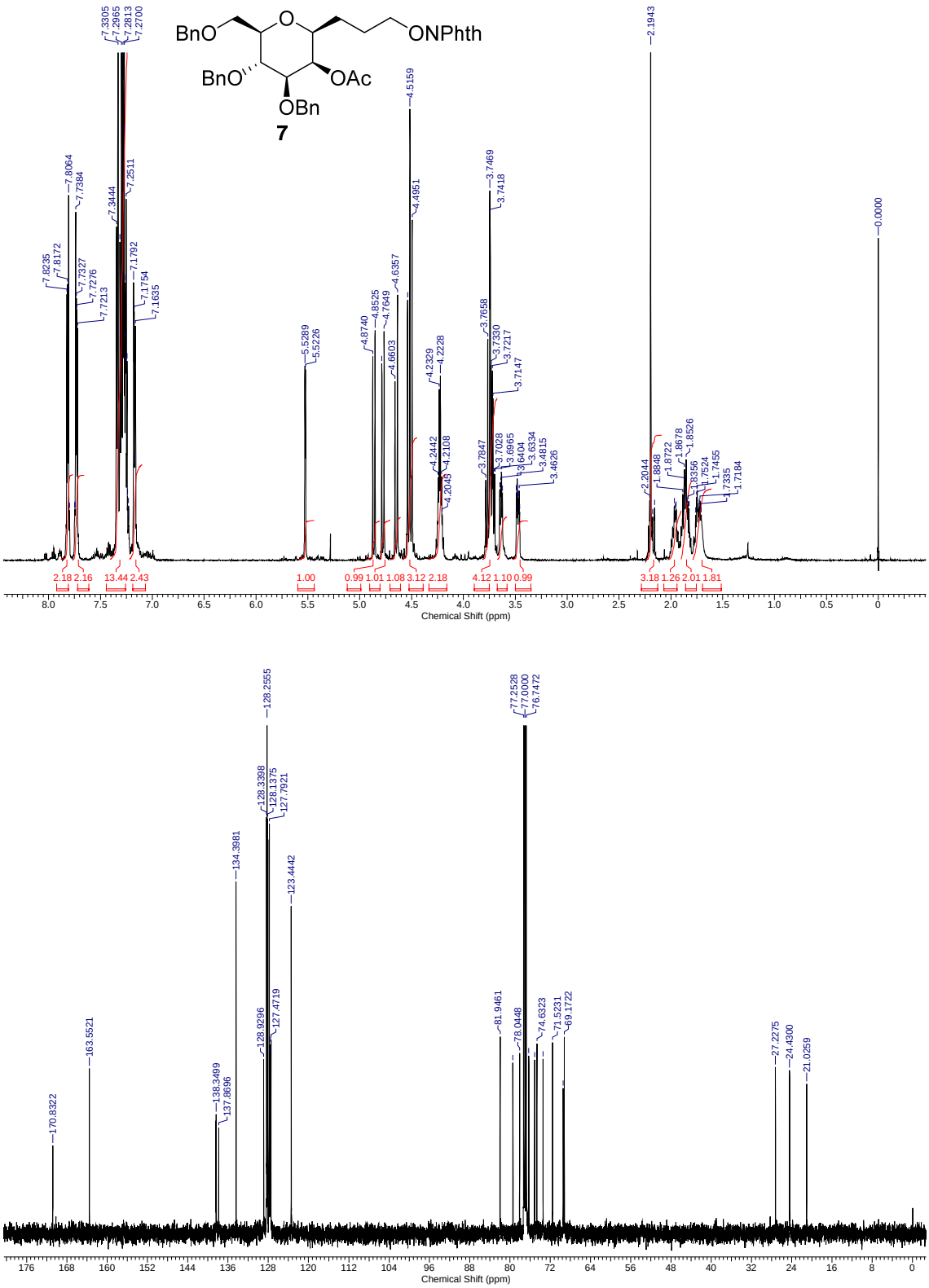

Fig. S11. ^{1}H NMR (500 MHz, $CDCl_3$) and $^{13}C\{H\}$ NMR (125.7 MHz, $CDCl_3$) of compound **7**.

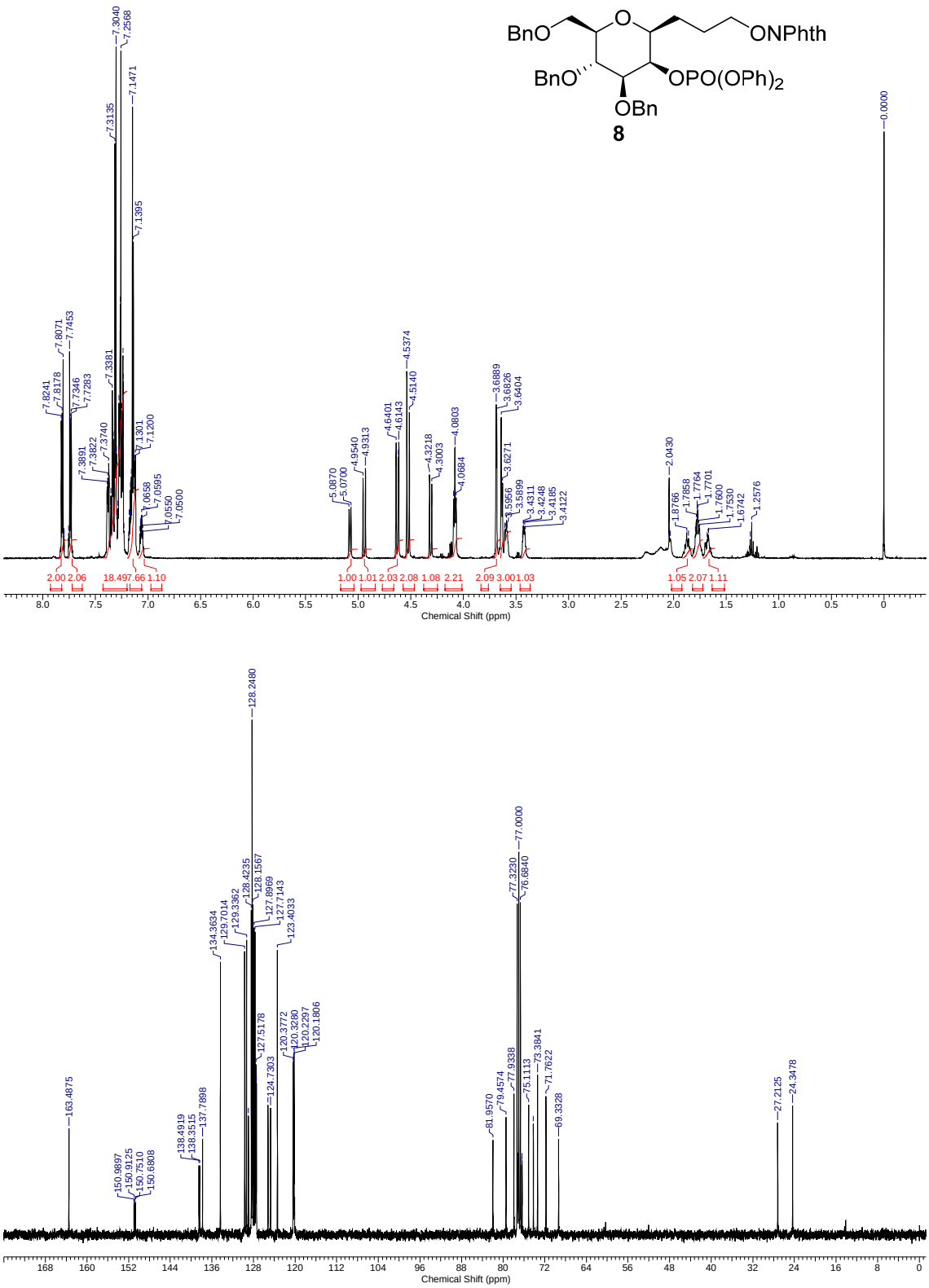

Fig. S12. ^{1}H NMR (500 MHz, $CDCl_3$) and $^{13}C\{H\}$ NMR (100.6 MHz, $CDCl_3$) of compound **8**.

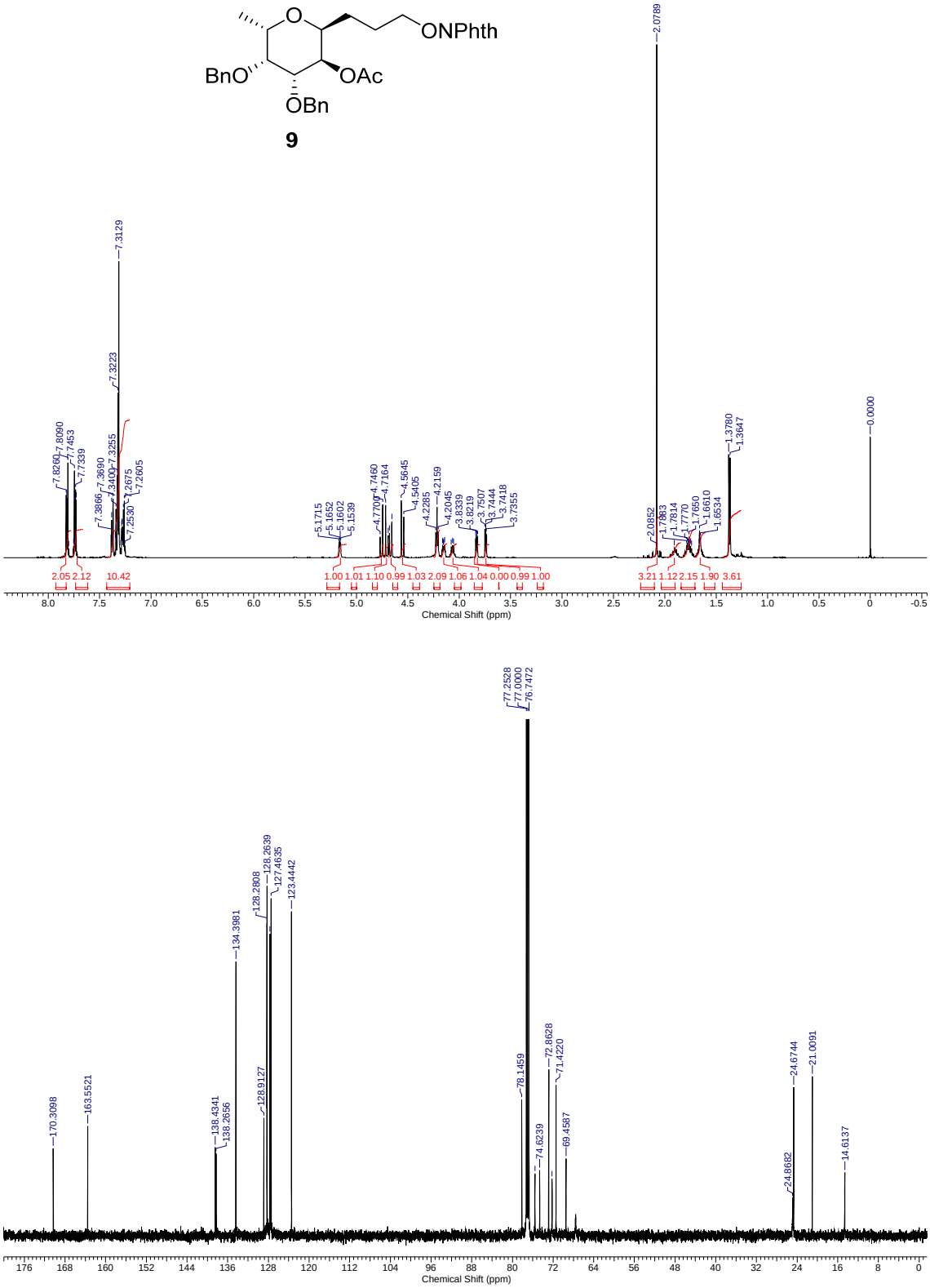

Fig. S13. ^{1}H NMR (500 MHz, $CDCl_3$) and $^{13}C\{H\}$ NMR (125.7 MHz, $CDCl_3$) of compound **9**.

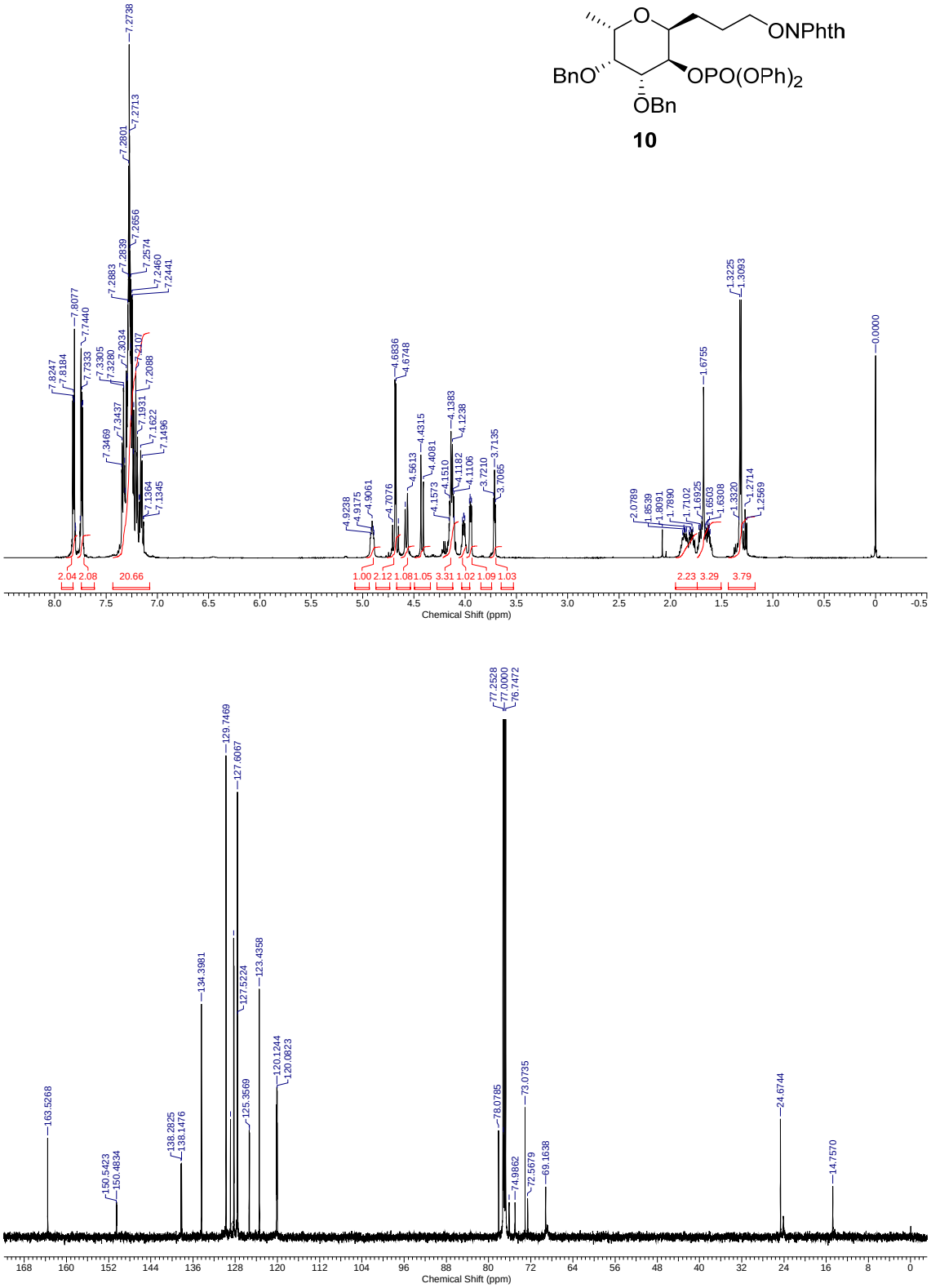

Fig. S14. ^{1}H NMR (500 MHz, $CDCl_3$) and $^{13}C\{H\}$ NMR (125.7 MHz, $CDCl_3$) of compound **10**.

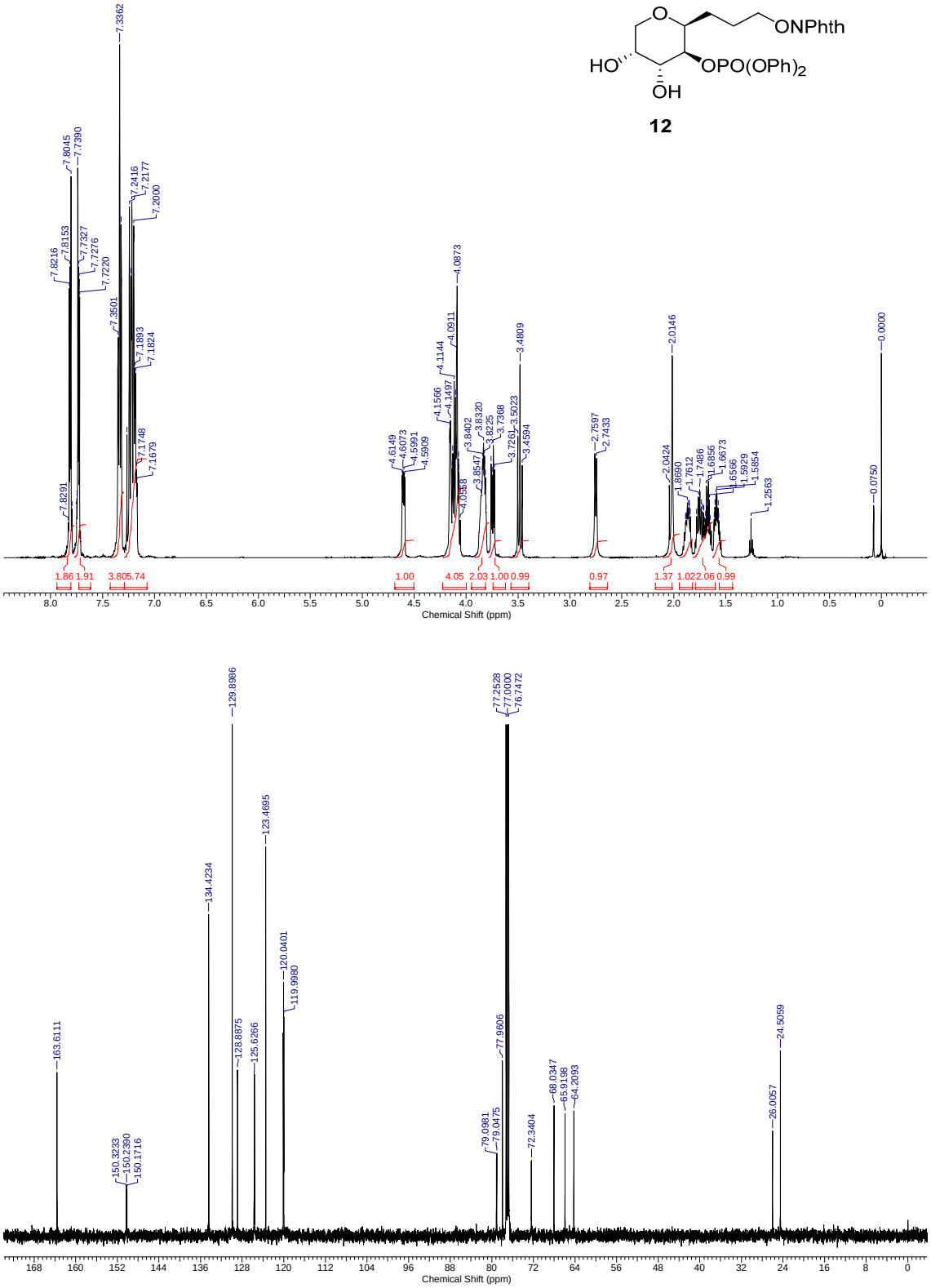

Fig. S15. ^{1}H NMR (500 MHz, $CDCl_3$) and $^{13}C\{H\}$ NMR (125.7 MHz, $CDCl_3$) of compound **12**.

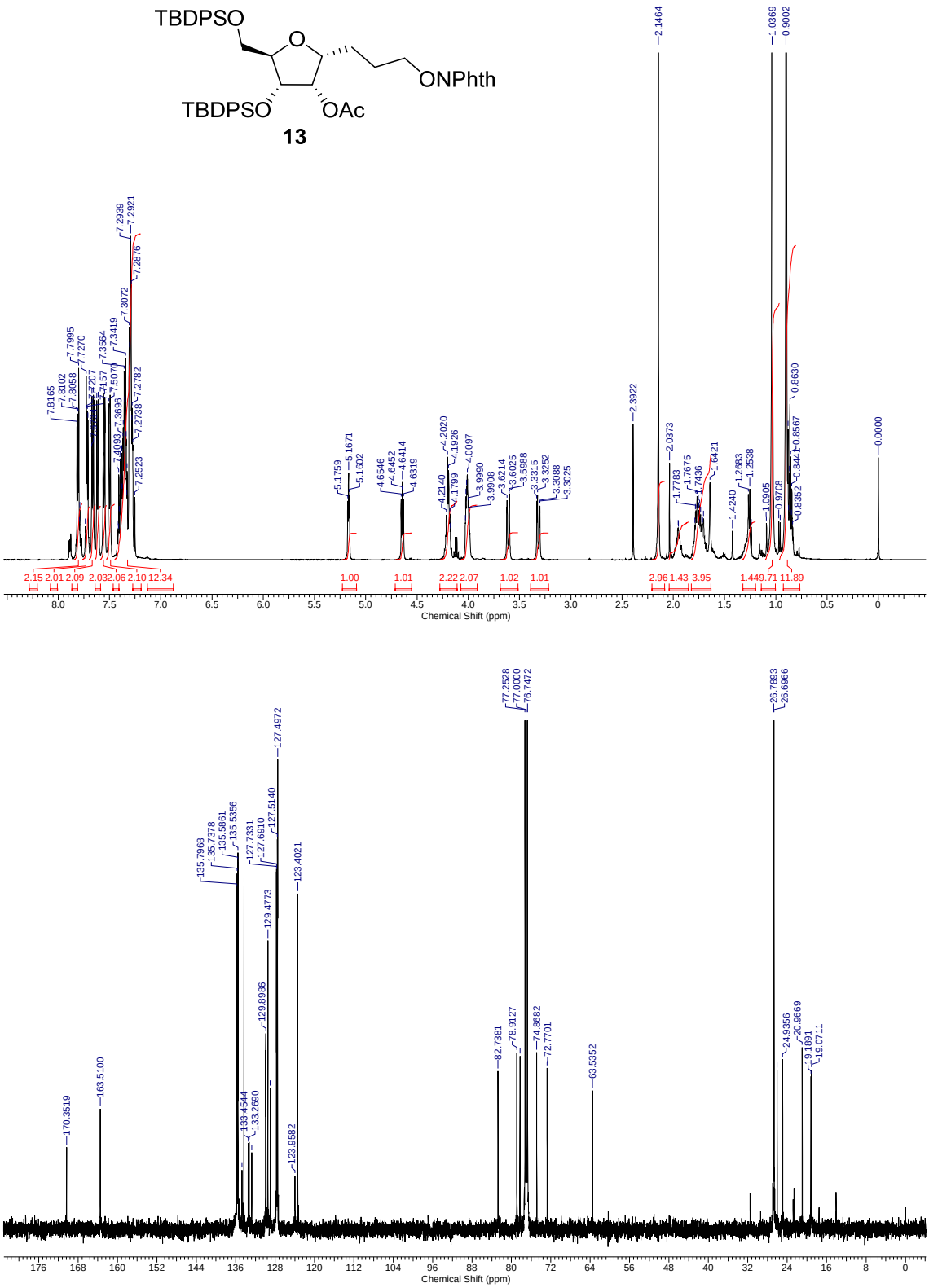

Fig. S16. ^{1}H NMR (500 MHz, $CDCl_3$) and $^{13}C\{H\}$ NMR (125.7 MHz, $CDCl_3$) of compound **13**.

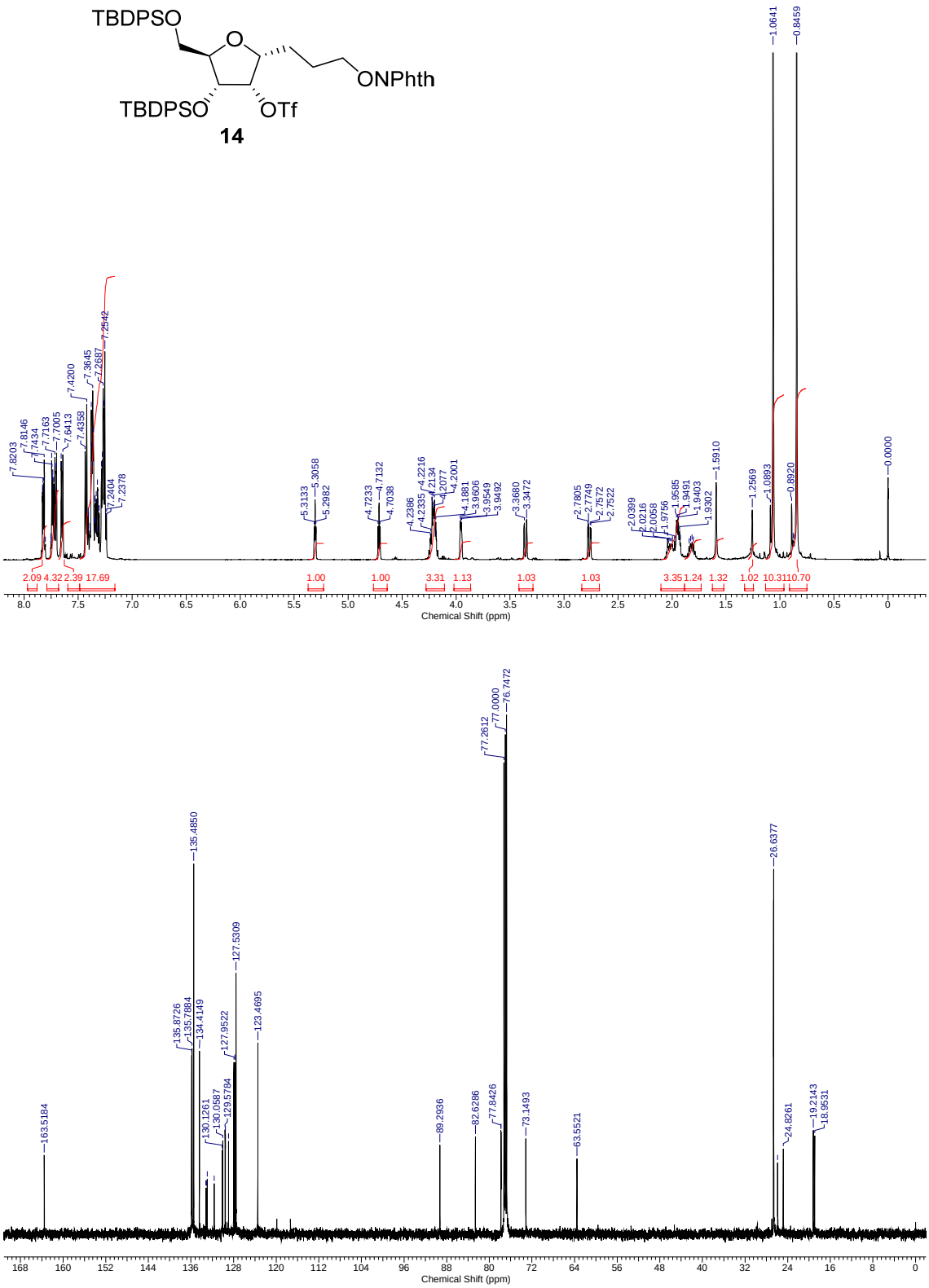

Fig. S17. ^{1}H NMR (500 MHz, $CDCl_3$) and $^{13}C\{H\}$ NMR (125.7 MHz, $CDCl_3$) of compound **14**.

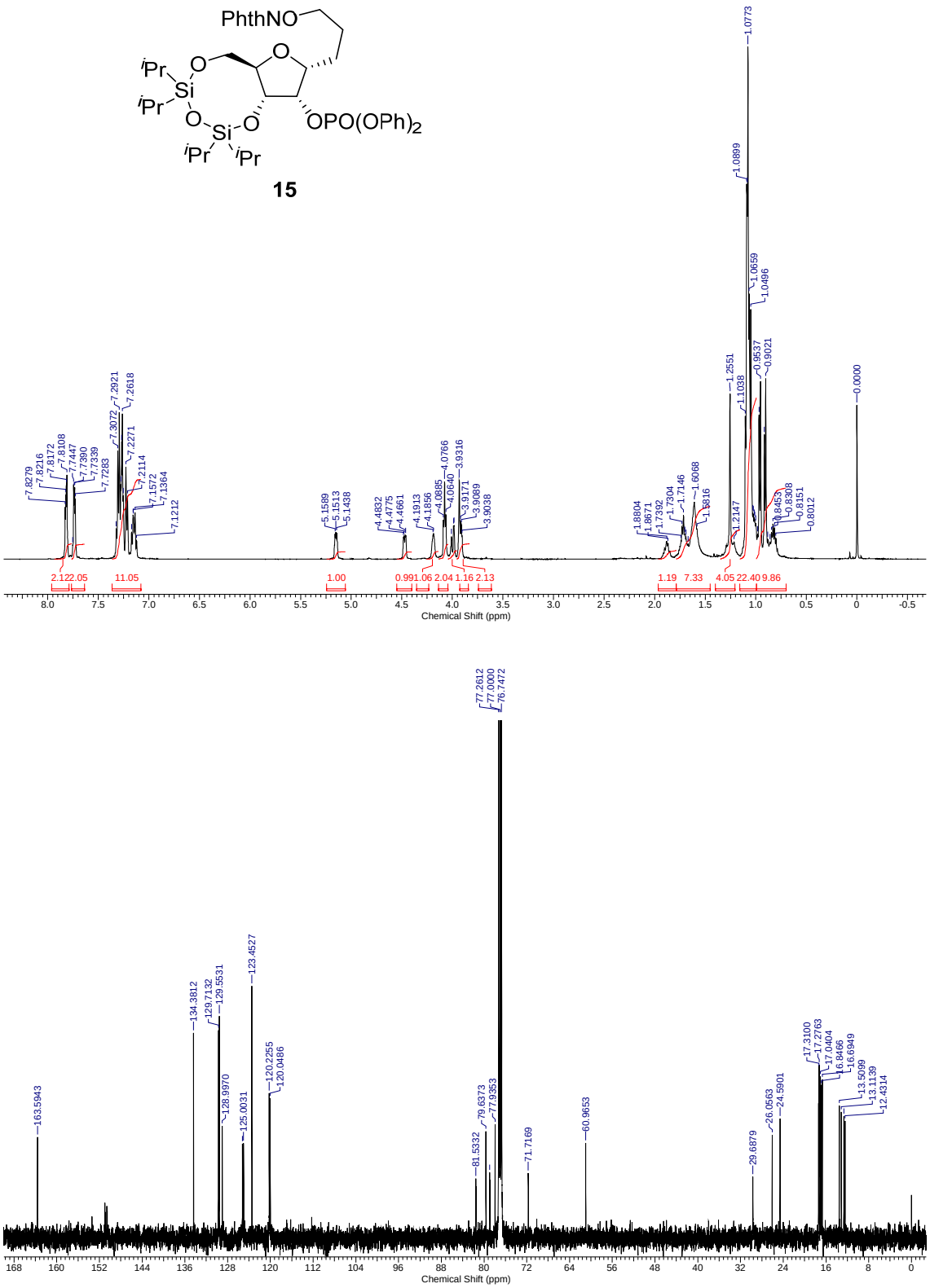

Fig. S18. ^{1}H NMR (500 MHz, $CDCl_3$) and $^{13}C\{H\}$ NMR (125.7 MHz, $CDCl_3$) of compound **15**.

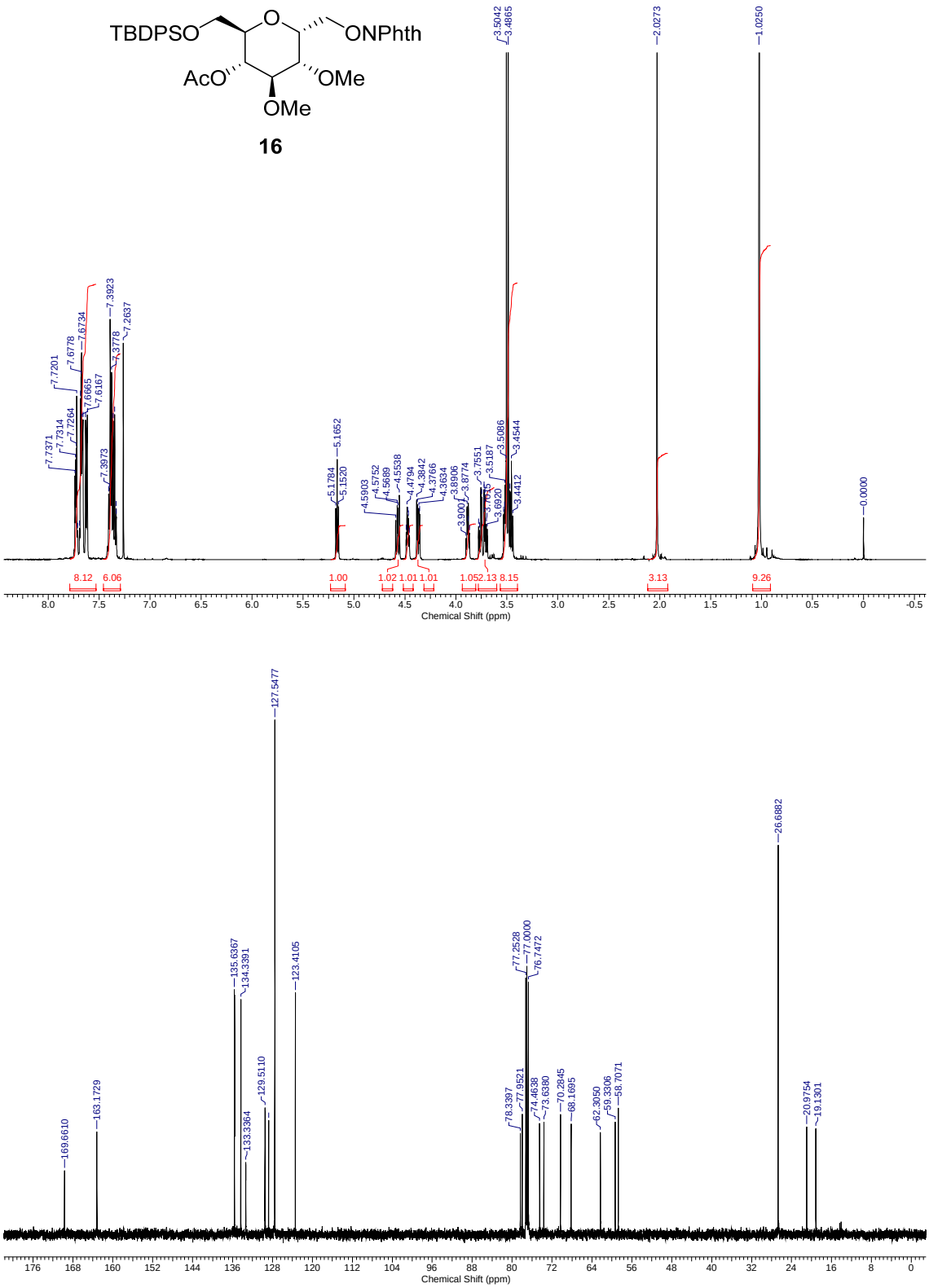

Fig. S19. ^{1}H NMR (500 MHz, $CDCl_3$) and $^{13}C\{H\}$ NMR (125.7 MHz, $CDCl_3$) of compound **16**.

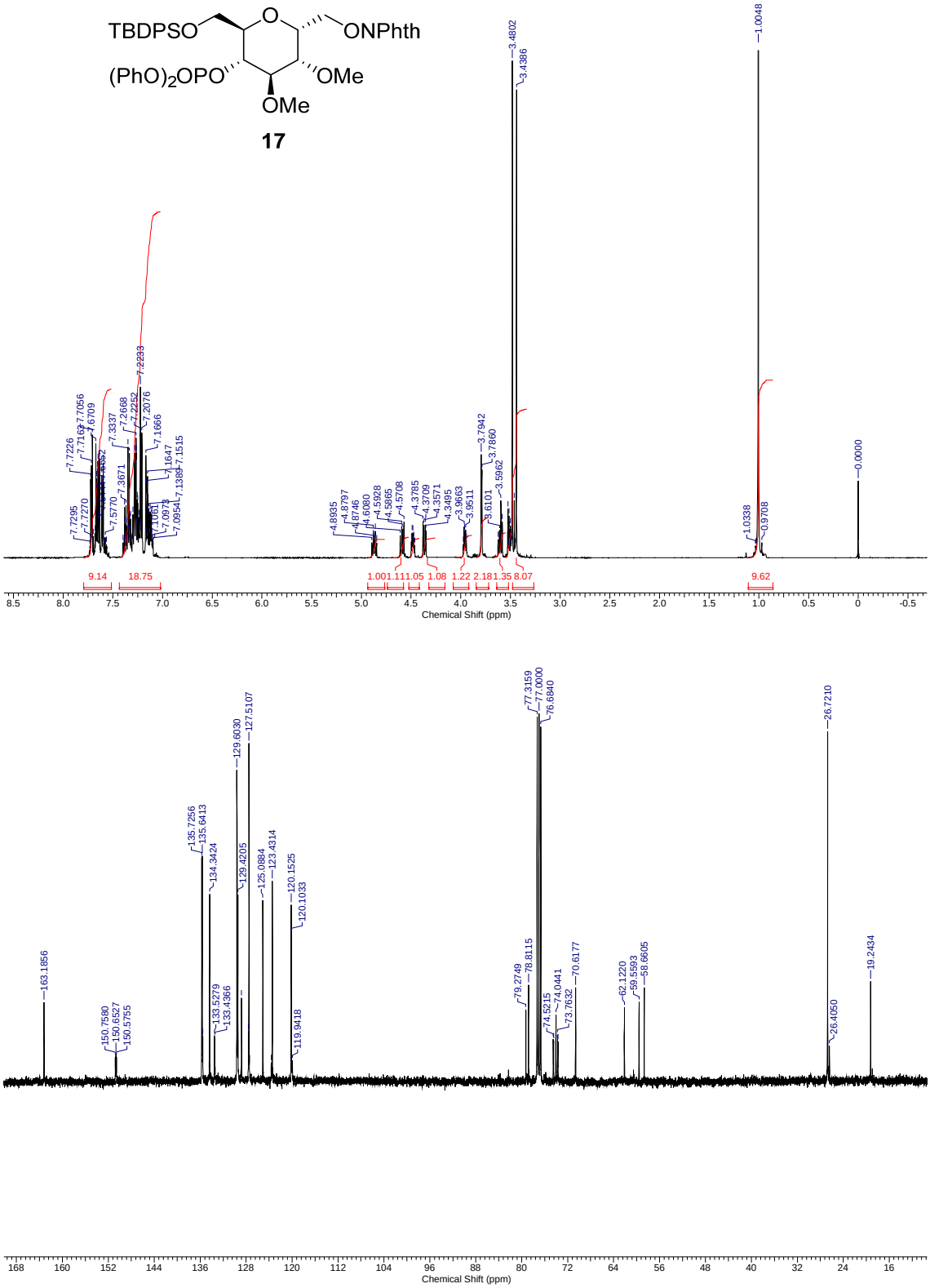

Fig. S20. ^{1}H NMR (500 MHz, $CDCl_3$) and $^{13}C\{H\}$ NMR (100.6 MHz, $CDCl_3$) of compound **17**.

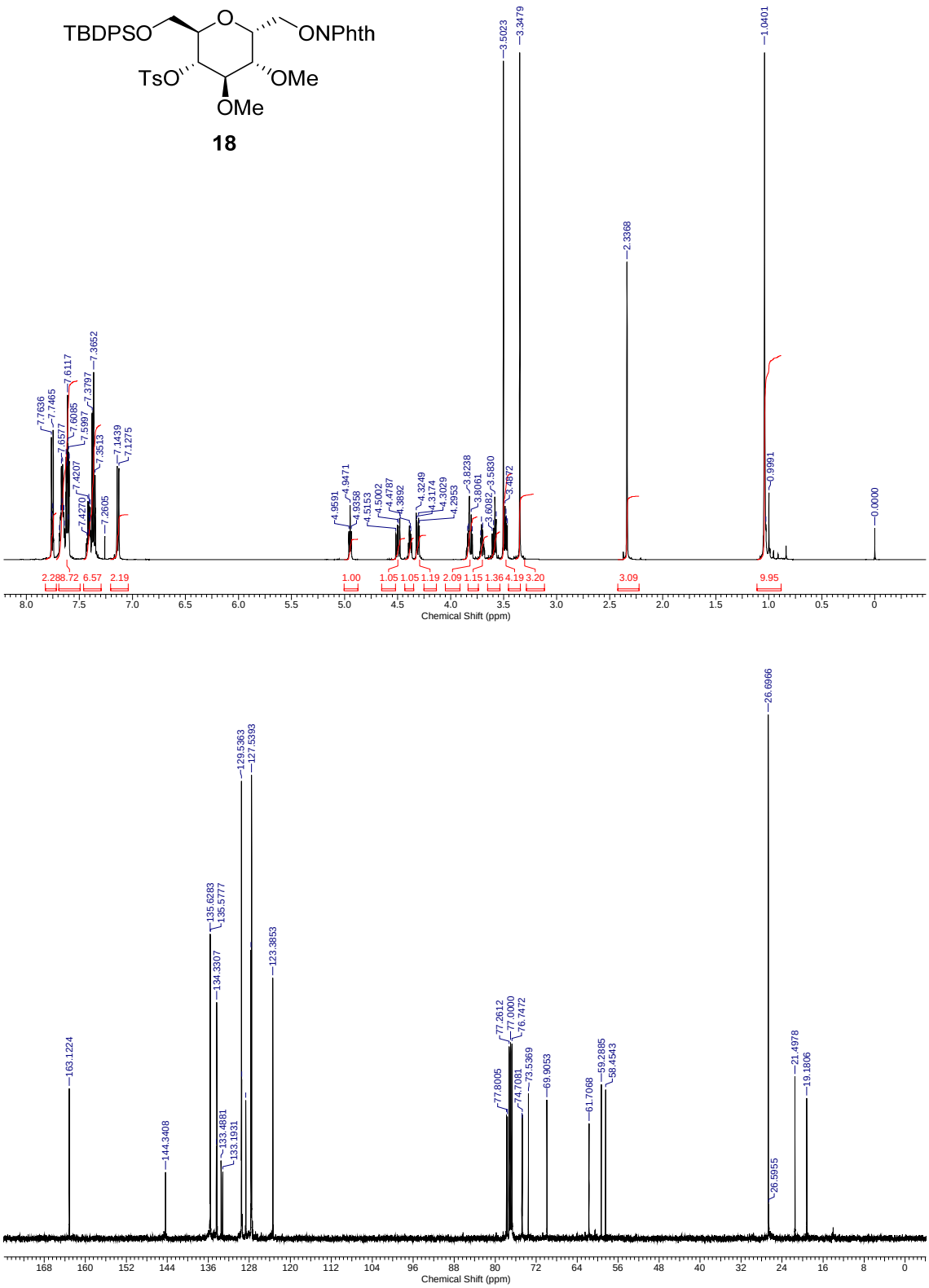

Fig. S21. ^{1}H NMR (500 MHz, $CDCl_3$) and $^{13}C\{H\}$ NMR (125.7 MHz, $CDCl_3$) of compound **18**.

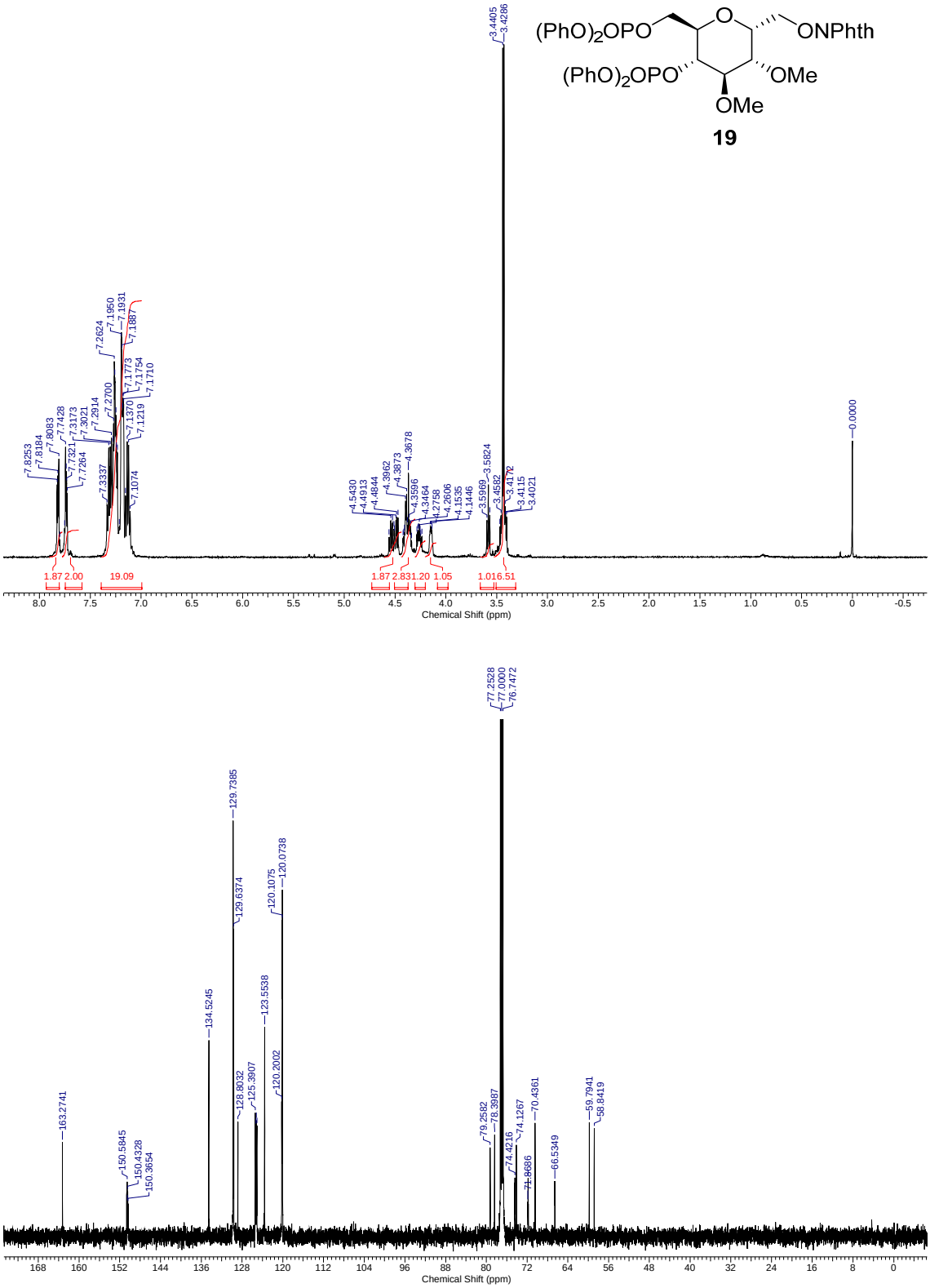

Fig. S22. ^{1}H NMR (500 MHz, $CDCl_3$) and $^{13}C\{H\}$ NMR (125.7 MHz, $CDCl_3$) of compound **19**.

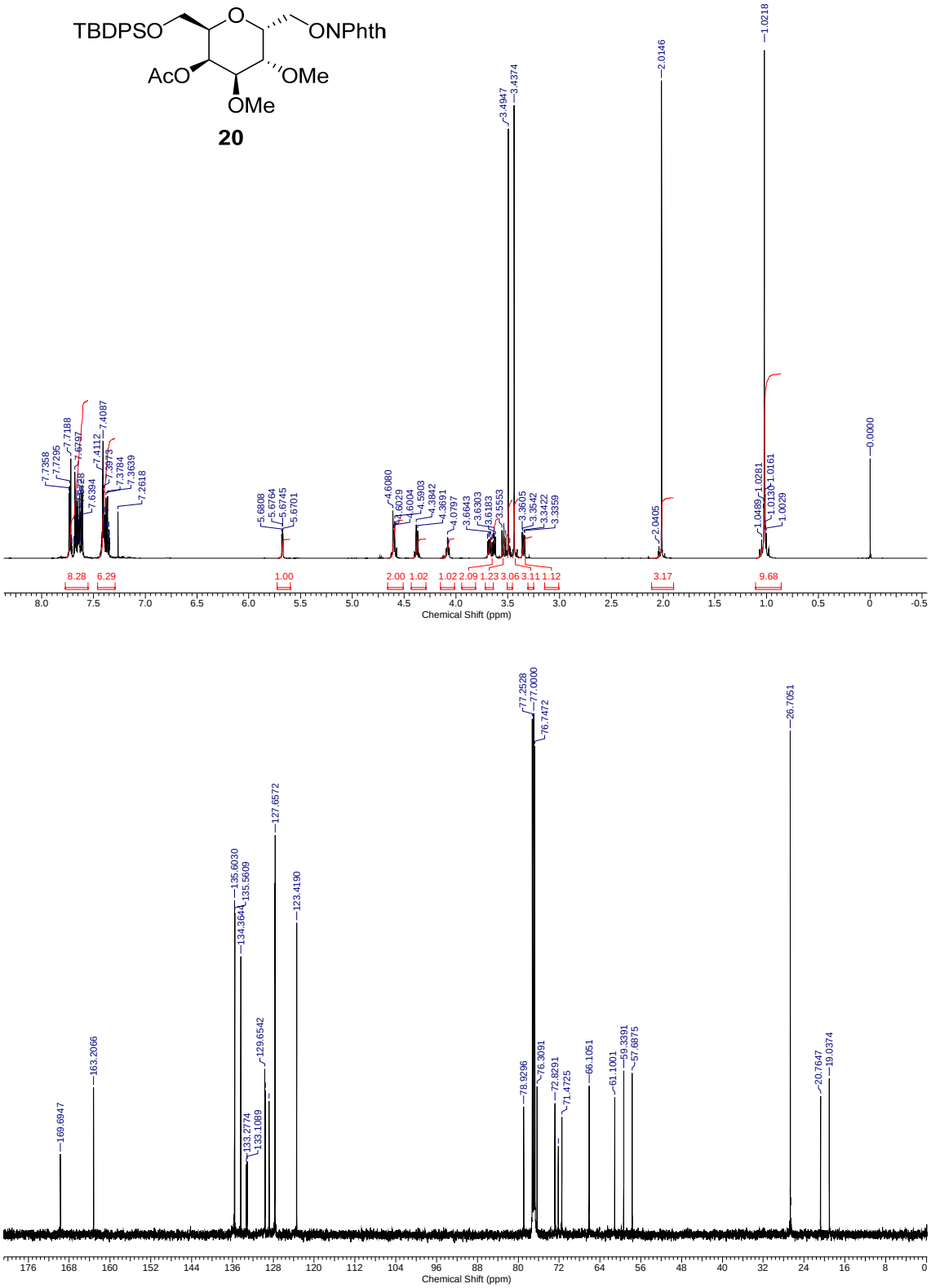

Fig. S23. ^{1}H NMR (500 MHz, $CDCl_3$) and $^{13}C\{H\}$ NMR (125.7 MHz, $CDCl_3$) of compound **20**.

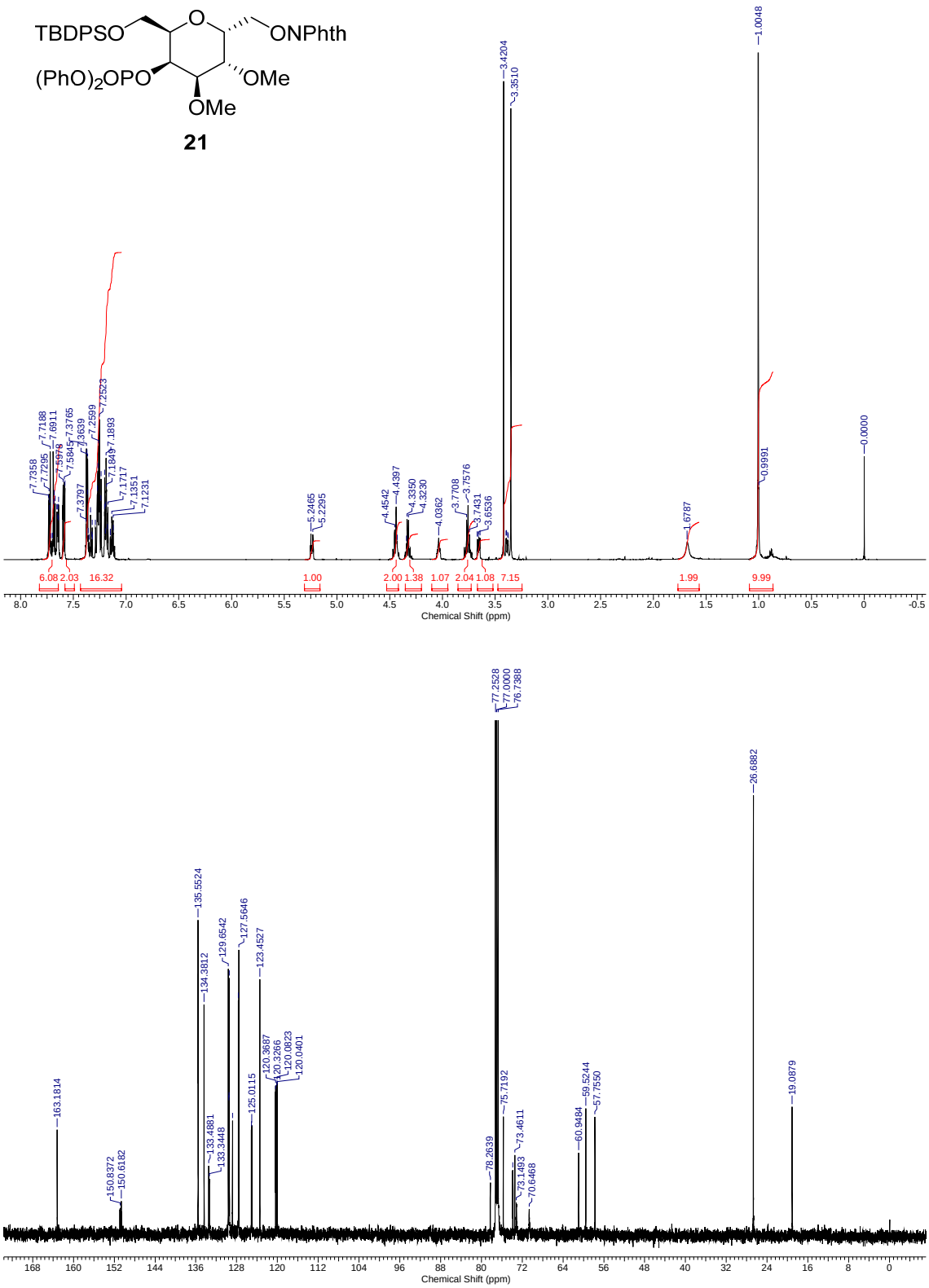

Fig. S24. ^{1}H NMR (500 MHz, $CDCl_3$) and $^{13}C\{H\}$ NMR (125.7 MHz, $CDCl_3$) of compound **21**.

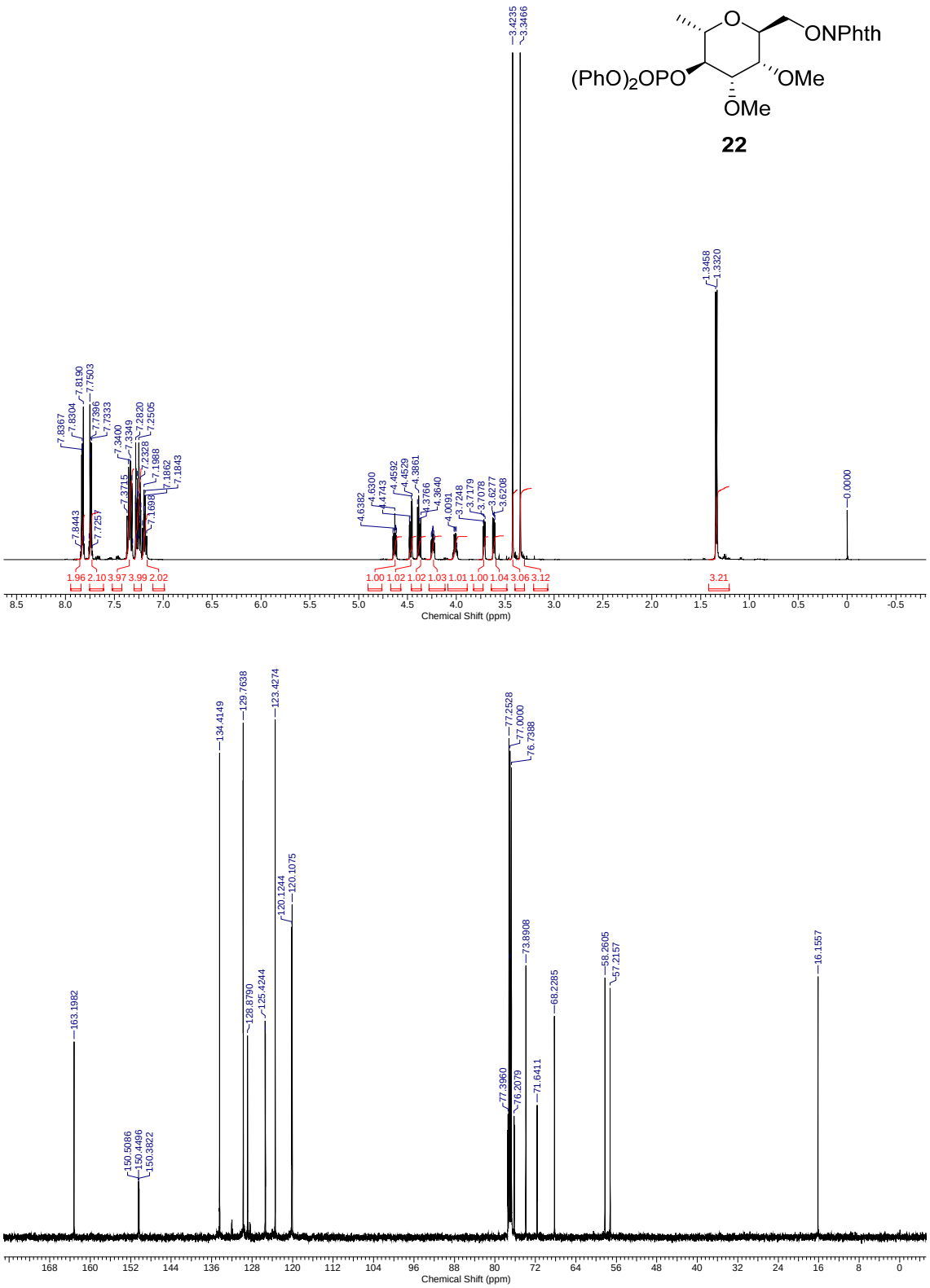

Fig. S25. ^{1}H NMR (500 MHz, $CDCl_3$) and $^{13}C\{H\}$ NMR (125.7 MHz, $CDCl_3$) of compound **22**.

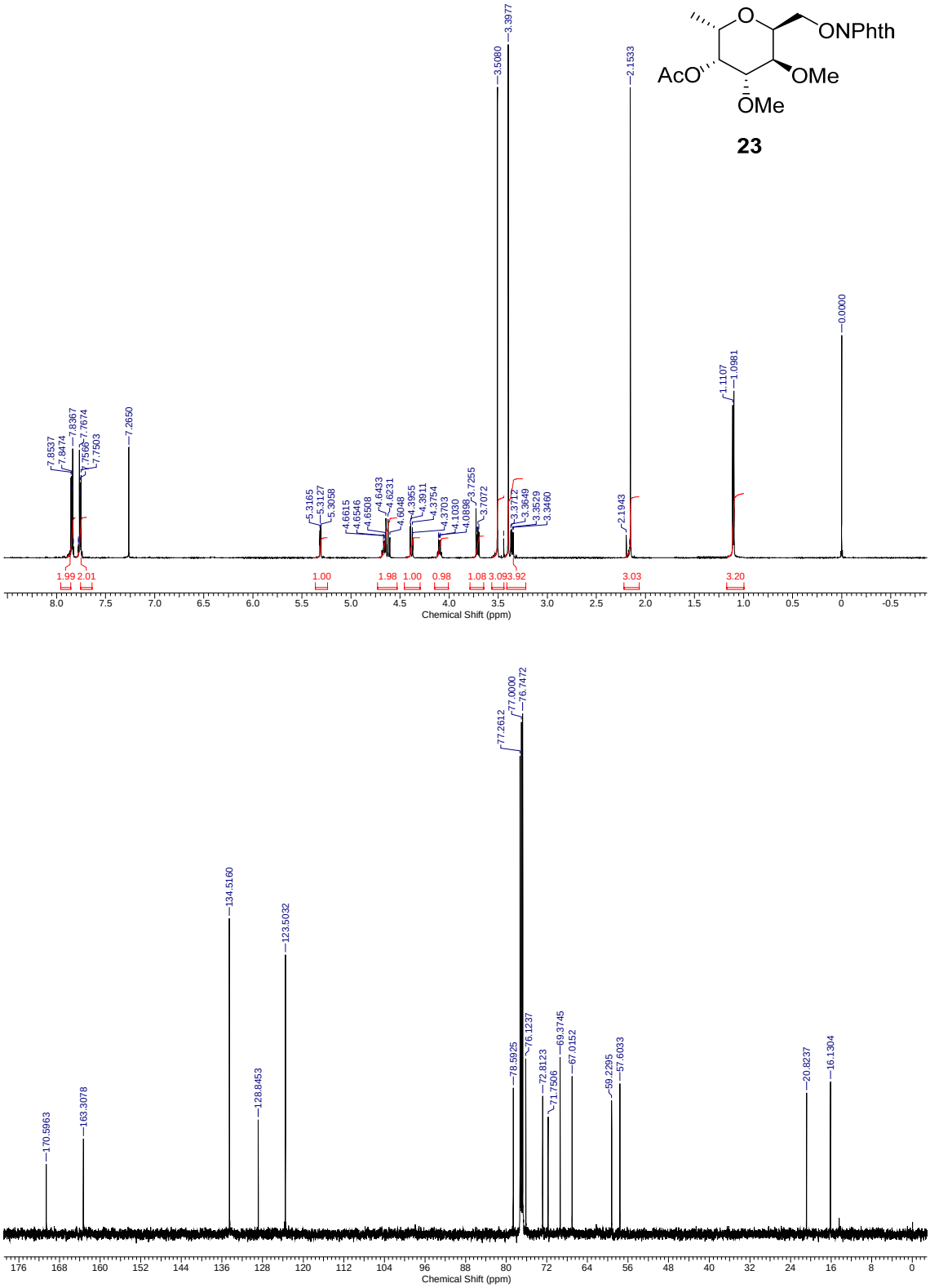

Fig. S26. ^{1}H NMR (500 MHz, $CDCl_3$) and $^{13}C\{H\}$ NMR (125.7 MHz, $CDCl_3$) of compound **23**.

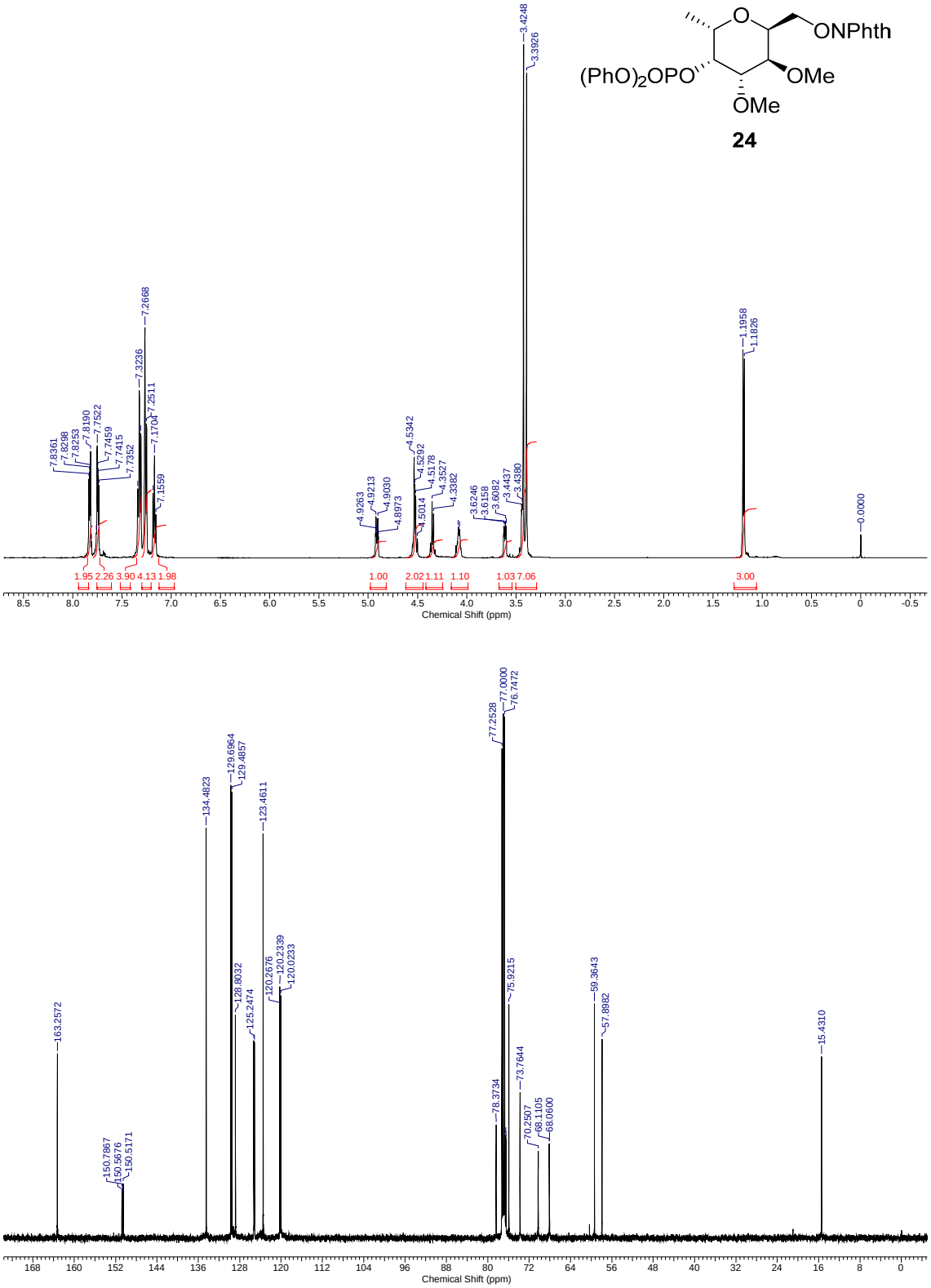

Fig. S27. ^{1}H NMR (500 MHz, $CDCl_3$) and $^{13}C\{H\}$ NMR (125.7 MHz, $CDCl_3$) of compound **24**.

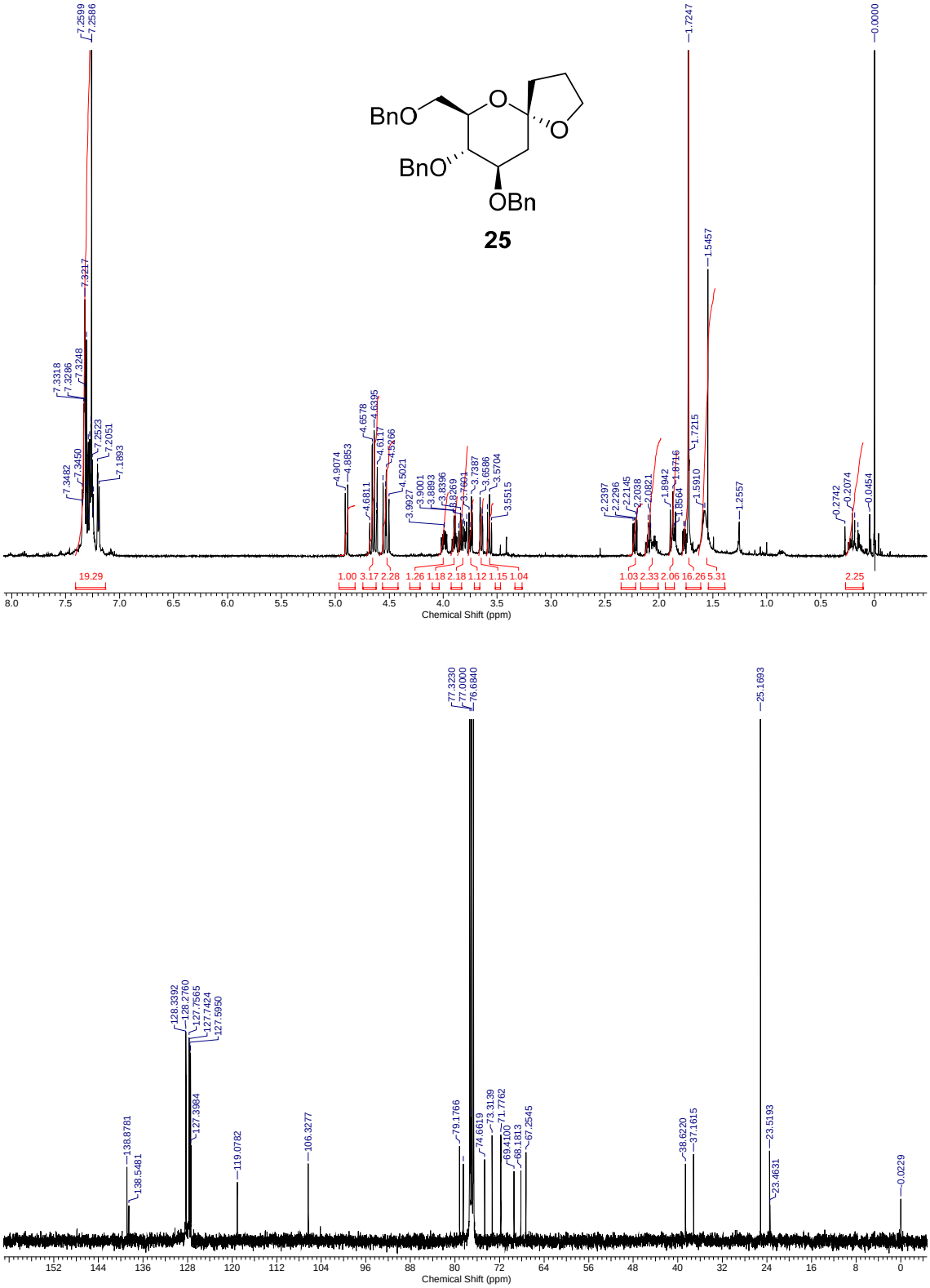

Fig. S28. ^{1}H NMR (500 MHz, $CDCl_3$) and $^{13}C\{H\}$ NMR (100.6 MHz, $CDCl_3$) of compound **25**.

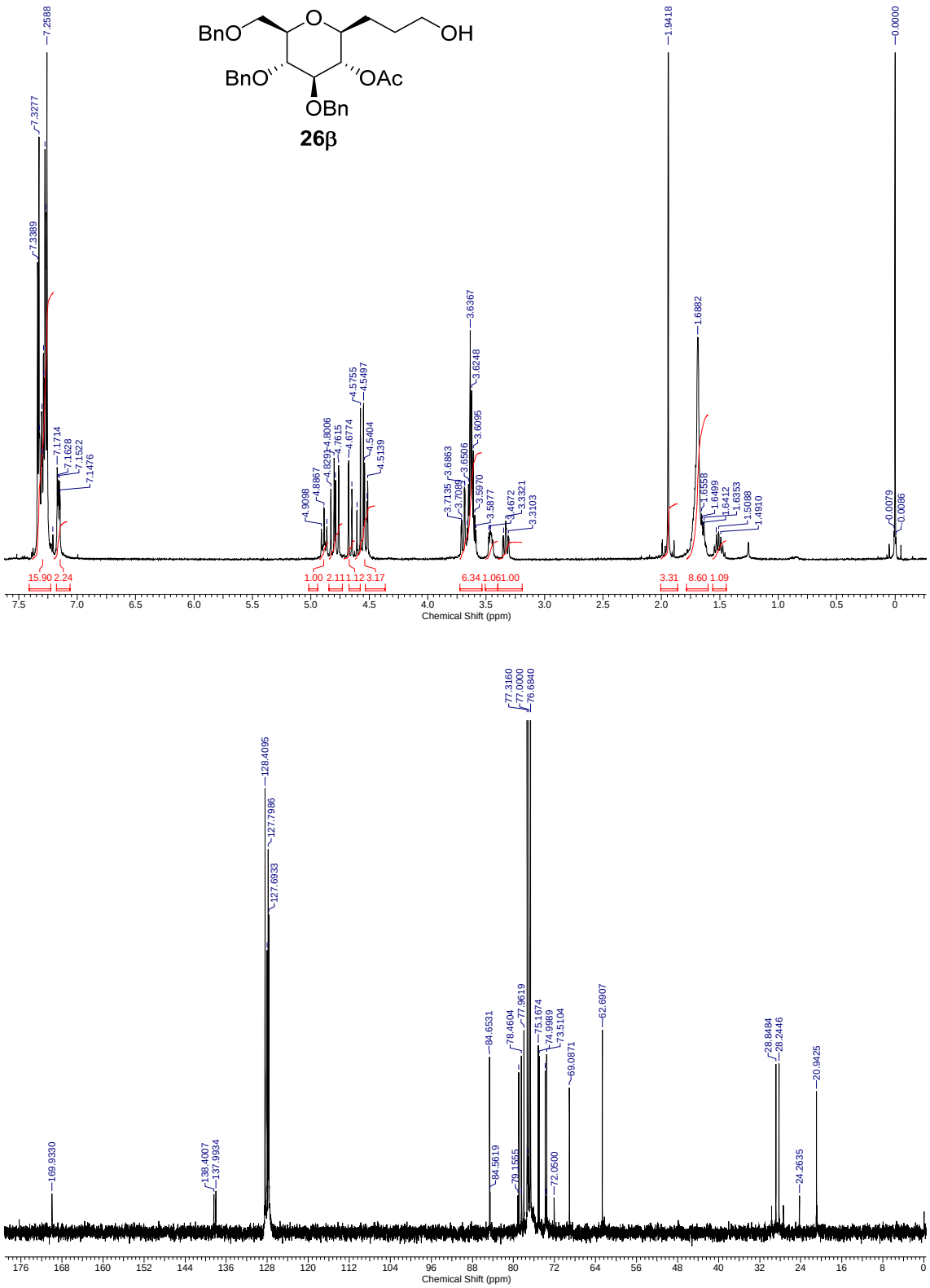

Fig. S29. ^{1}H NMR (400 MHz, $CDCl_3$) and $^{13}C\{H\}$ NMR (100.6 MHz, $CDCl_3$) of compound **26β**.

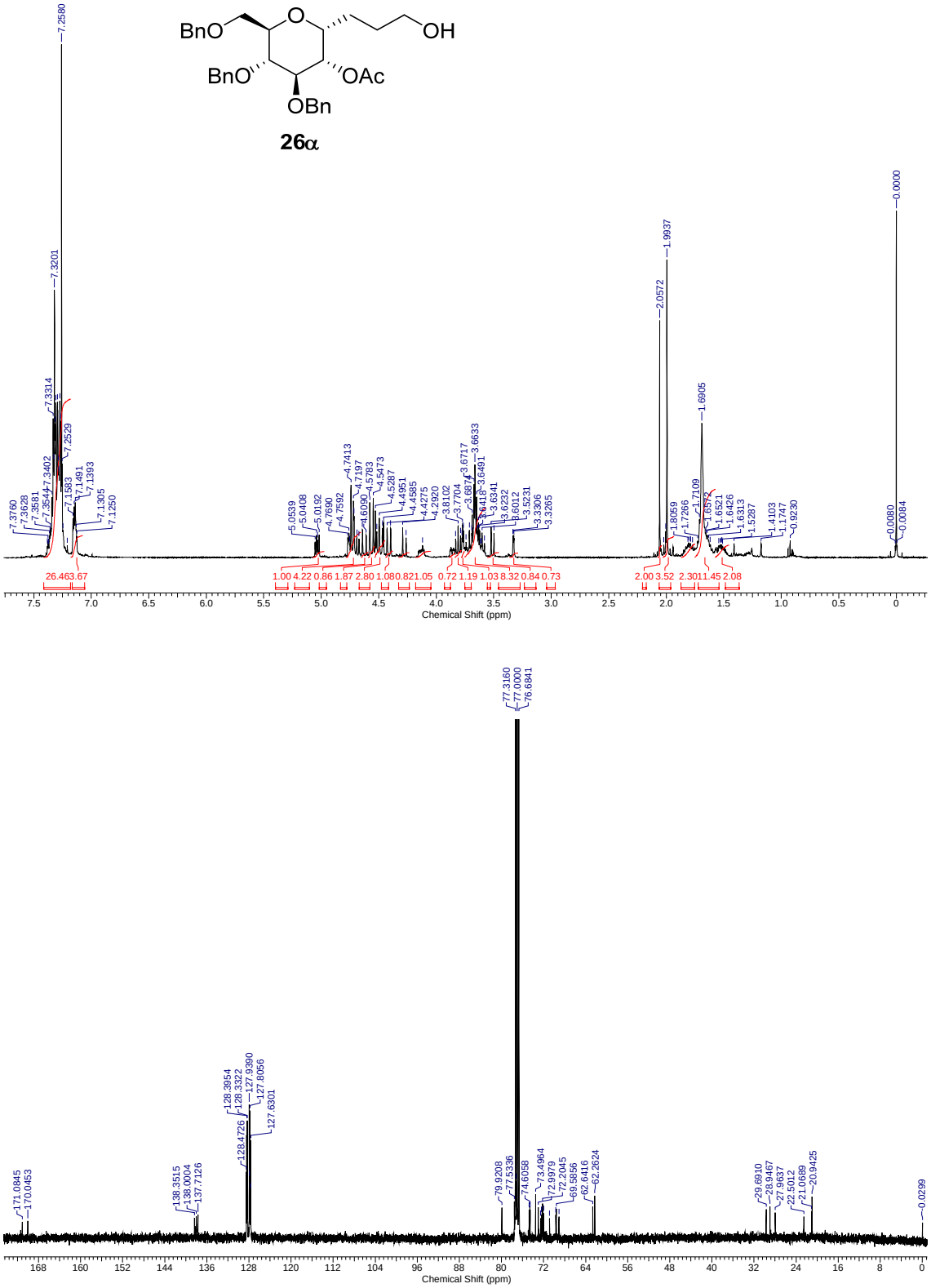

Fig. S30. ^{1}H NMR (400 MHz, $CDCl_3$) and $^{13}C\{H\}$ NMR (100.6 MHz, $CDCl_3$) of compound **26α**.

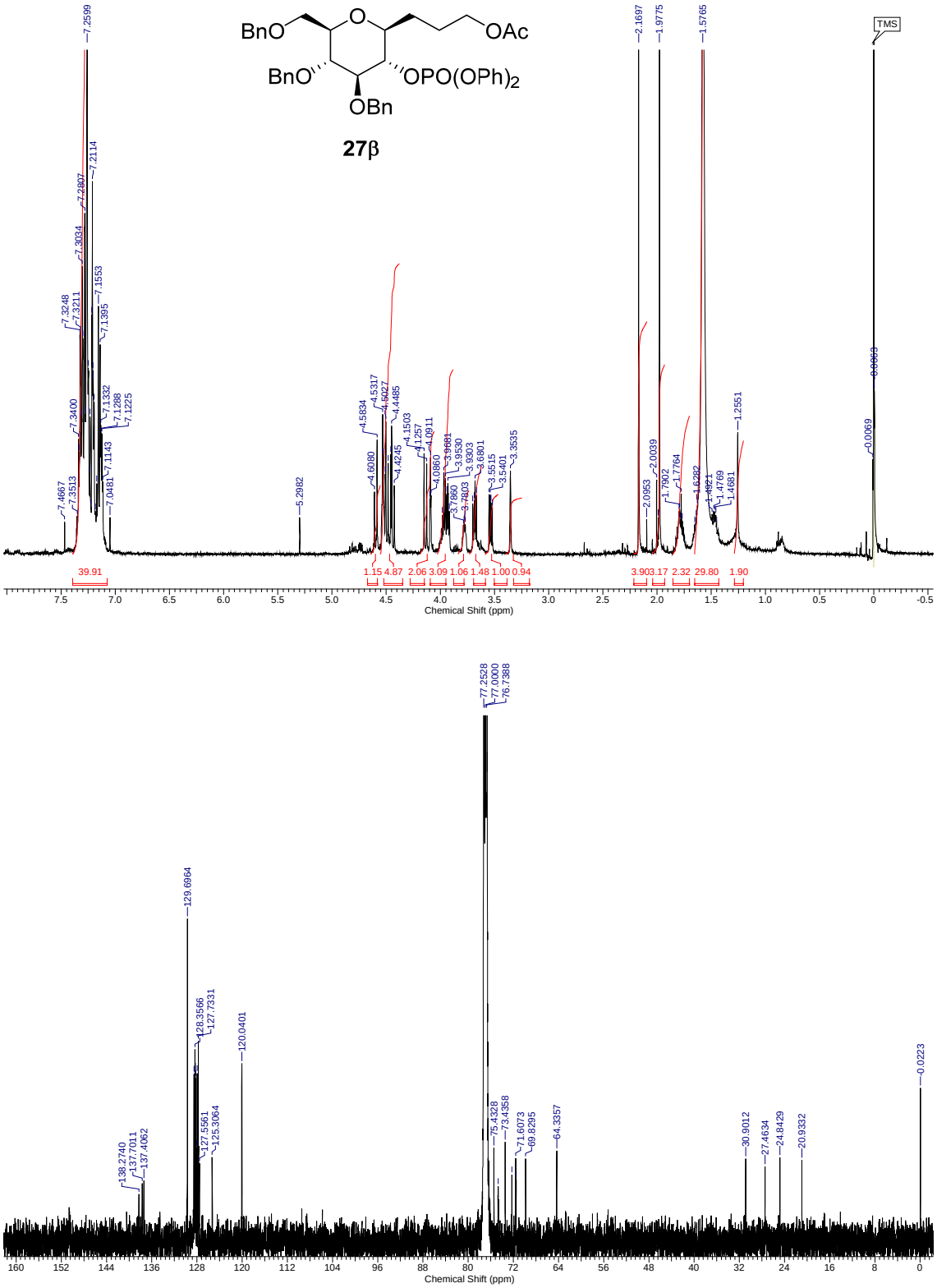

Fig. S31. ^{1}H NMR (500 MHz, $CDCl_3$) and $^{13}C\{H\}$ NMR (125.7 MHz, $CDCl_3$) of compound **27β**.

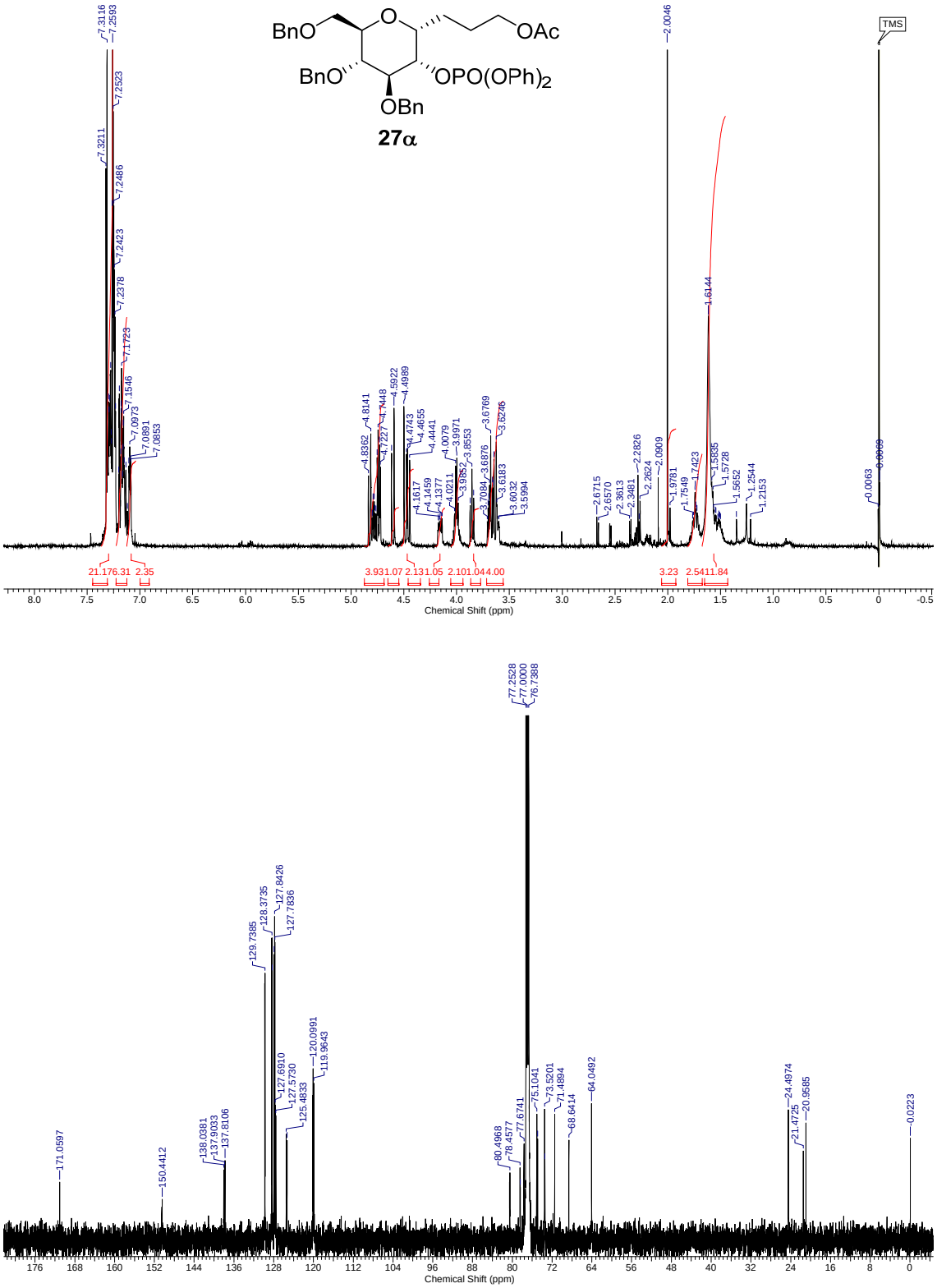

Fig. S32. ^{1}H NMR (500 MHz, $CDCl_3$) and $^{13}C\{H\}$ NMR (125.7 MHz, $CDCl_3$) of compound **27α**.

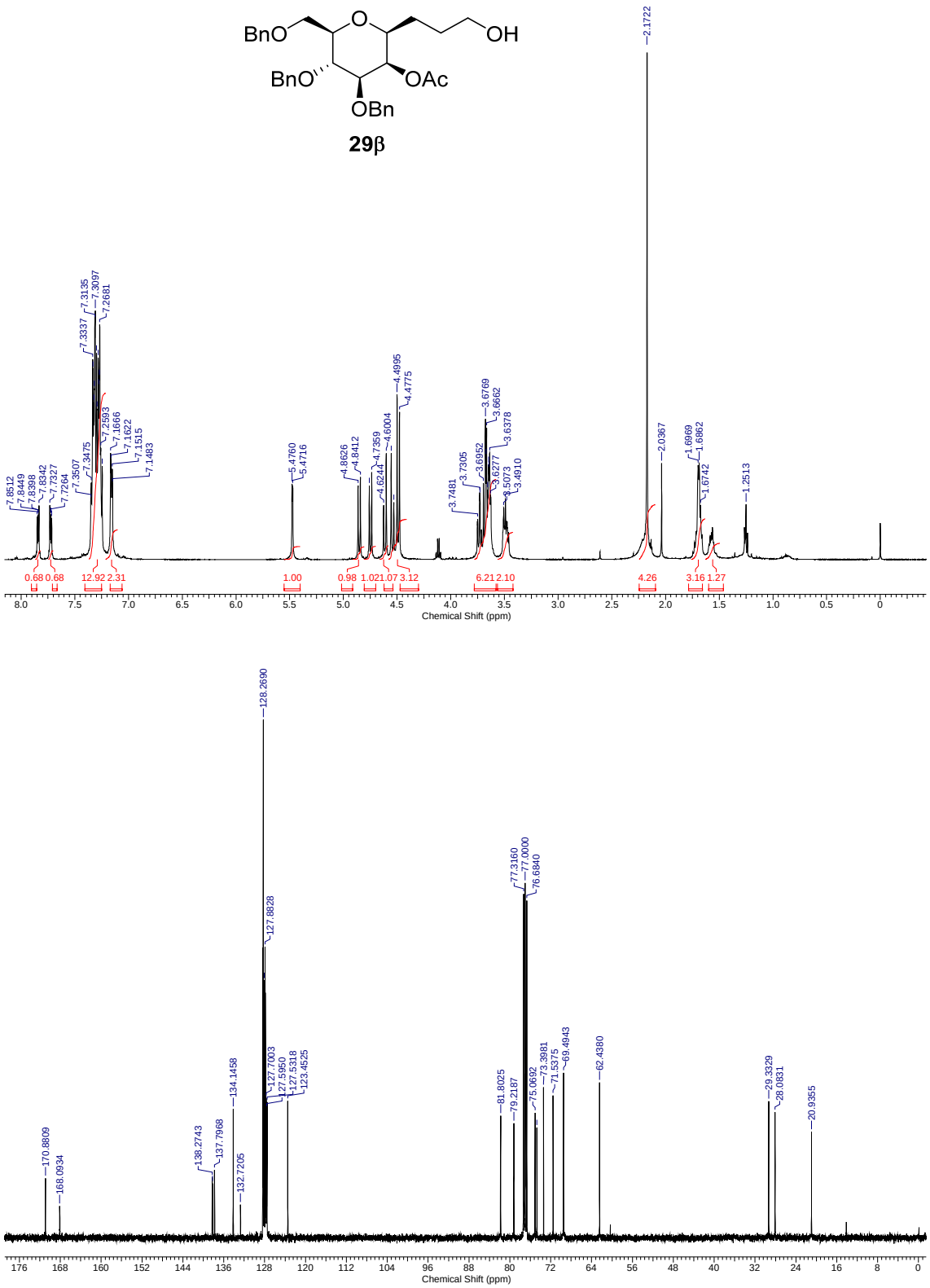

Fig. S33. ^{1}H NMR (500 MHz, $CDCl_3$) and $^{13}C\{H\}$ NMR (100.6 MHz, $CDCl_3$) of compound **29β**.

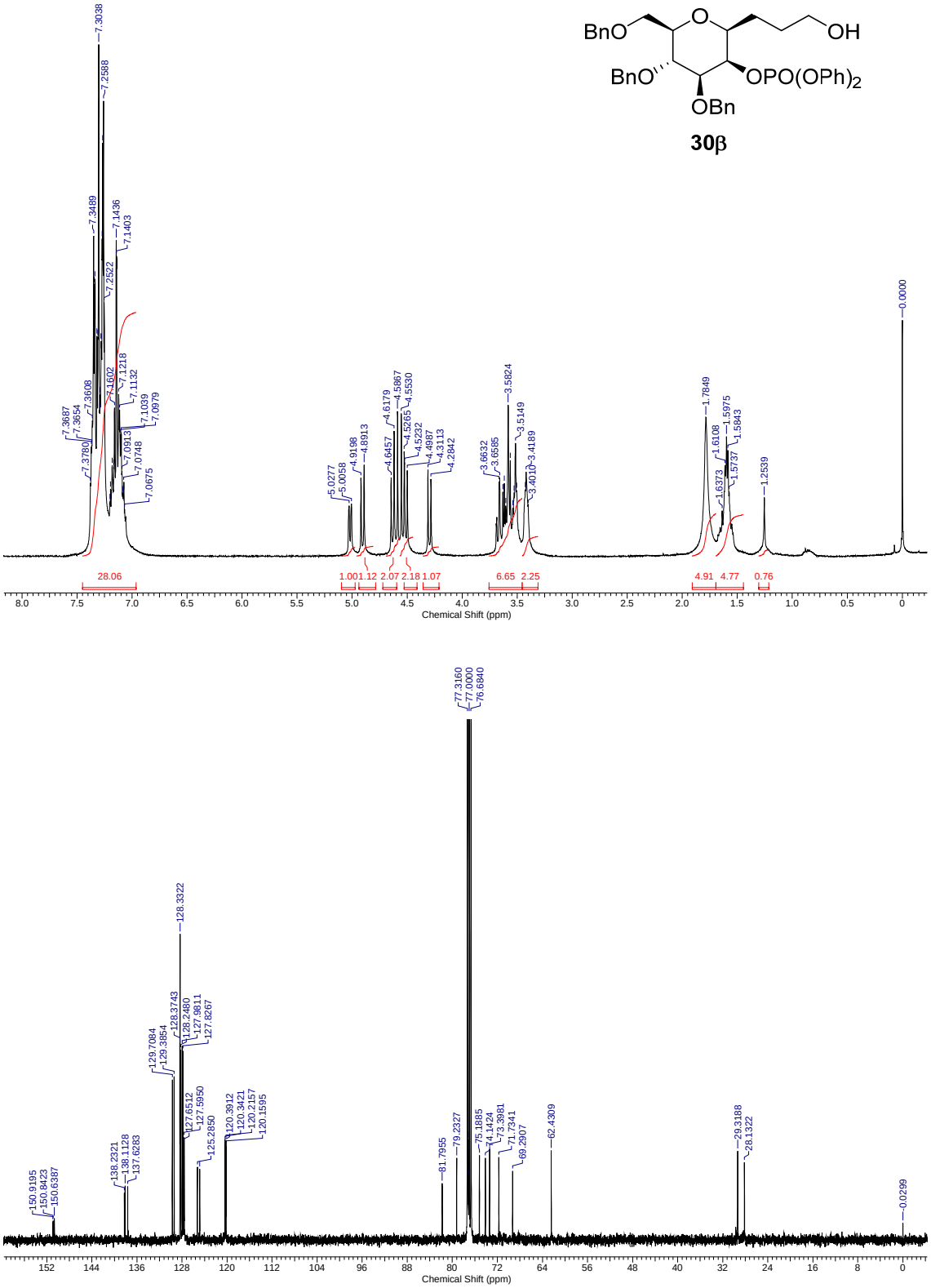

Fig. S34. ^{1}H NMR (400 MHz, $CDCl_3$) and $^{13}C\{H\}$ NMR (100.6 MHz, $CDCl_3$) of compound **30β**.

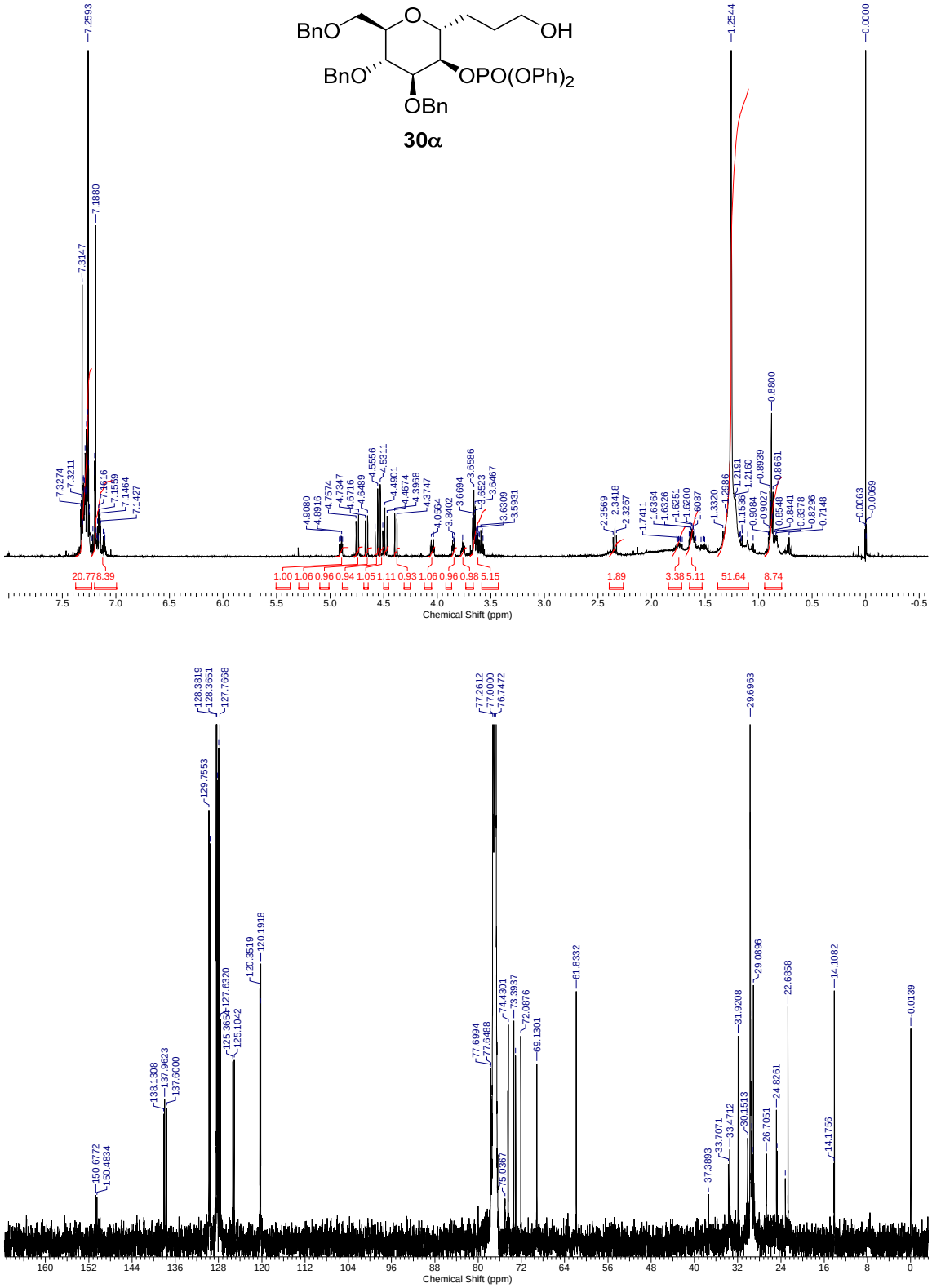

Fig. S35. ^{1}H NMR (500 MHz, $CDCl_3$) and $^{13}C\{H\}$ NMR (125.7 MHz, $CDCl_3$) of compound **30α**.

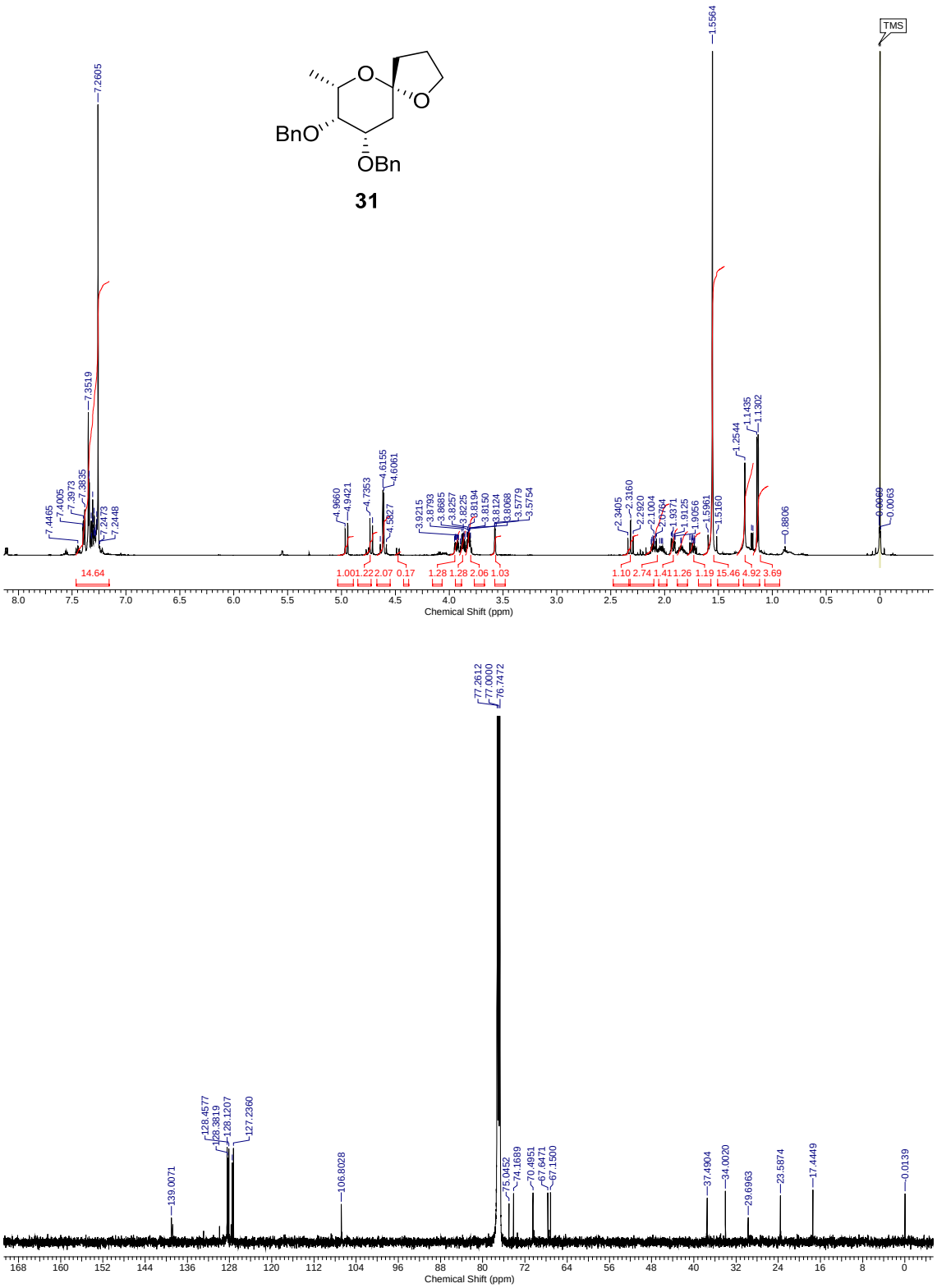

Fig. S36. ^{1}H NMR (500 MHz, $CDCl_3$) and $^{13}C\{H\}$ NMR (125.7 MHz, $CDCl_3$) of compound **31**.

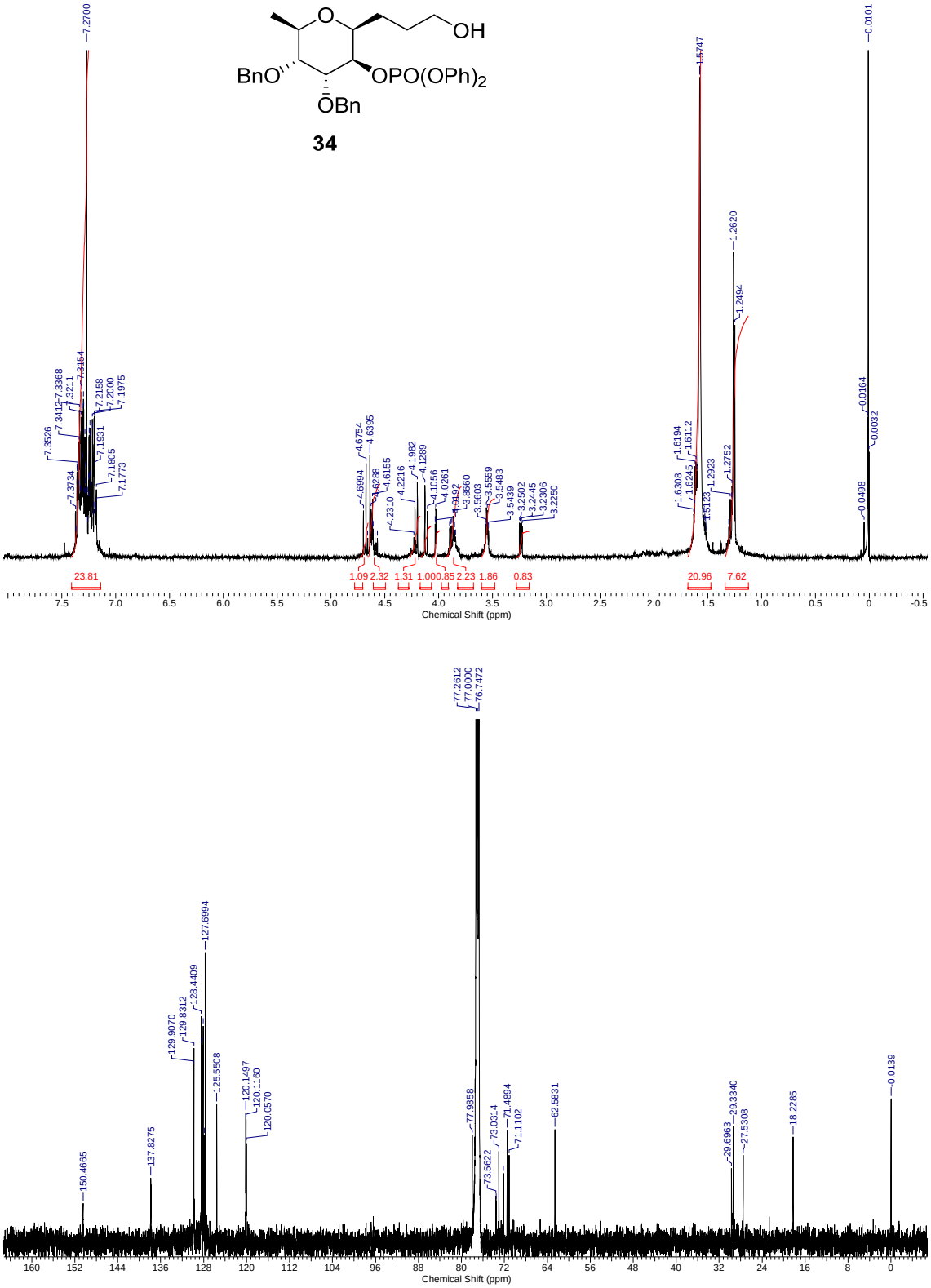

Fig. S37. ^{1}H NMR (500 MHz, $CDCl_3$) and $^{13}C\{H\}$ NMR (125.7 MHz, $CDCl_3$) of compound **34**.

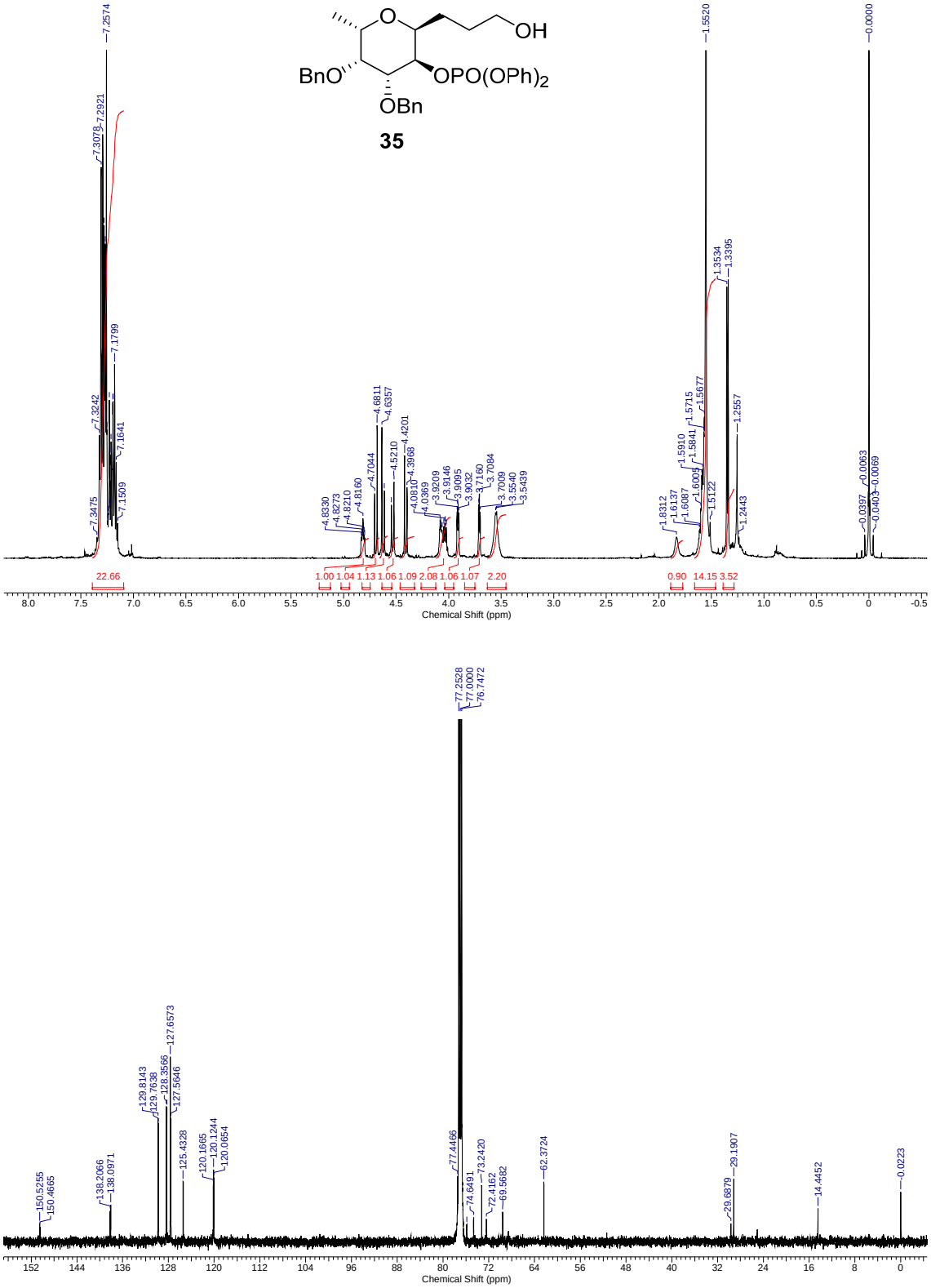

Fig. S38. ^{1}H NMR (500 MHz, $CDCl_3$) and $^{13}C\{H\}$ NMR (125.7 MHz, $CDCl_3$) of compound **35**.

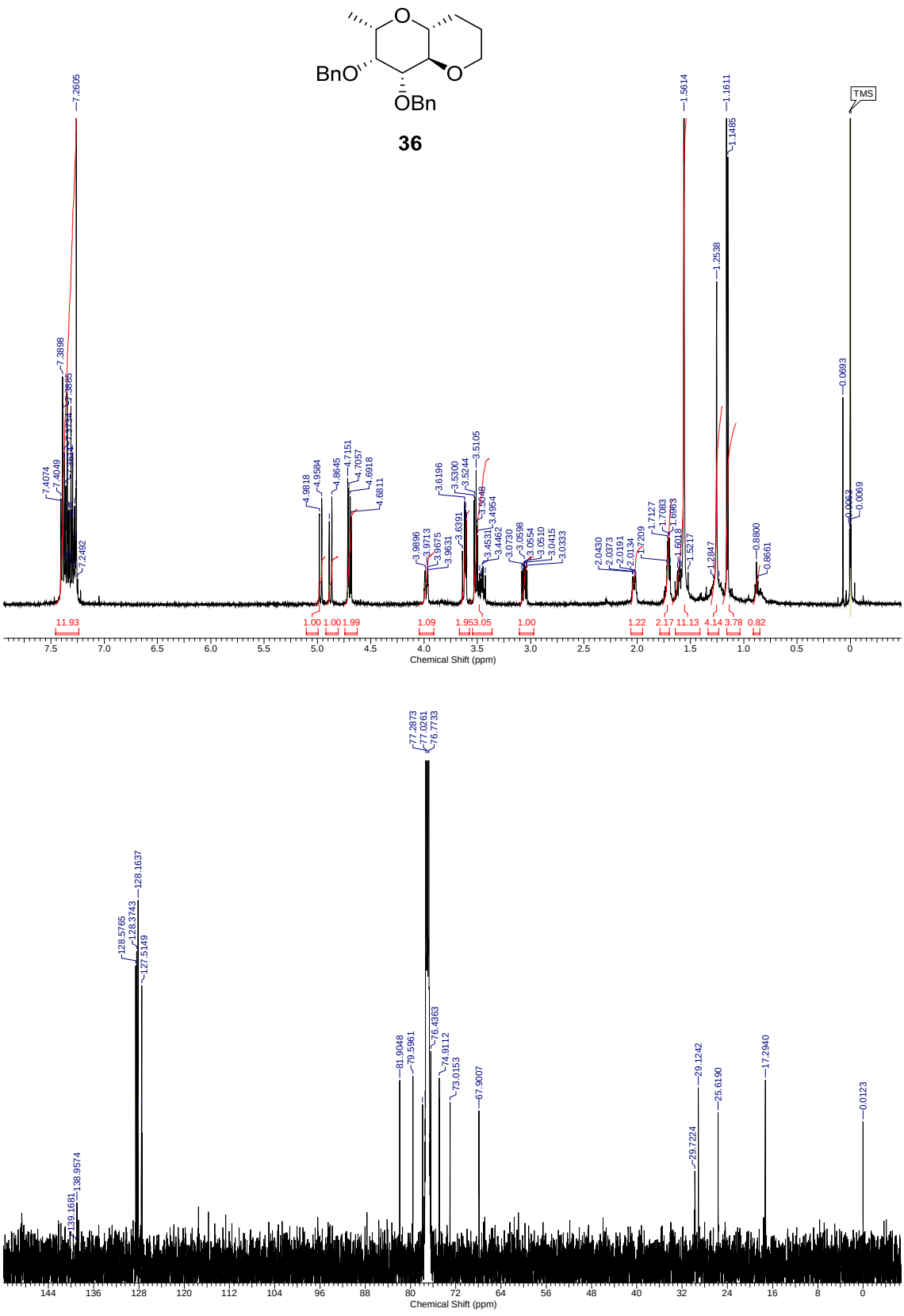

Fig. S39. ^{1}H NMR (500 MHz, $CDCl_3$) and ^{13}C{H} NMR (125.7 MHz, $CDCl_3$) of compound **36**.

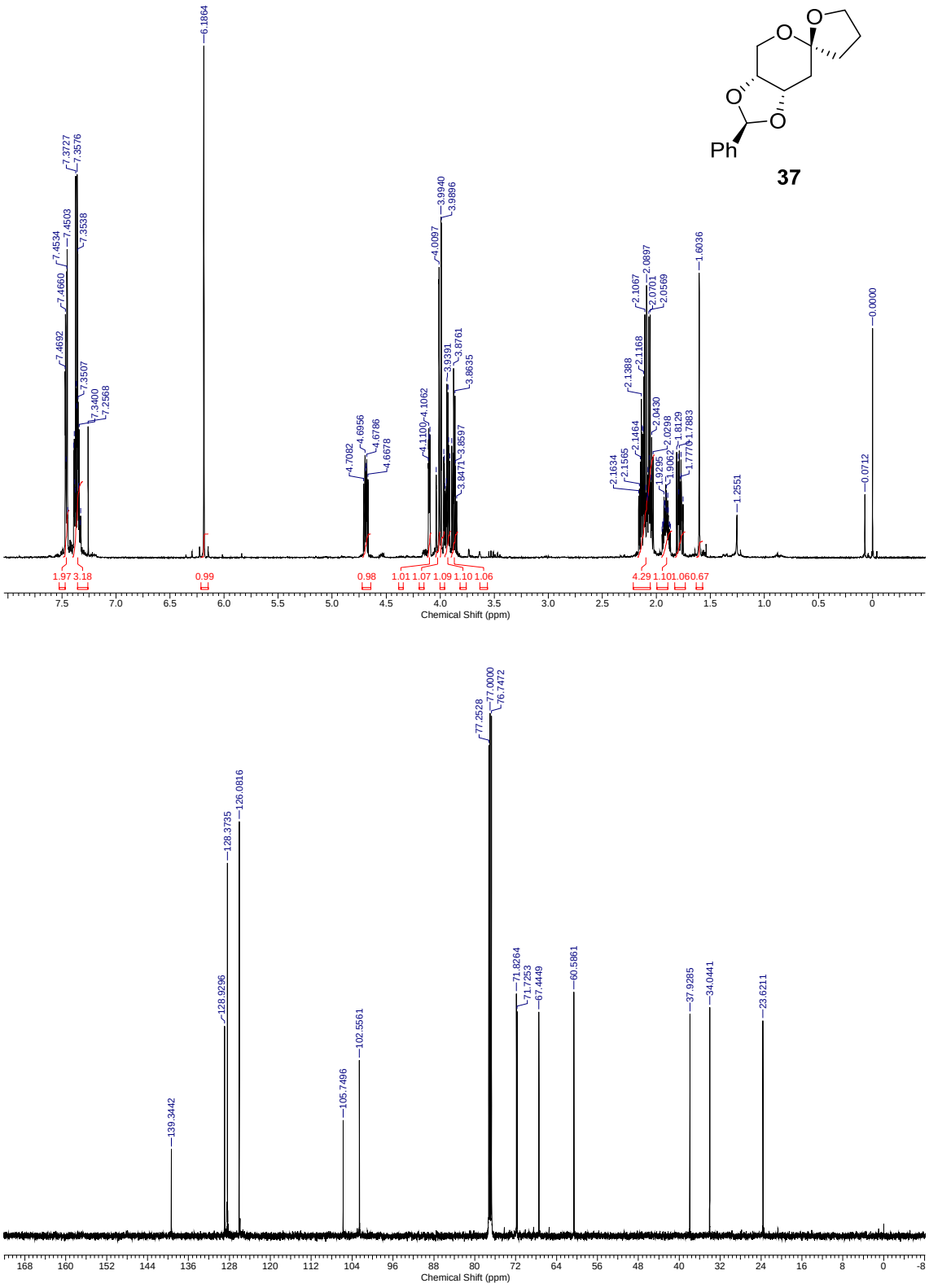

Fig. S40. ^{1}H NMR (500 MHz, $CDCl_3$) and ^{13}C{H} NMR (125.7 MHz, $CDCl_3$) of compound **37**.

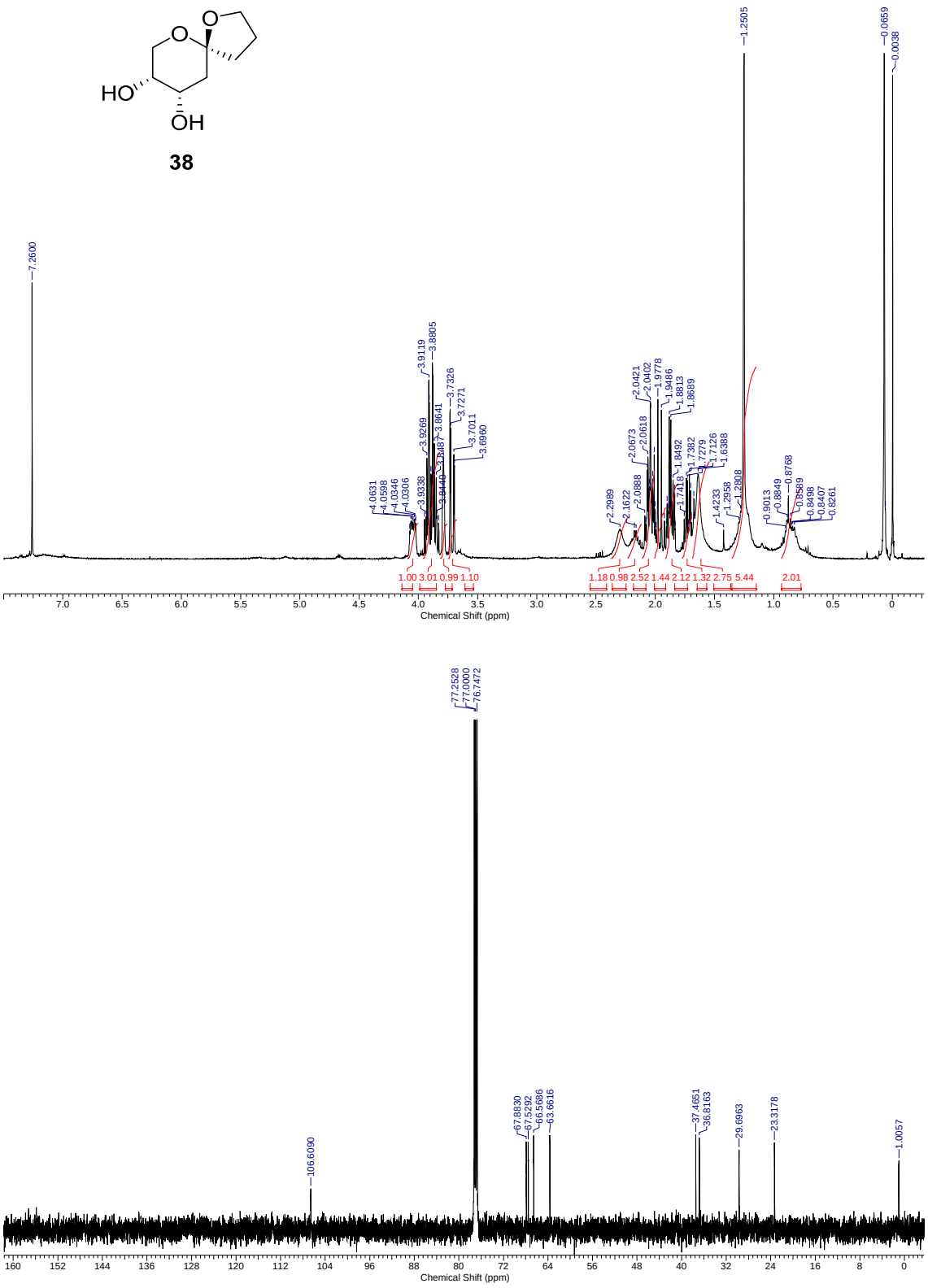

Fig. S41. ^{1}H NMR (400 MHz, $CDCl_3$) and $^{13}C\{H\}$ NMR (125.7 MHz, $CDCl_3$) of compound **38**.

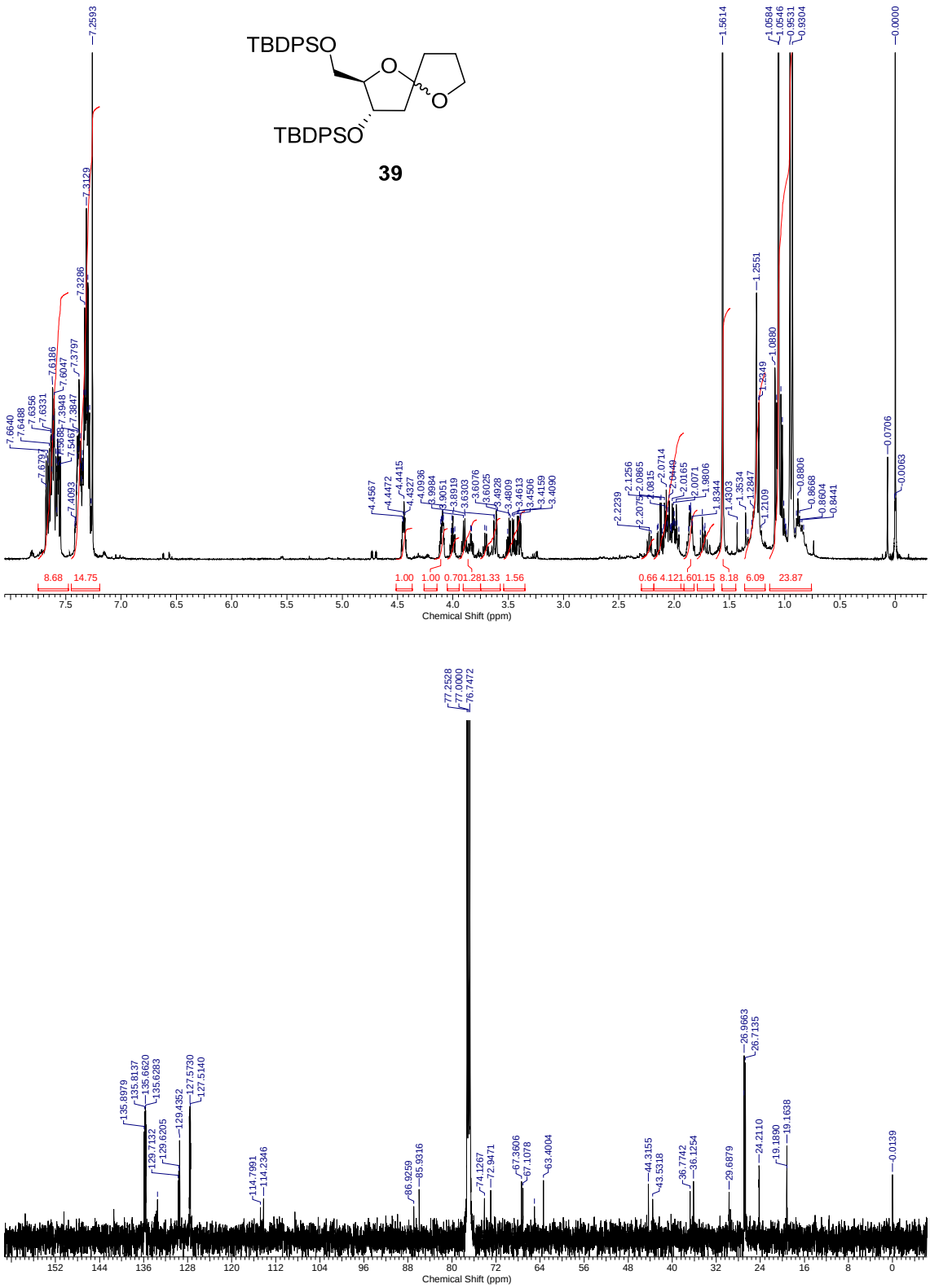

Fig. S42. ^{1}H NMR (500 MHz, $CDCl_3$) and $^{13}C\{H\}$ NMR (125.7 MHz, $CDCl_3$) of compound **39**.

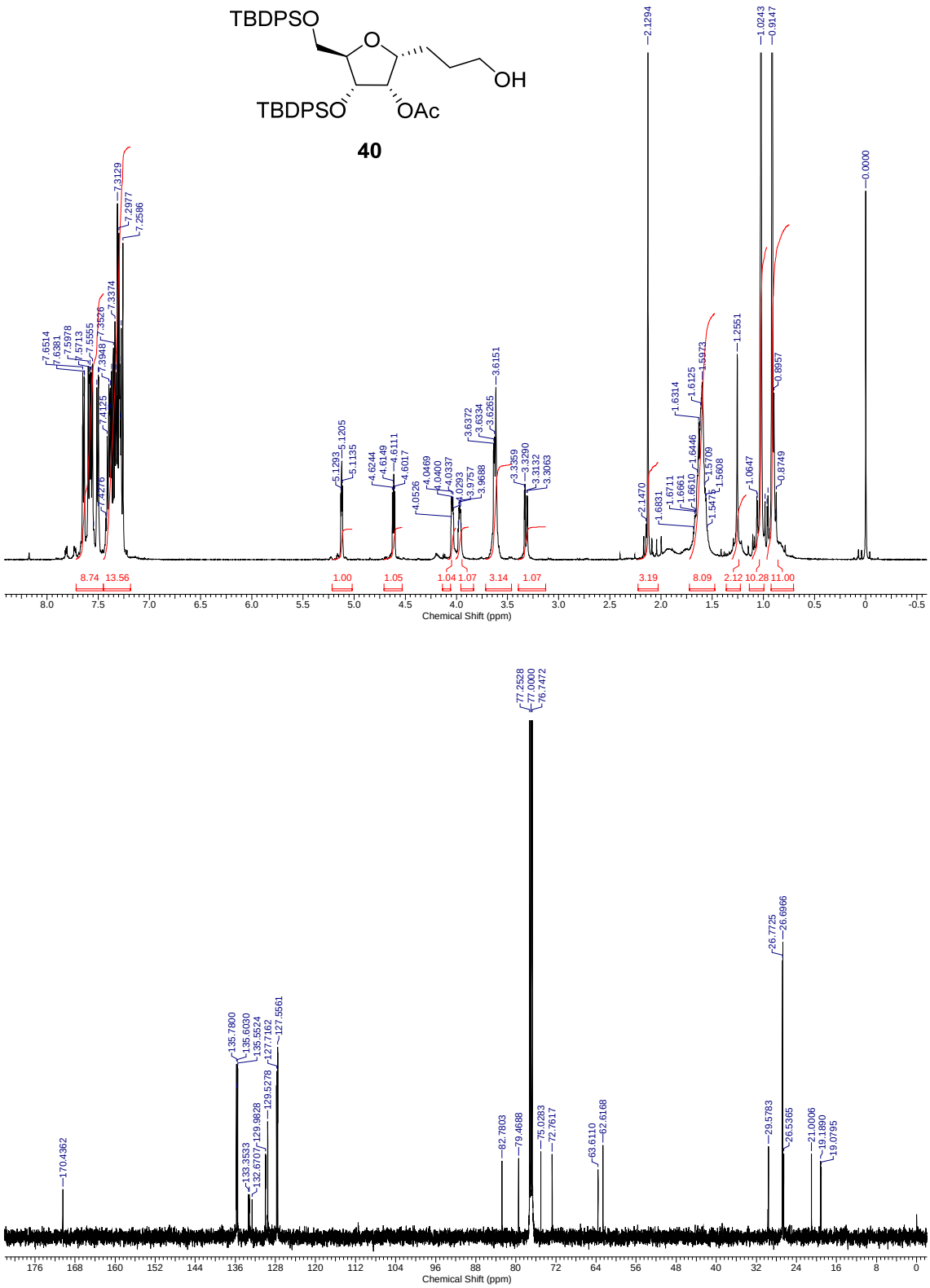

Fig. S43. ^{1}H NMR (500 MHz, $CDCl_3$) and $^{13}C\{H\}$ NMR (125.7 MHz, $CDCl_3$) of compound **40**.

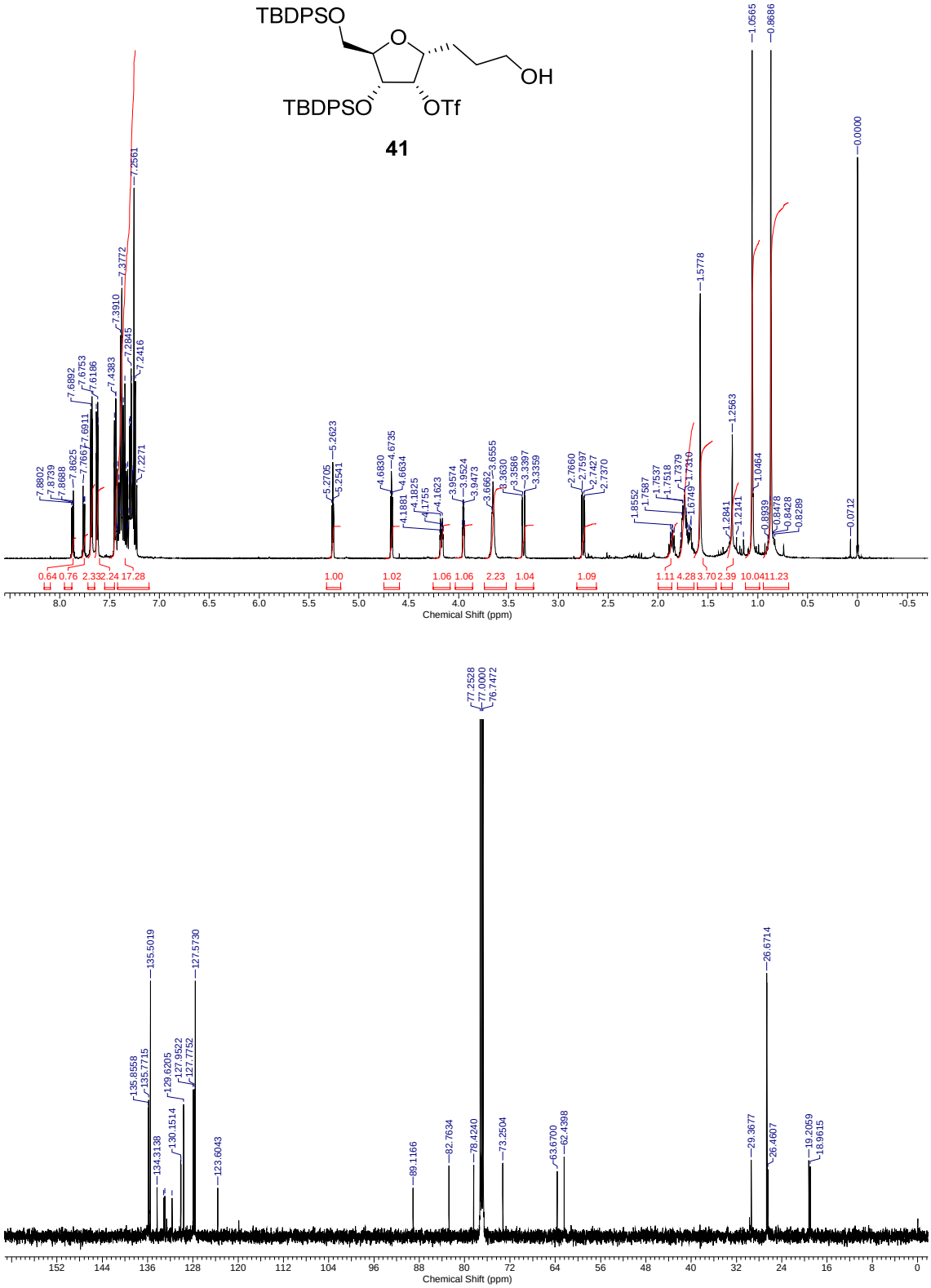

Fig. S44. ^{1}H NMR (500 MHz, $CDCl_3$) and $^{13}C\{H\}$ NMR (125.7 MHz, $CDCl_3$) of compound **41**.

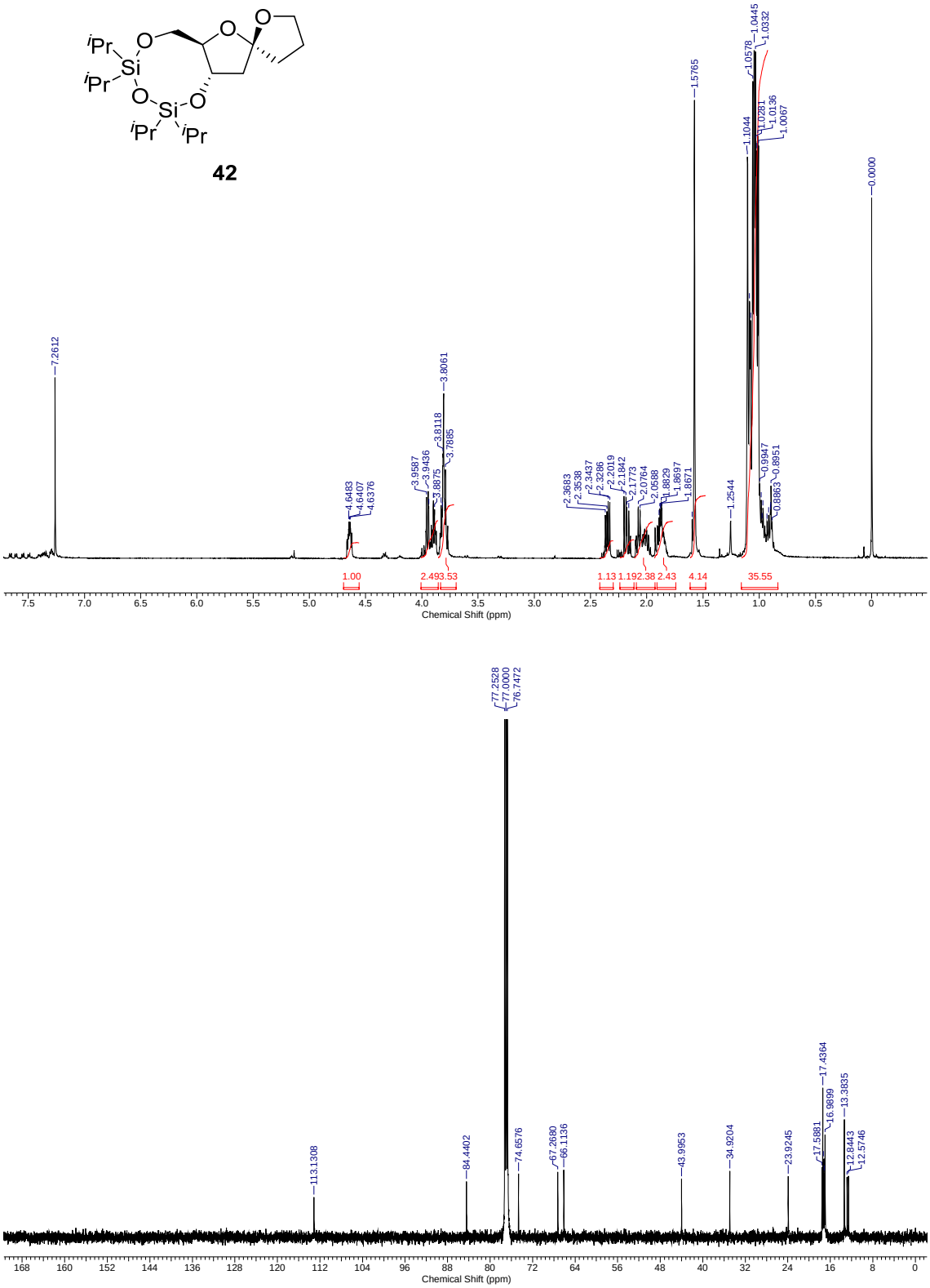

Fig. S45. ^{1}H NMR (500 MHz, $CDCl_3$) and $^{13}C\{H\}$ NMR (125.7 MHz, $CDCl_3$) of compound **42**.

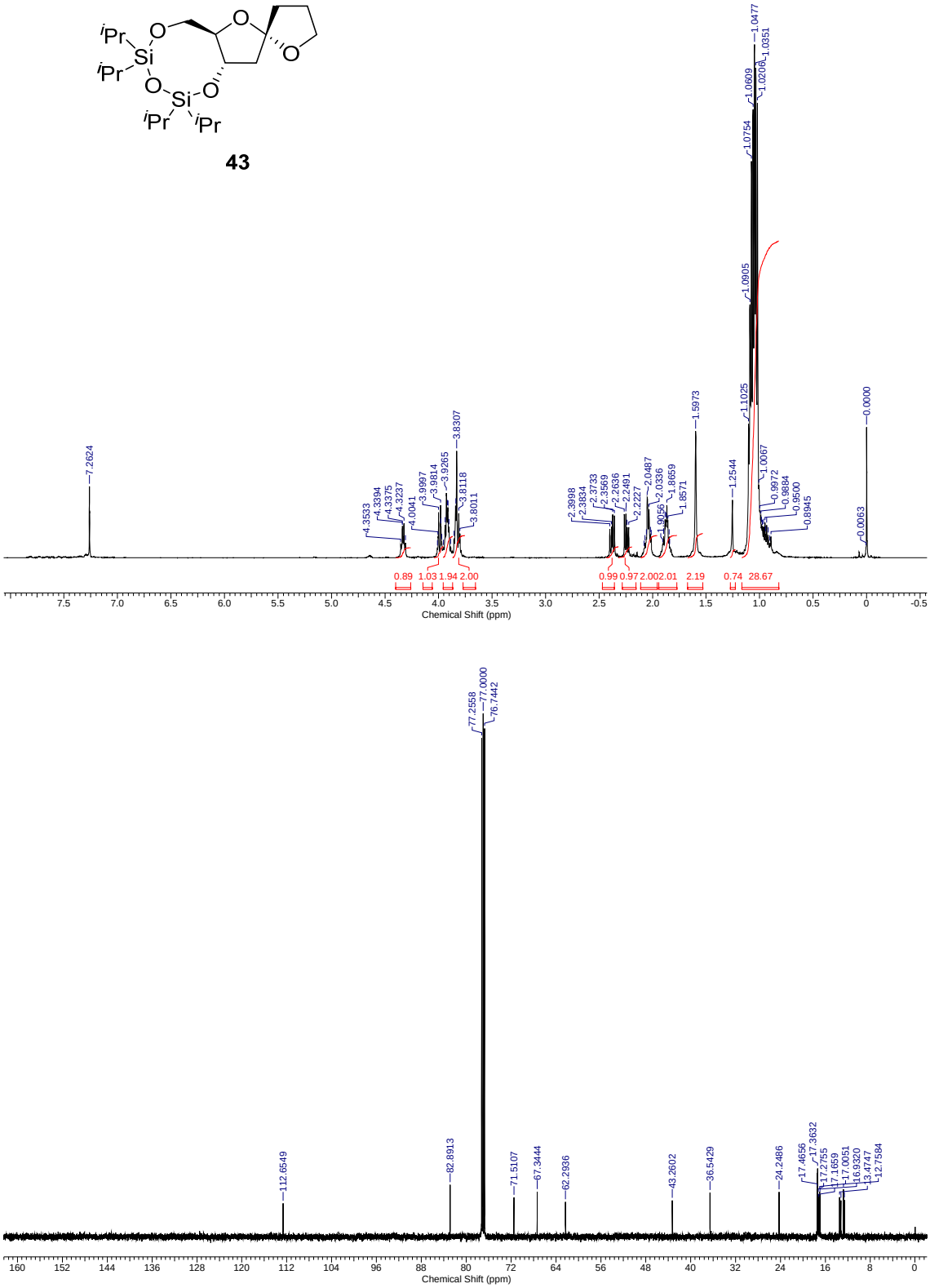

Fig. S46. ^{1}H NMR (500 MHz, $CDCl_3$) and $^{13}C\{H\}$ NMR (125.7 MHz, $CDCl_3$) of compound **43**.

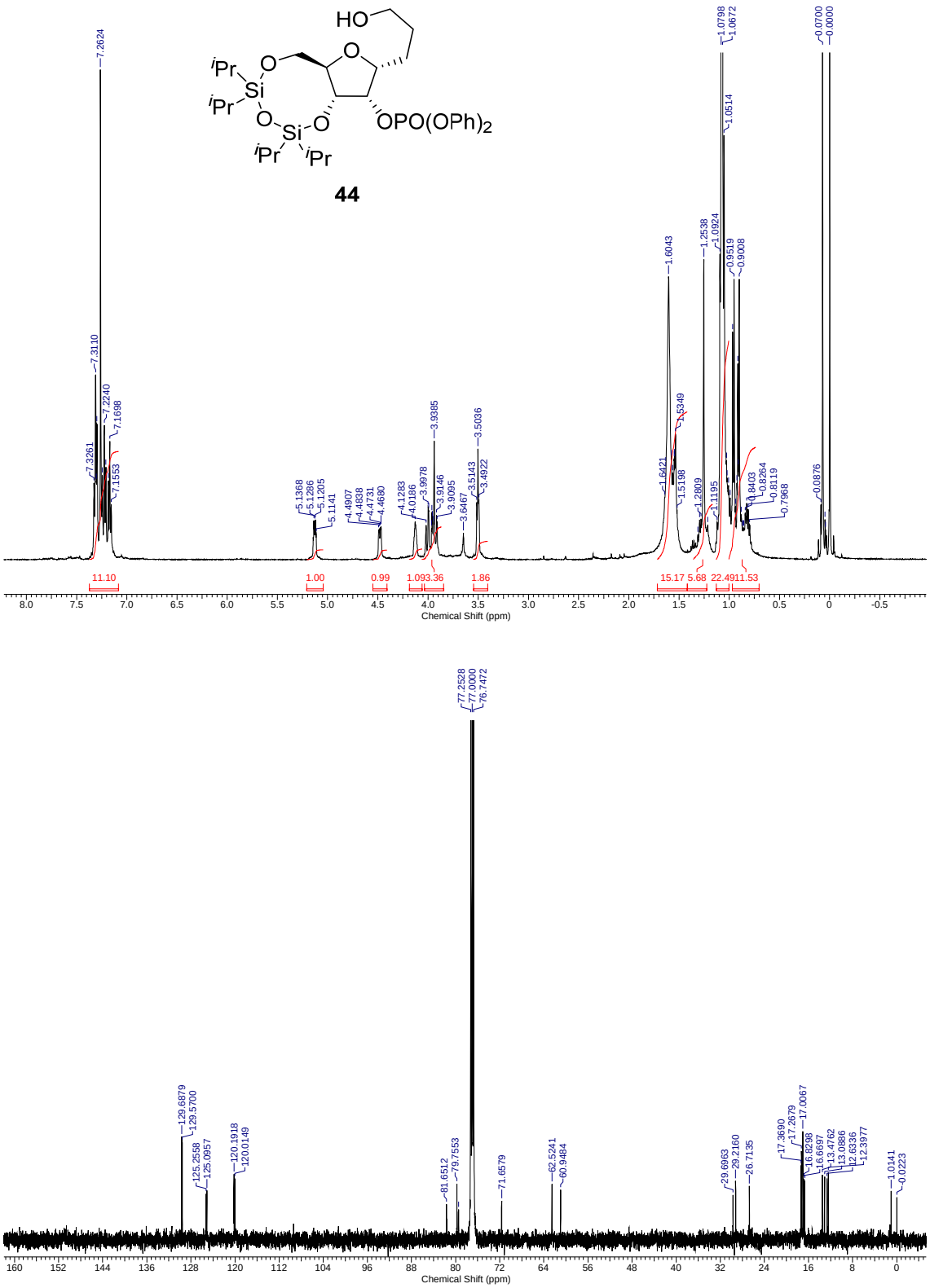

Fig. S47. ^{1}H NMR (500 MHz, $CDCl_3$) and $^{13}C\{H\}$ NMR (125.7 MHz, $CDCl_3$) of compound **44**.

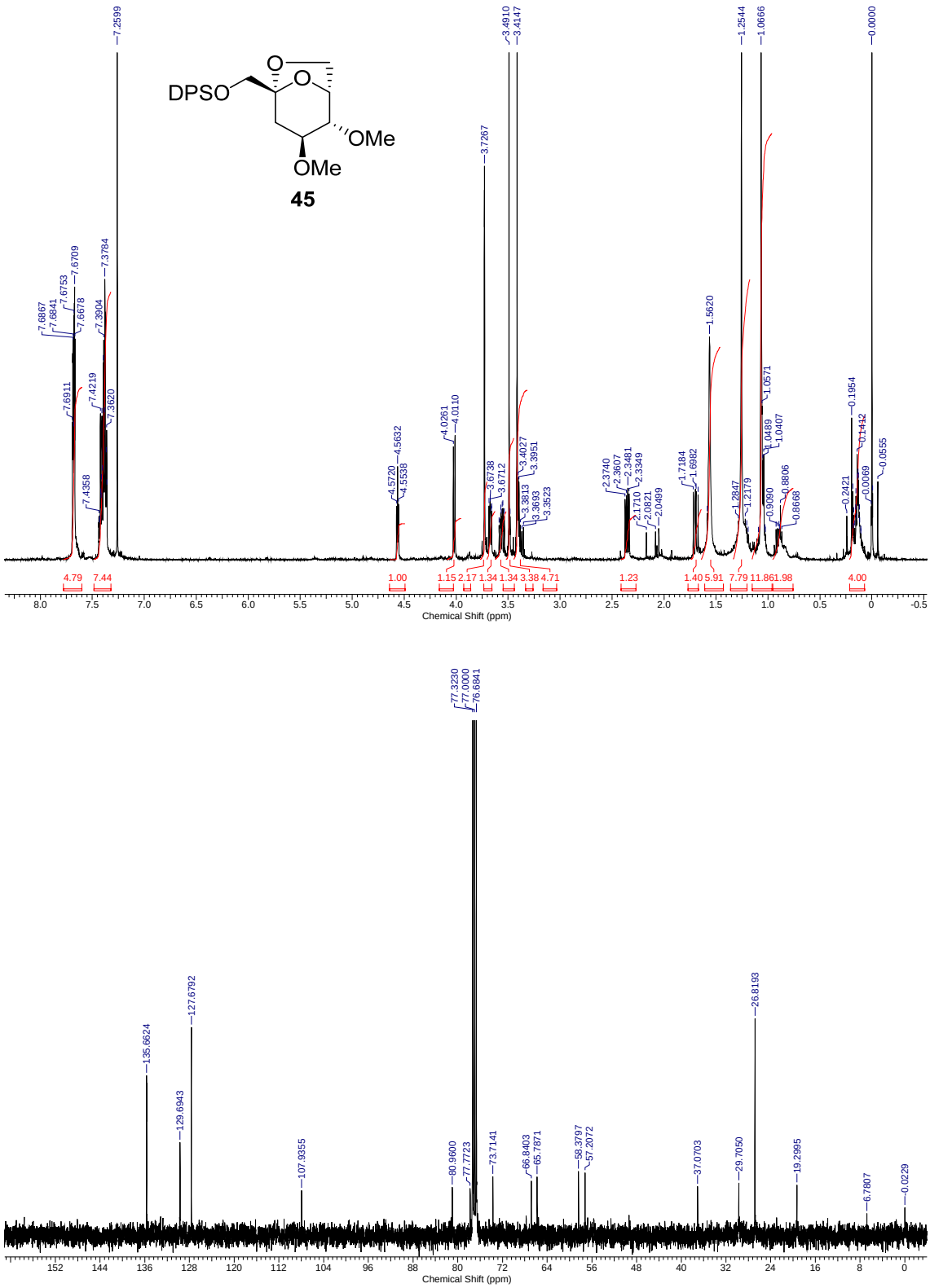

Fig. S48. ^{1}H NMR (500 MHz, $CDCl_3$) and $^{13}C\{H\}$ NMR (100.6 MHz, $CDCl_3$) of compound **45**.

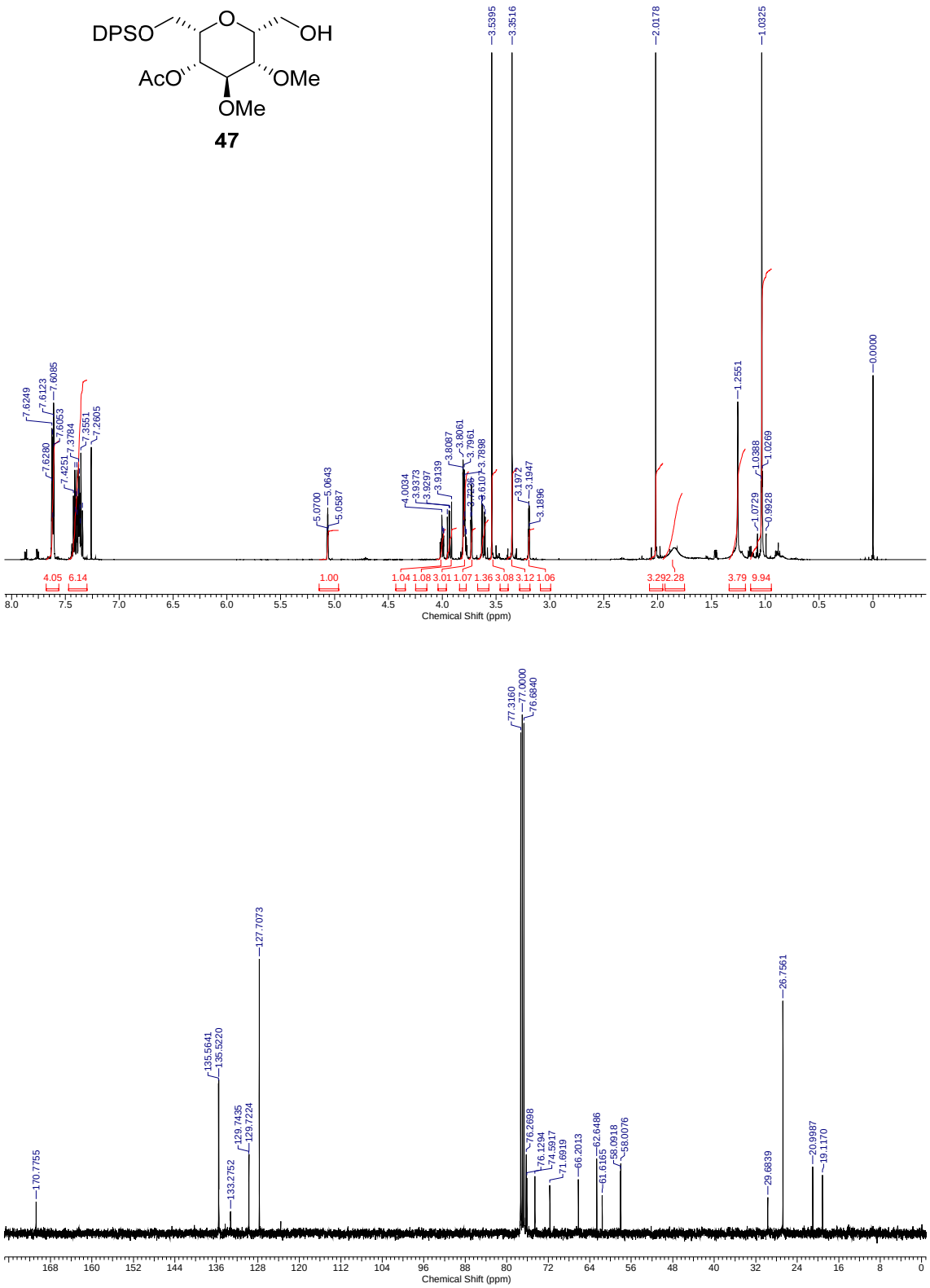

Fig. S49. ^{1}H NMR (500 MHz, $CDCl_3$) and $^{13}C\{H\}$ NMR (100.6 MHz, $CDCl_3$) of compound **47**.

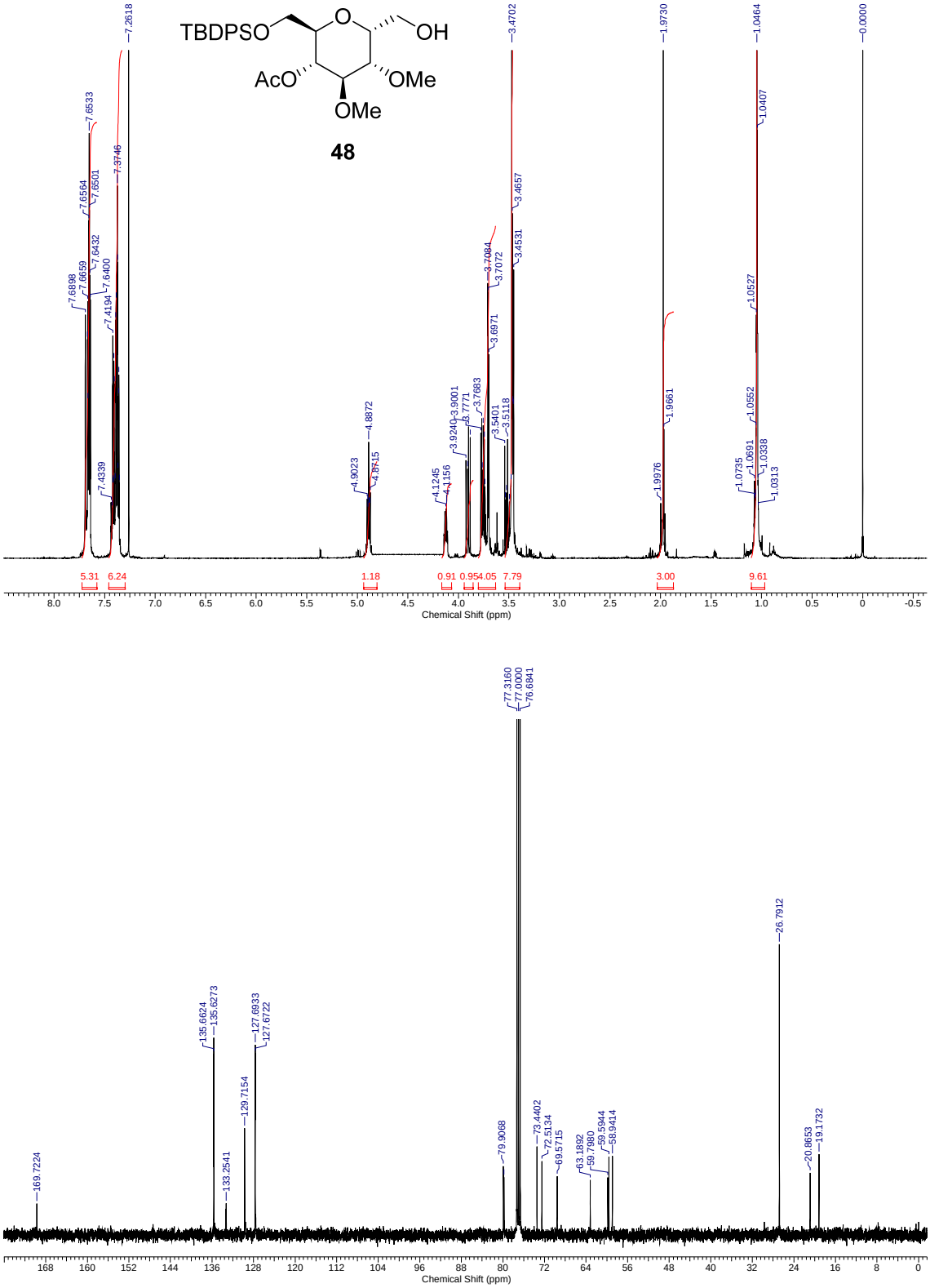

Fig. S50. ^{1}H NMR (500 MHz, $CDCl_3$) and $^{13}C\{H\}$ NMR (100.6 MHz, $CDCl_3$) of compound **48**.

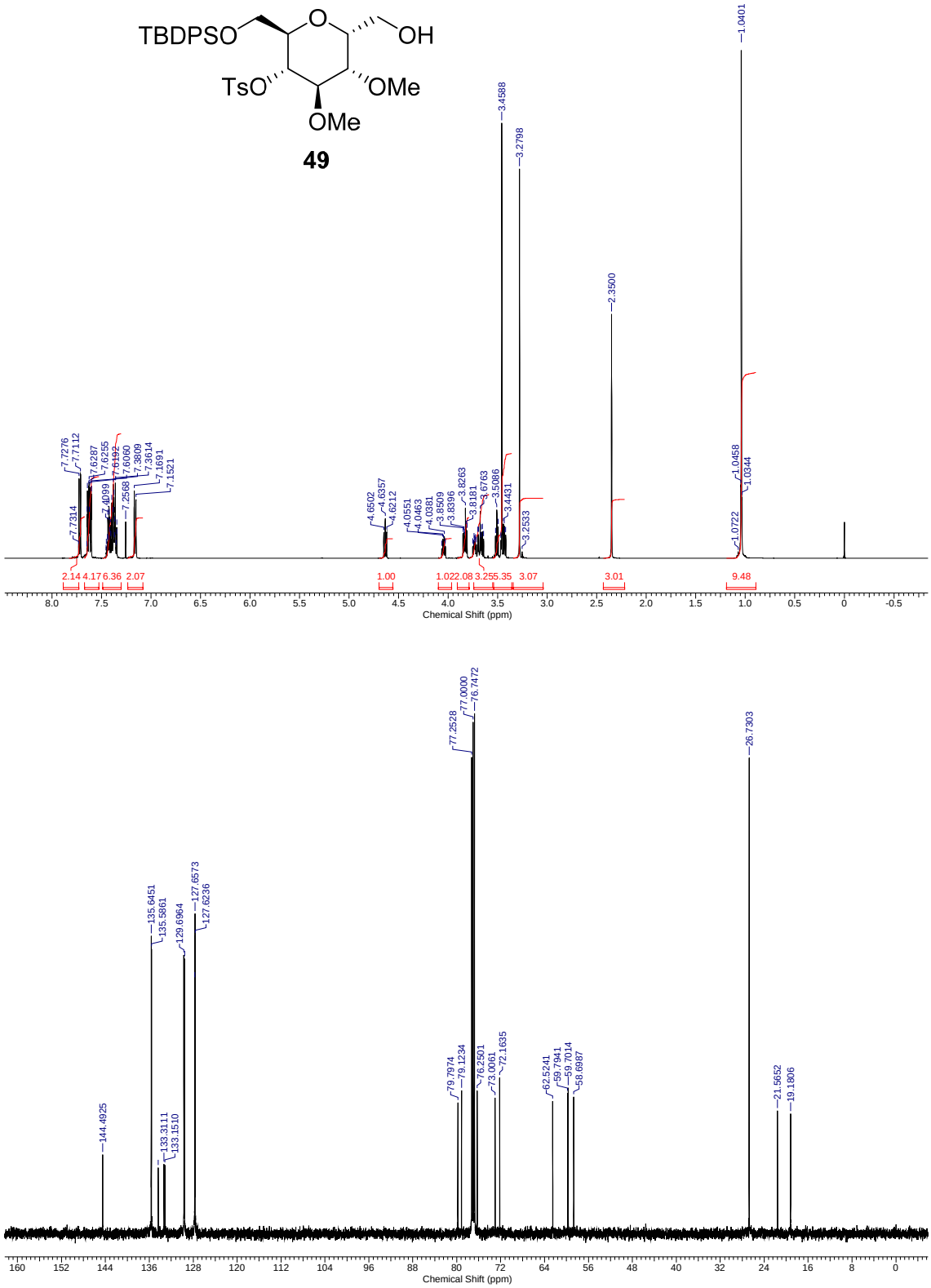

Fig. S51. ^{1}H NMR (500 MHz, $CDCl_3$) and $^{13}C\{H\}$ NMR (100.6 MHz, $CDCl_3$) of compound **49**.

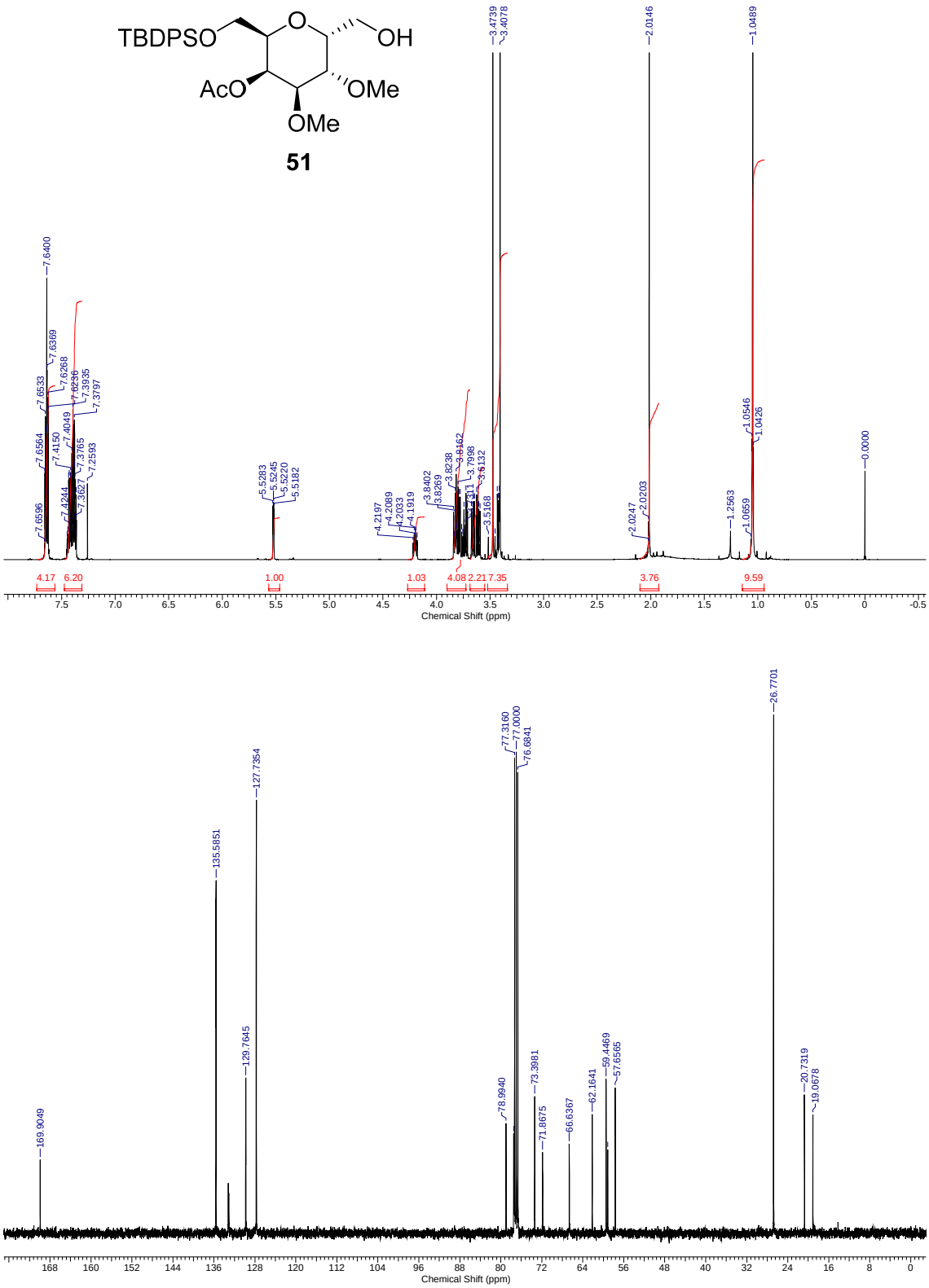

Fig. S52. ^{1}H NMR (500 MHz, $CDCl_3$) and $^{13}C\{H\}$ NMR (100.6 MHz, $CDCl_3$) of compound **51**.

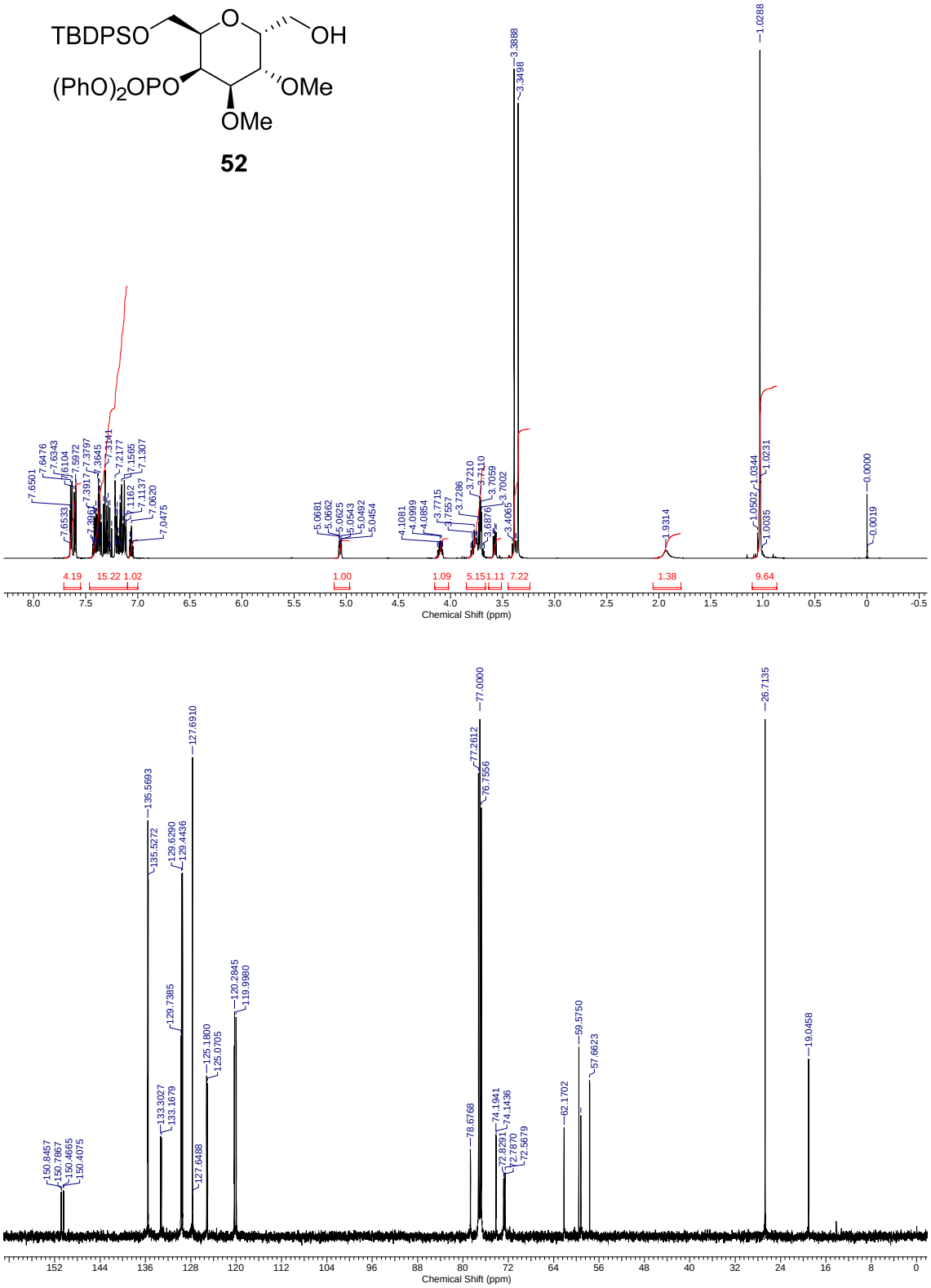

Fig. S53. ^{1}H NMR (500 MHz, $CDCl_3$) and $^{13}C\{H\}$ NMR (125.7 MHz, $CDCl_3$) of compound **52**.

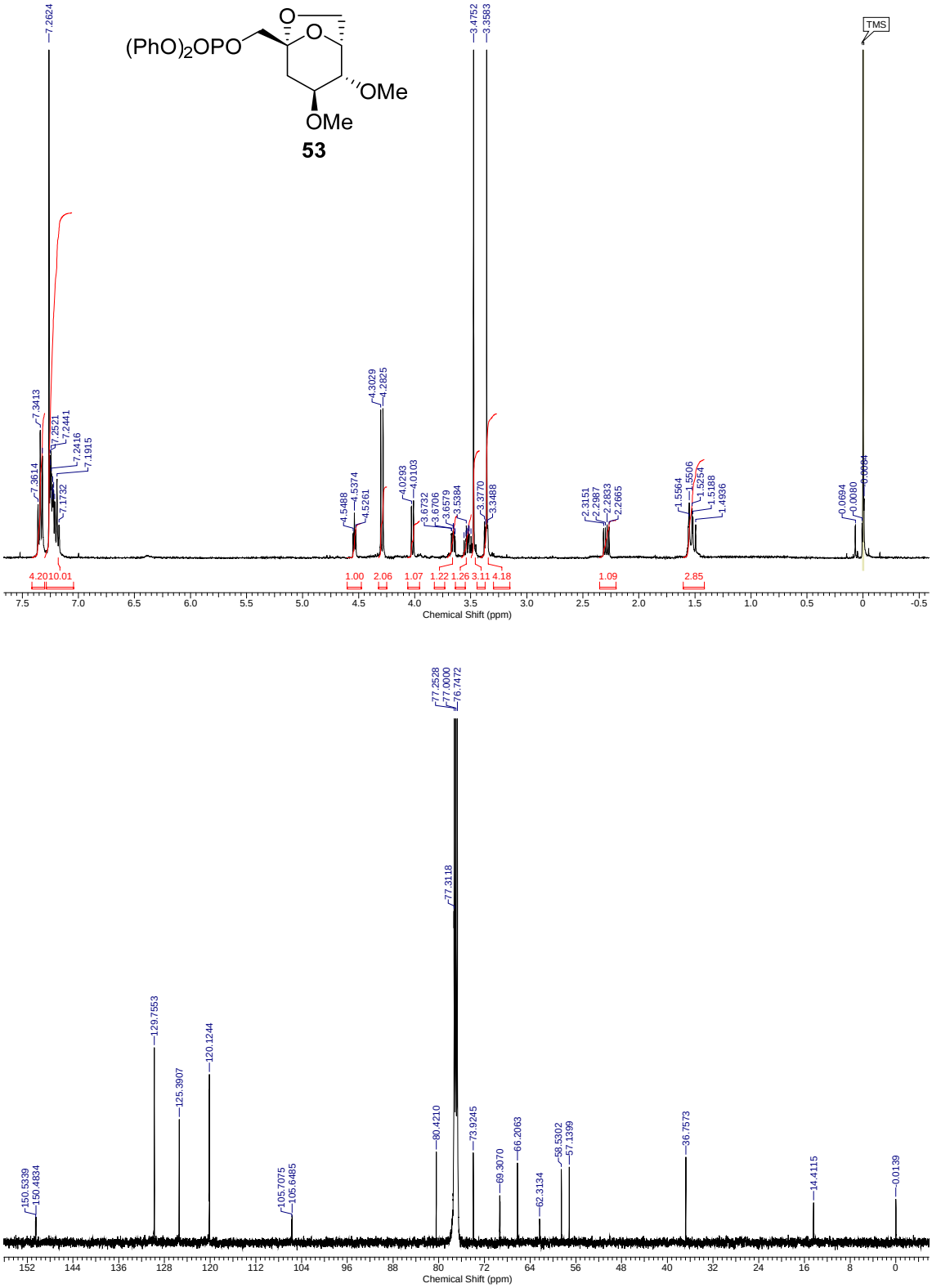

Fig. S54. ^{1}H NMR (500 MHz, $CDCl_3$) and $^{13}C\{H\}$ NMR (125.7 MHz, $CDCl_3$) of compound **53**.

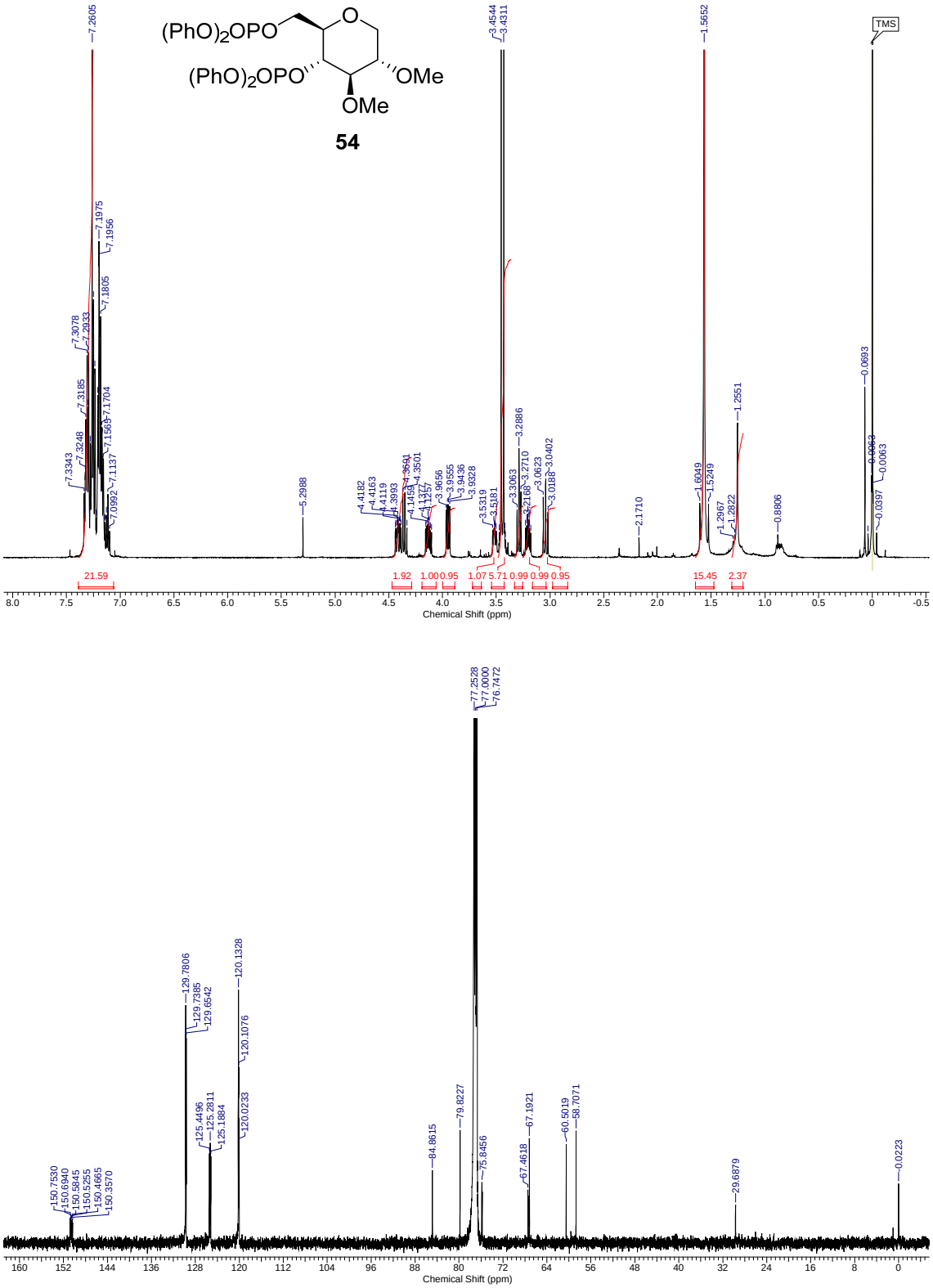

Fig. S55. ^{1}H NMR (500 MHz, $CDCl_3$) and $^{13}C\{H\}$ NMR (125.7 MHz, $CDCl_3$) of compound **54**.

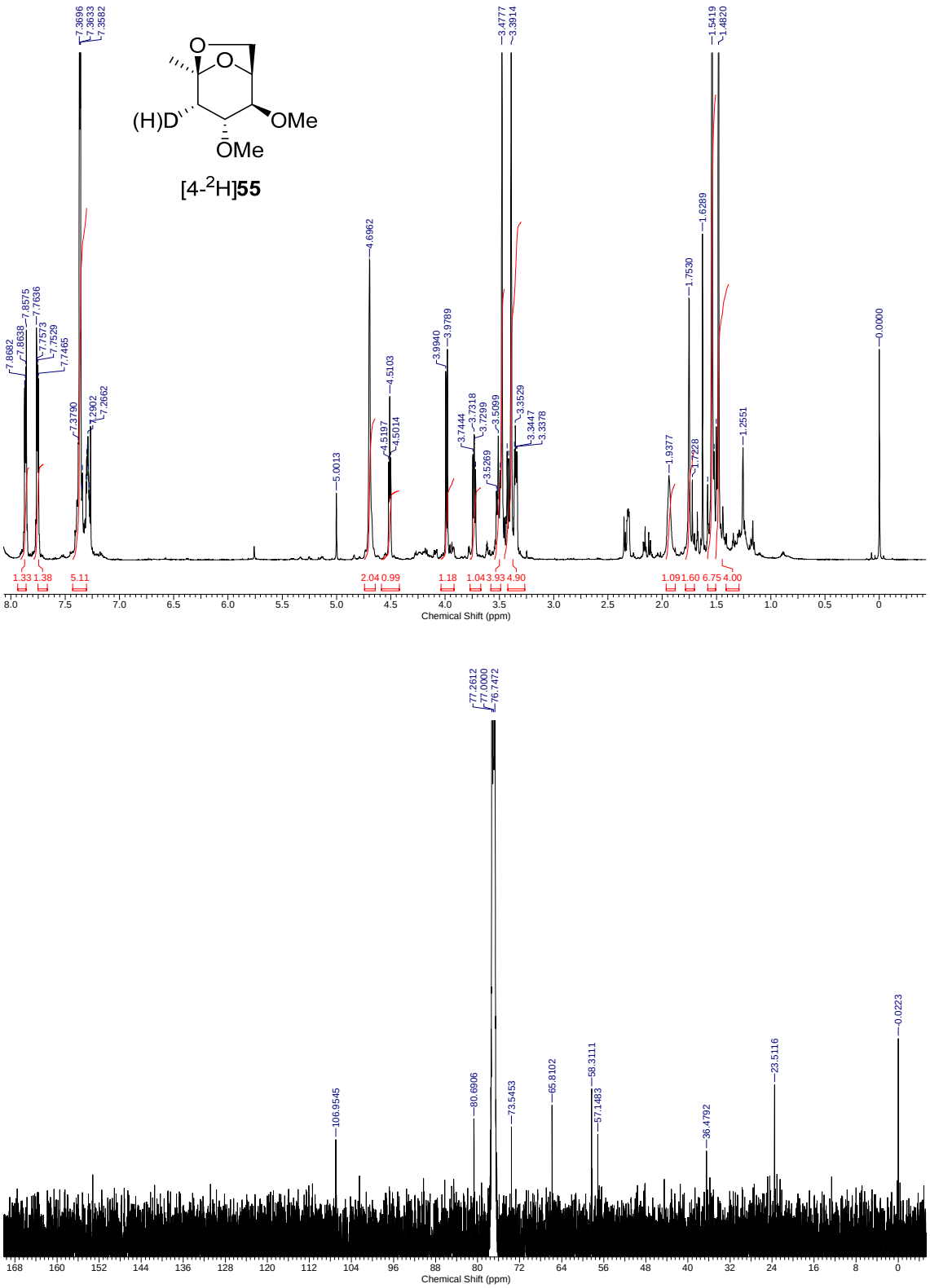

Fig. S56. ^{1}H NMR (500 MHz, $CDCl_3$) and $^{13}C\{H\}$ NMR (125.7 MHz, $CDCl_3$) of compound [4-^{2}H]**55**.

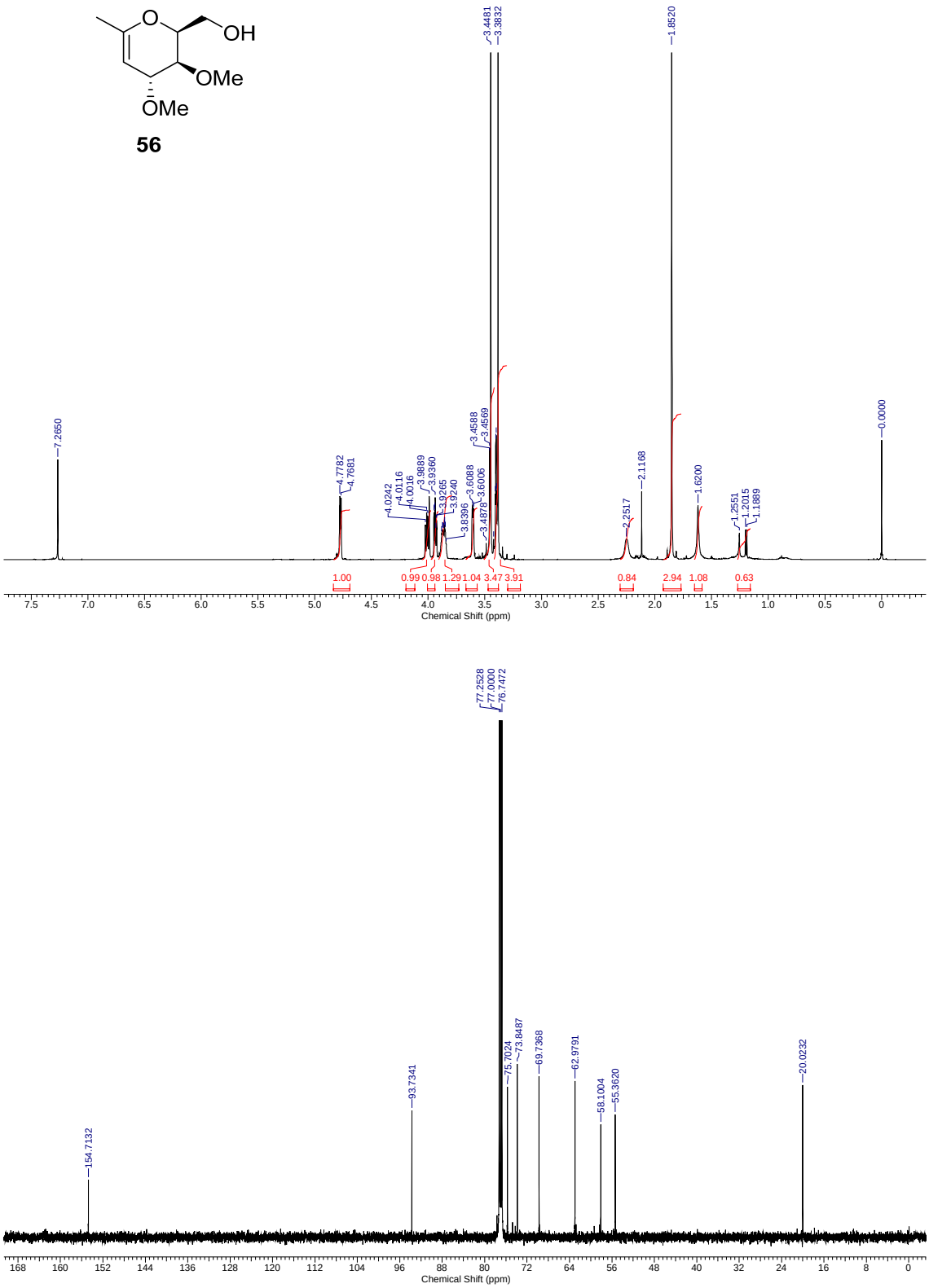

Fig. S57. ^{1}H NMR (500 MHz, $CDCl_3$) and $^{13}C\{H\}$ NMR (125.7 MHz, $CDCl_3$) of compound **56**.

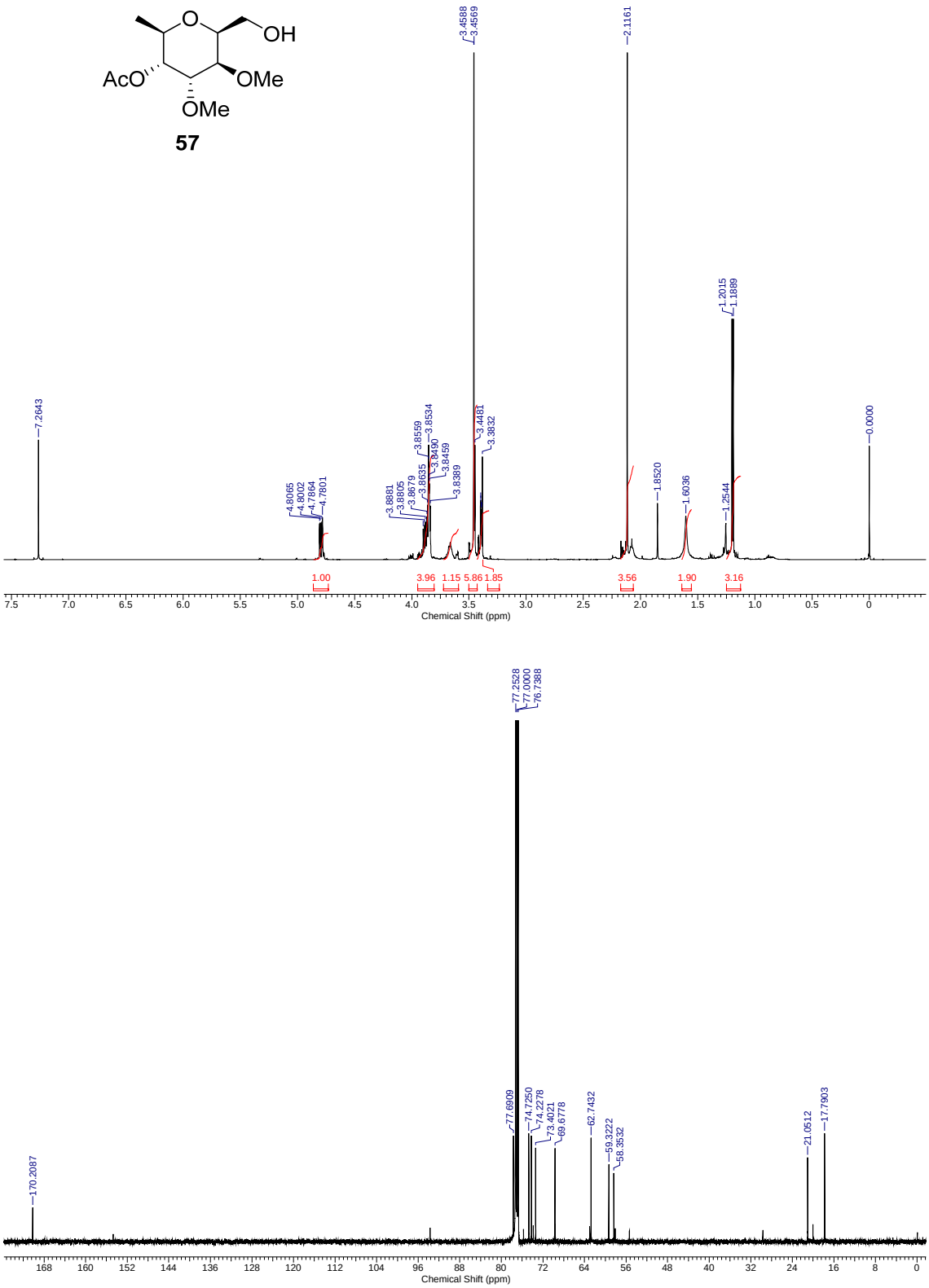

Fig. S58. ^{1}H NMR (500 MHz, $CDCl_3$) and $^{13}C\{H\}$ NMR (125.7 MHz, $CDCl_3$) of compound **57**.

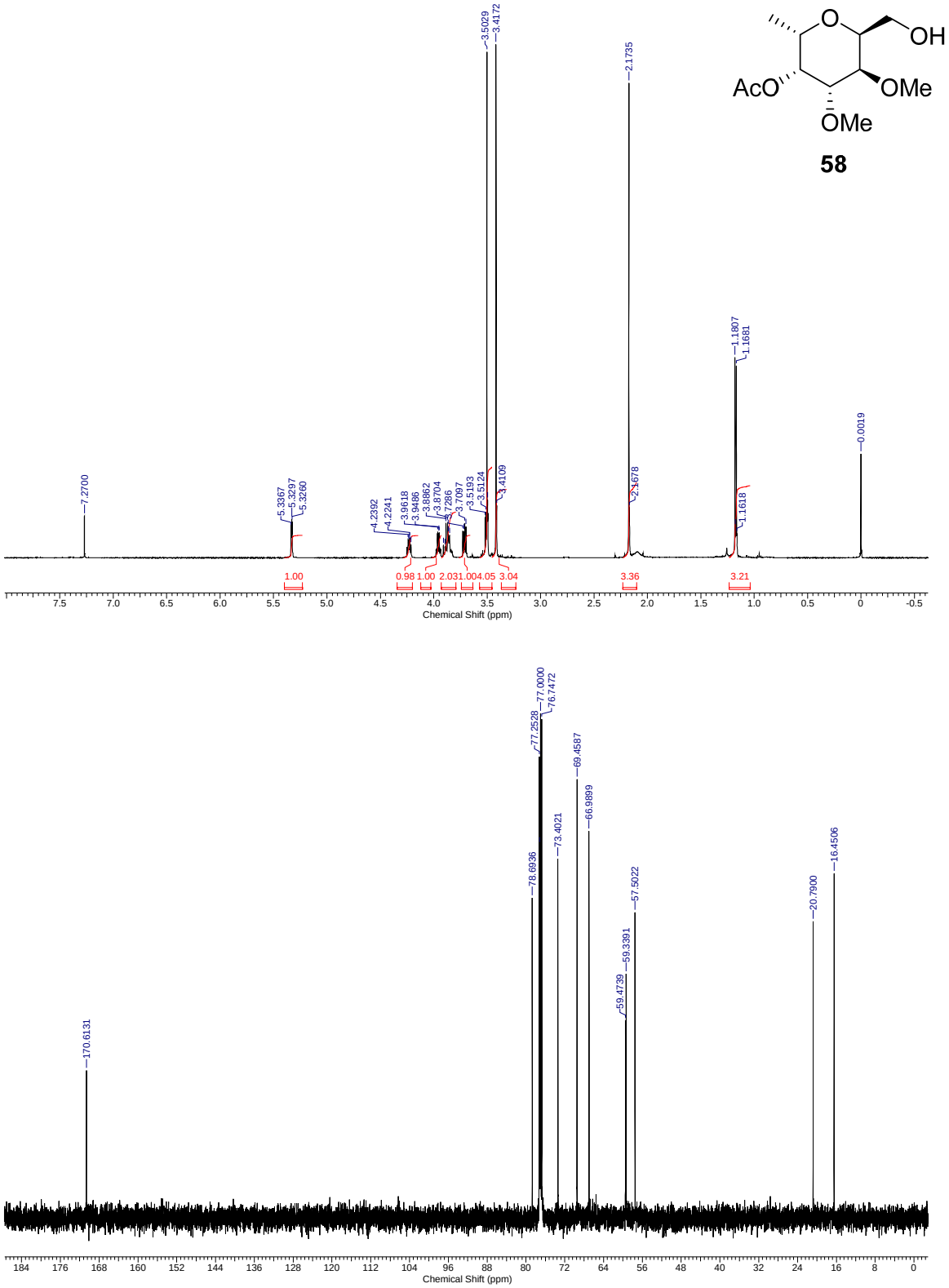

Fig. S59. ^{1}H NMR (500 MHz, $CDCl_3$) and $^{13}C\{H\}$ NMR (125.7 MHz, $CDCl_3$) of compound **58**.

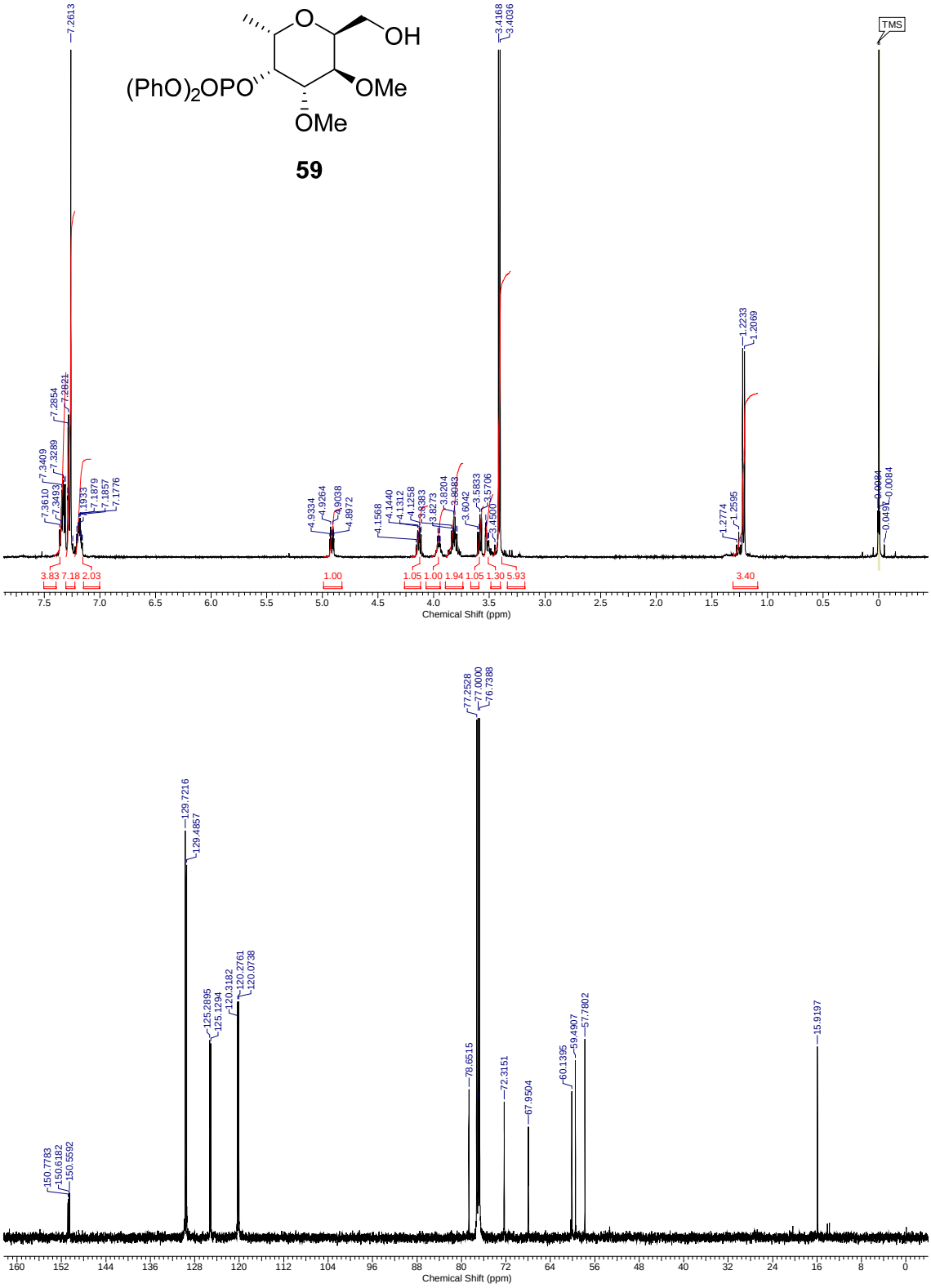

Fig. S60. ^{1}H NMR (400 MHz, $CDCl_3$) and $^{13}C\{H\}$ NMR (125.7 MHz, $CDCl_3$) of compound **59**.

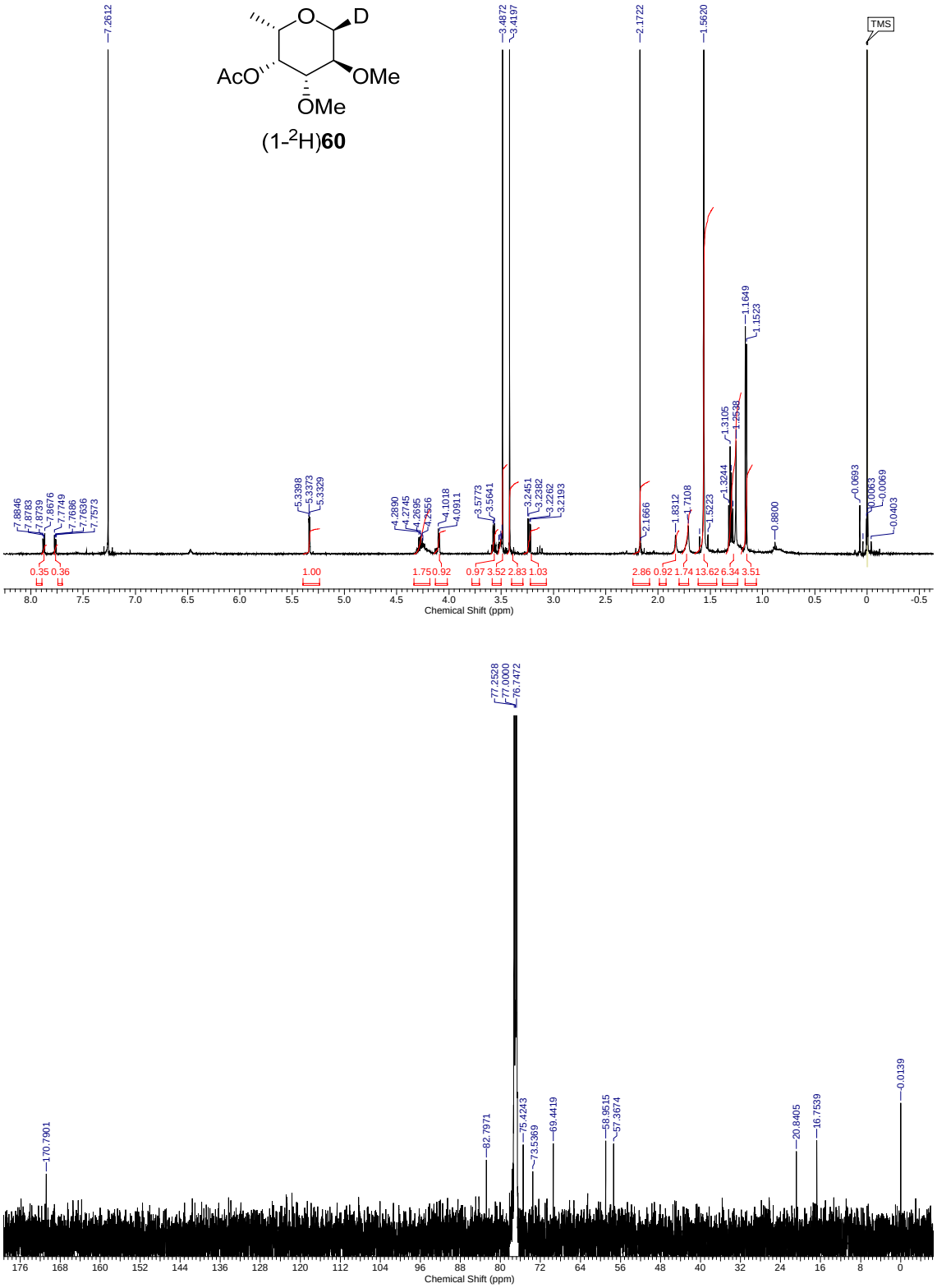

Fig. S61. ^{1}H NMR (500 MHz, $CDCl_3$) and $^{13}C\{H\}$ NMR (125.7 MHz, $CDCl_3$) of compound (1-^{2}H)**60**.

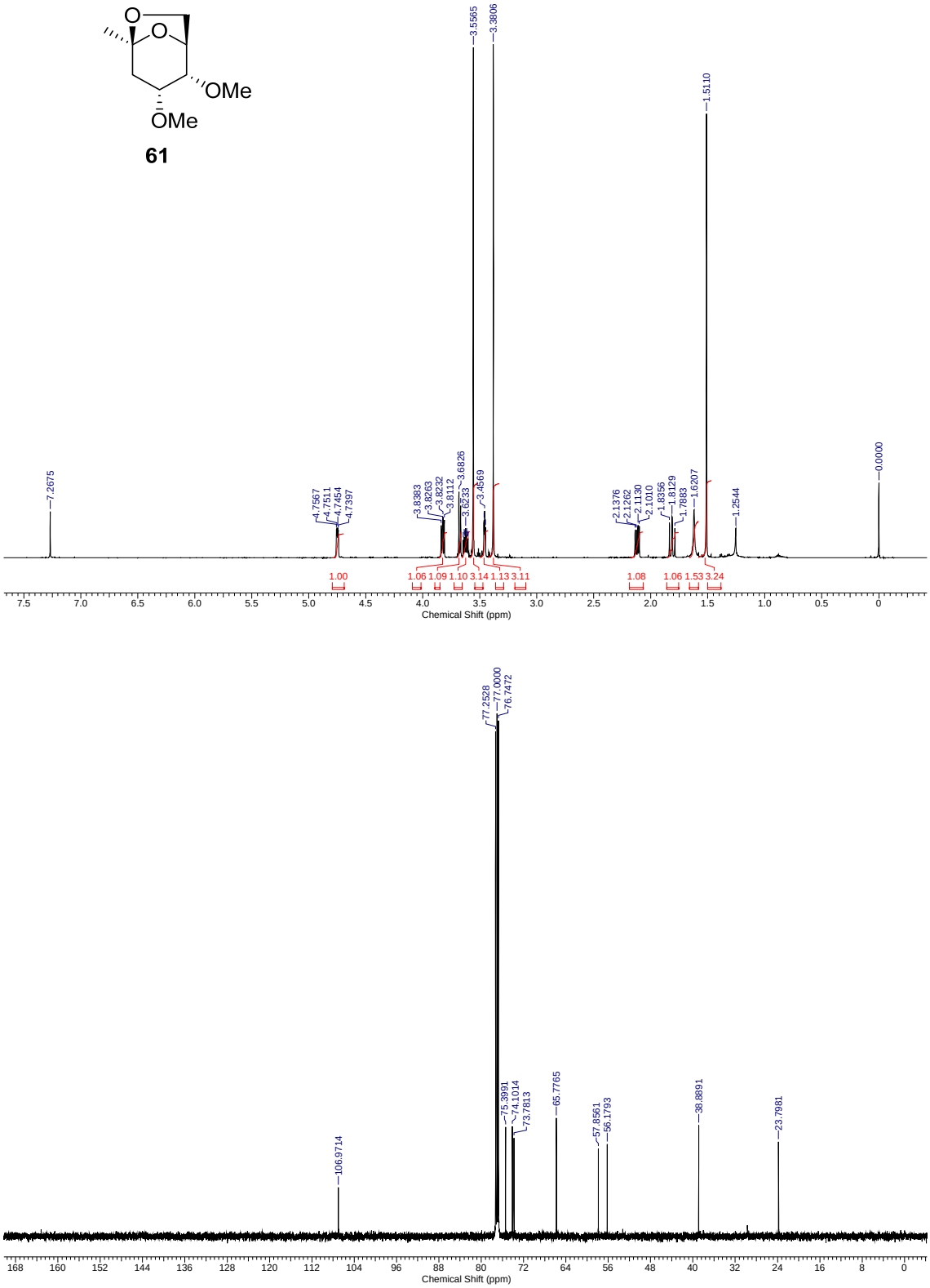

Fig. S62. ^{1}H NMR (500 MHz, $CDCl_3$) and $^{13}C\{H\}$ NMR (125.7 MHz, $CDCl_3$) of compound **61**.

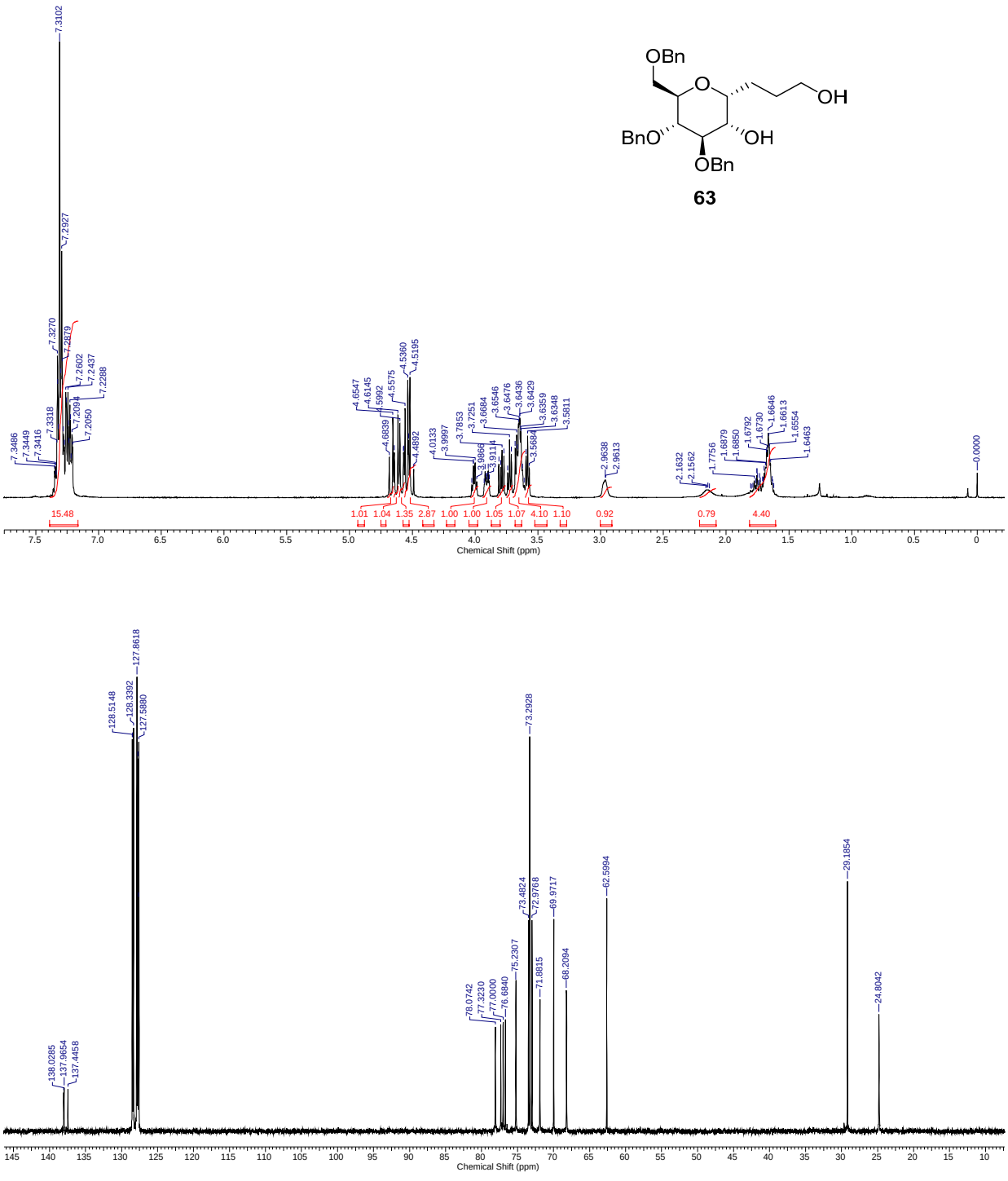

Fig. S63. ^{1}H NMR (400 MHz, $CDCl_3$) and ^{13}C{H} NMR (100.6 MHz, $CDCl_3$) of compound **63**.

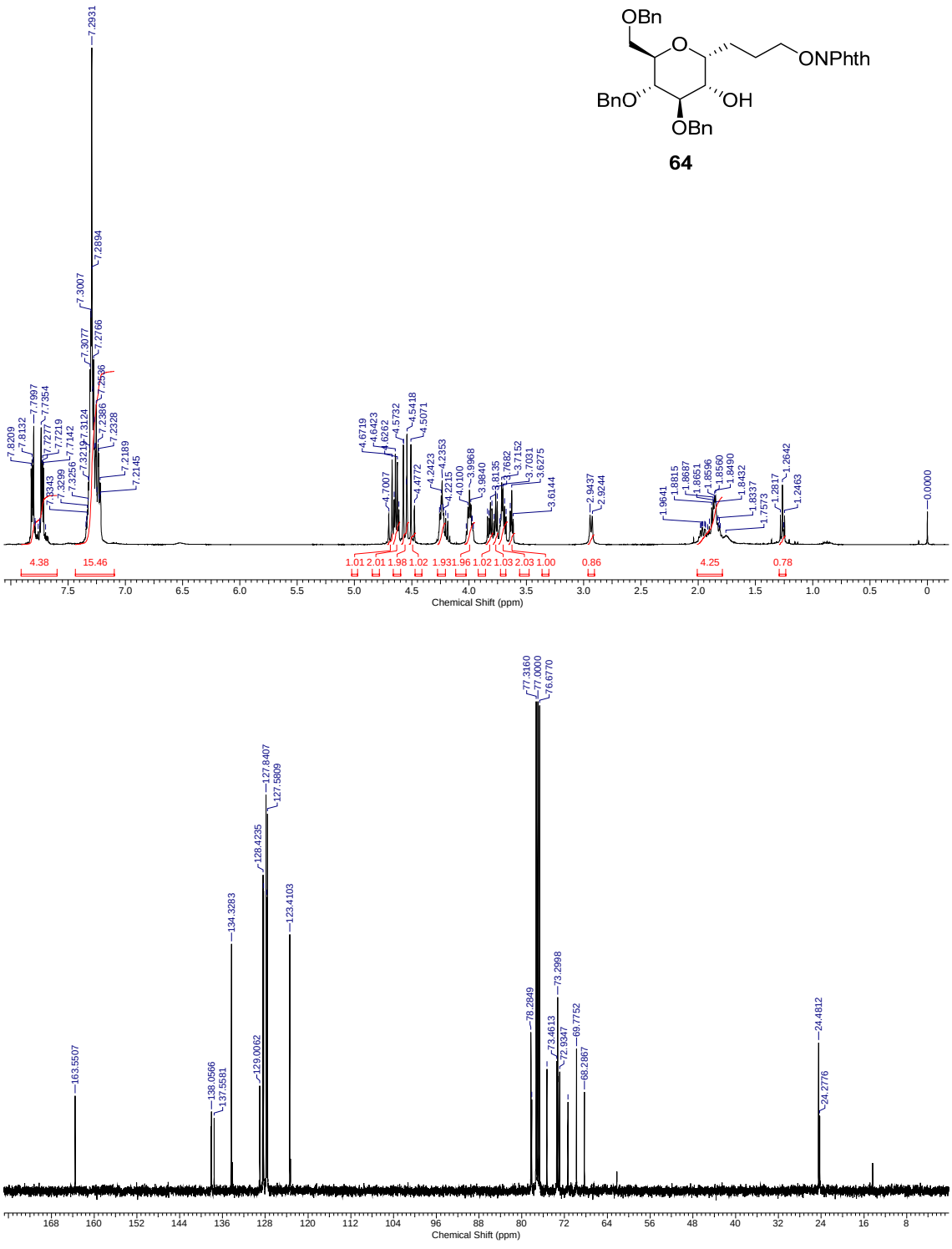

Fig. S64. ^{1}H NMR (400 MHz, $CDCl_3$) and ^{13}C{H} NMR (100.6 MHz, $CDCl_3$) of compound **64**.

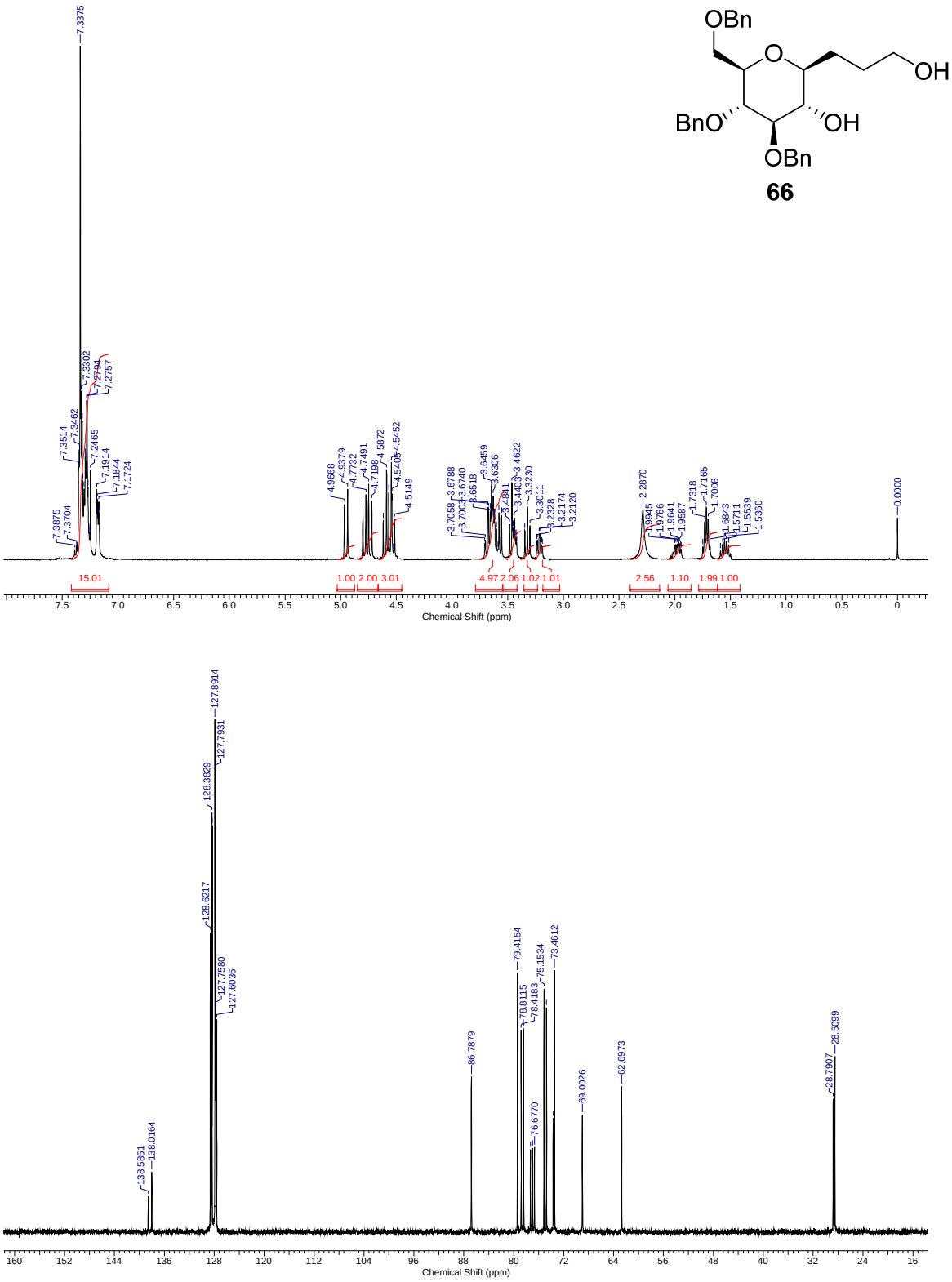

Fig. S65. ^{1}H NMR (400 MHz, $CDCl_3$) and $^{13}C\{H\}$ NMR (100.6 MHz, $CDCl_3$) of compound **66**.

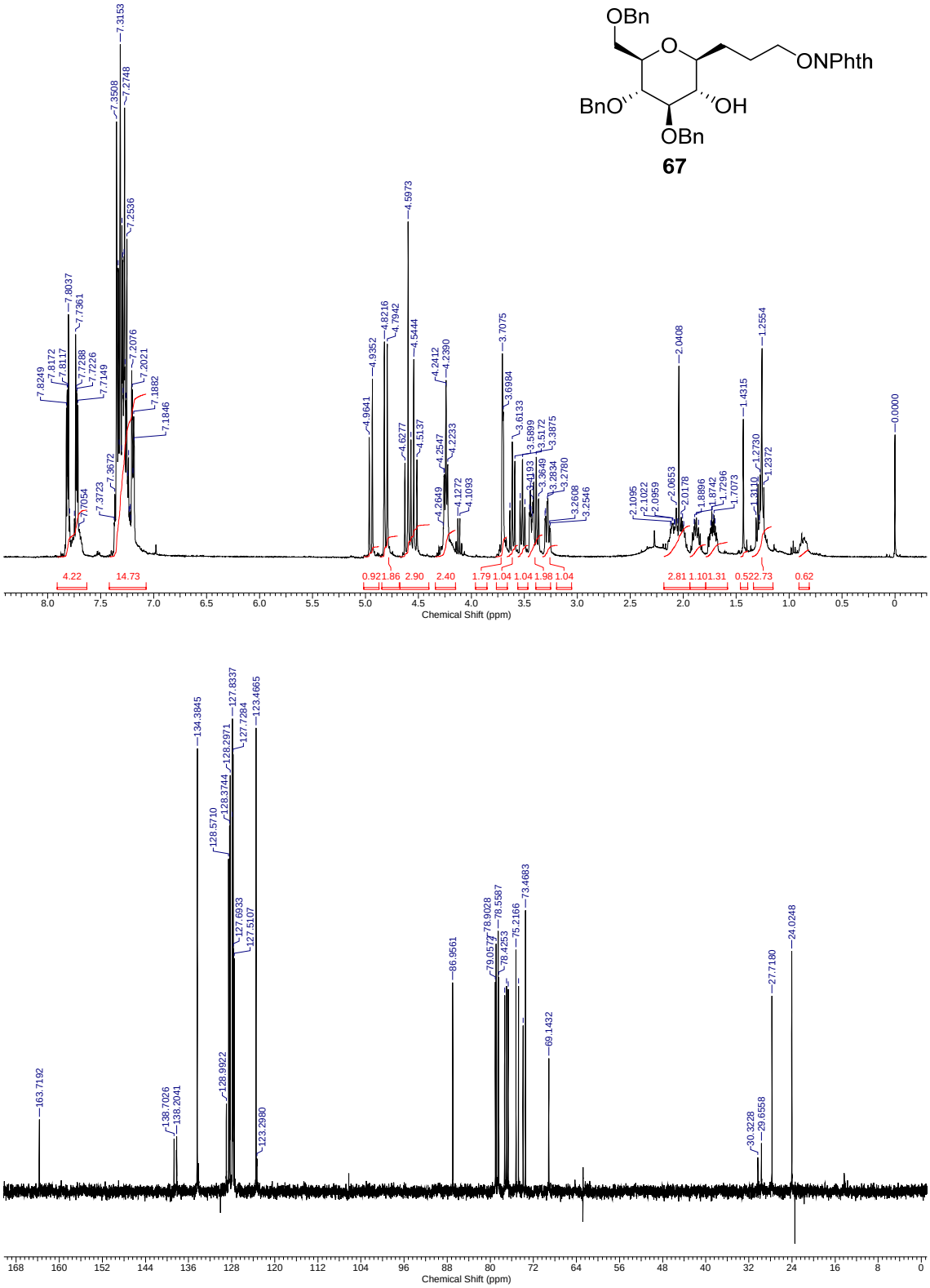

Fig. S66. ^{1}H NMR (400 MHz, $CDCl_3$) and $^{13}C\{H\}$ NMR (100.6 MHz, $CDCl_3$) of compound **67**.

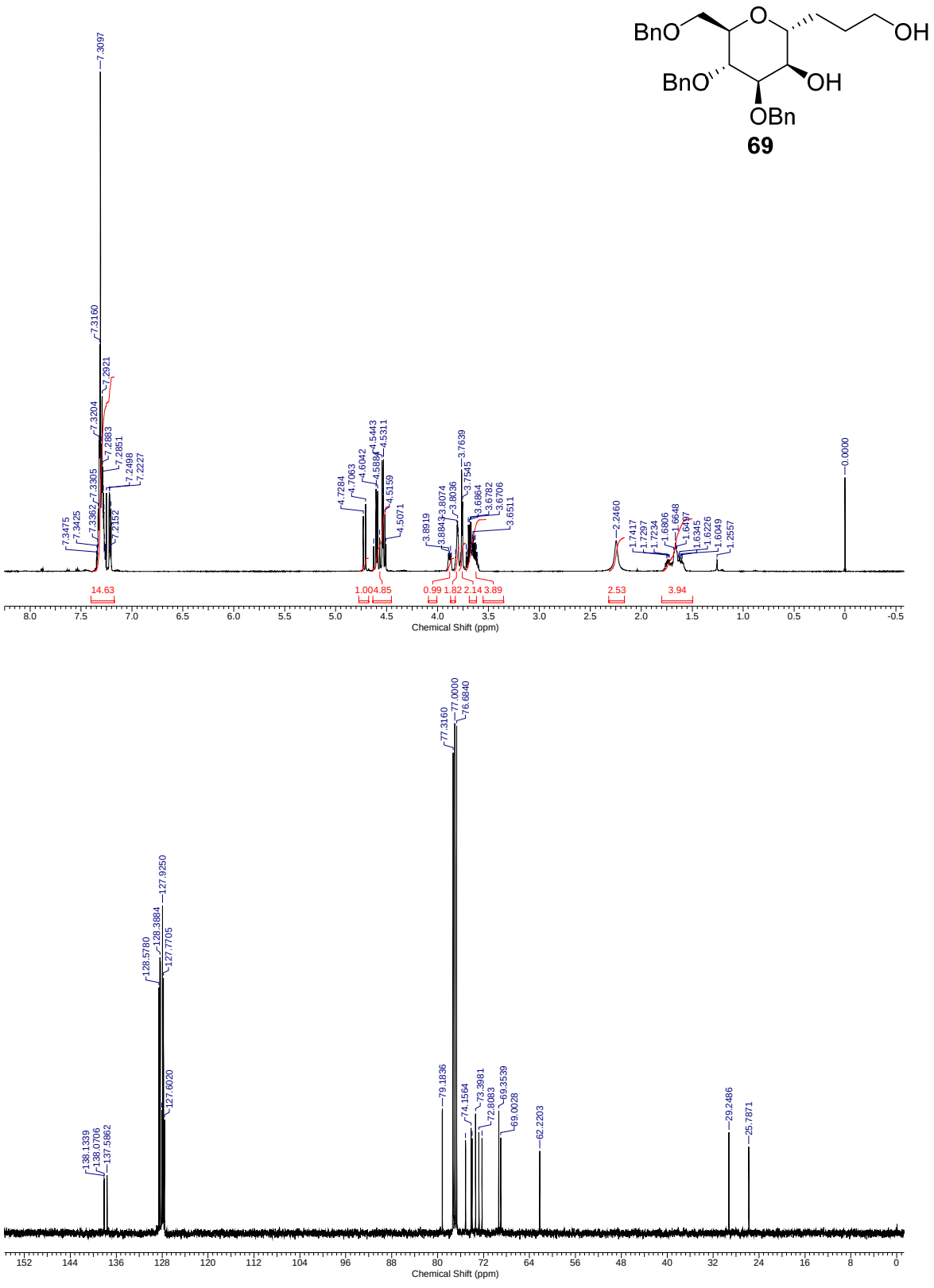

Fig. S67. ^{1}H NMR (500 MHz, $CDCl_3$) and $^{13}C\{H\}$ NMR (100.6 MHz, $CDCl_3$) of compound **69**.

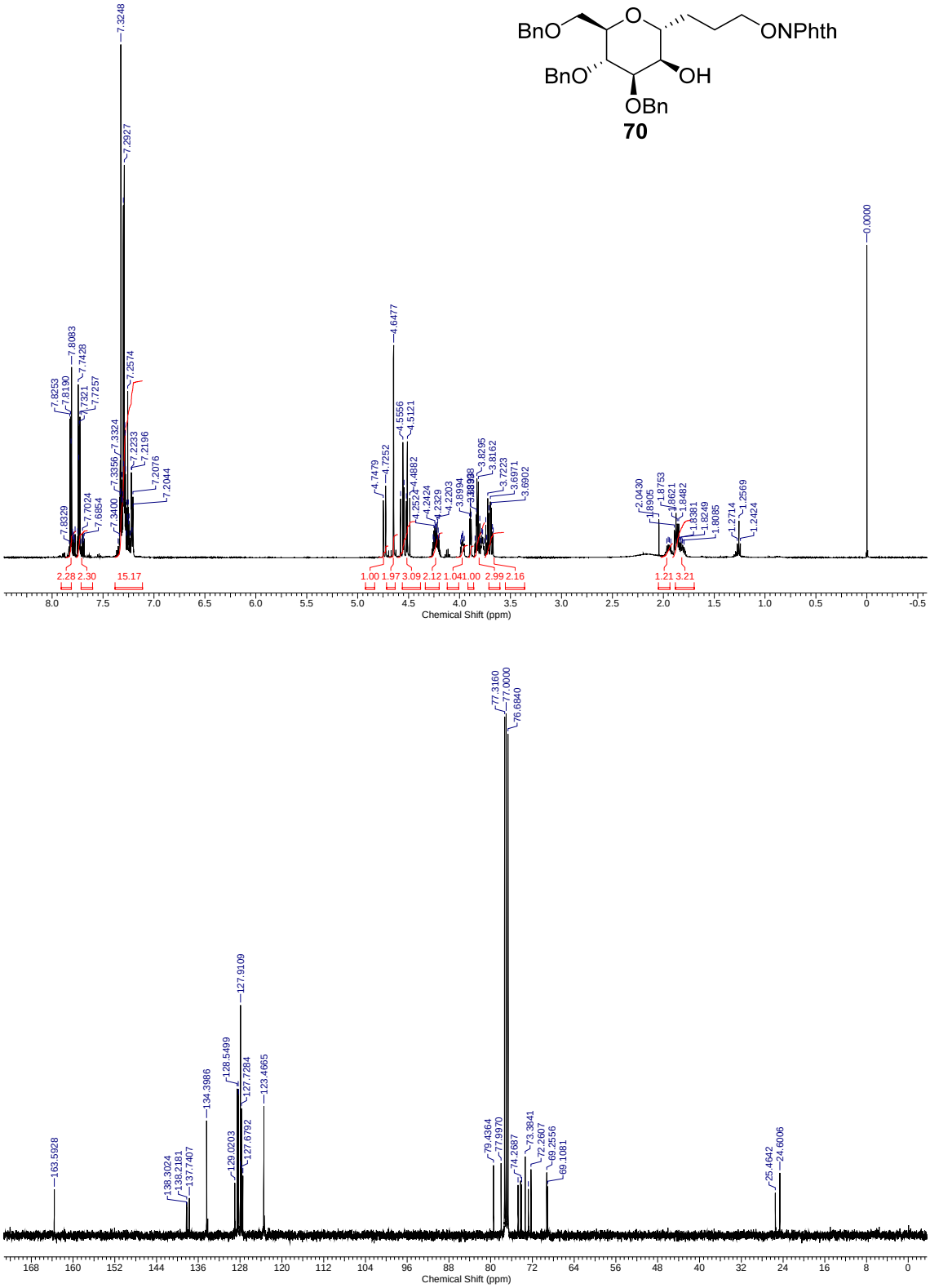

Fig. S68. ^{1}H NMR (500 MHz, $CDCl_3$) and $^{13}C\{H\}$ NMR (100.6 MHz, $CDCl_3$) of compound **70**.

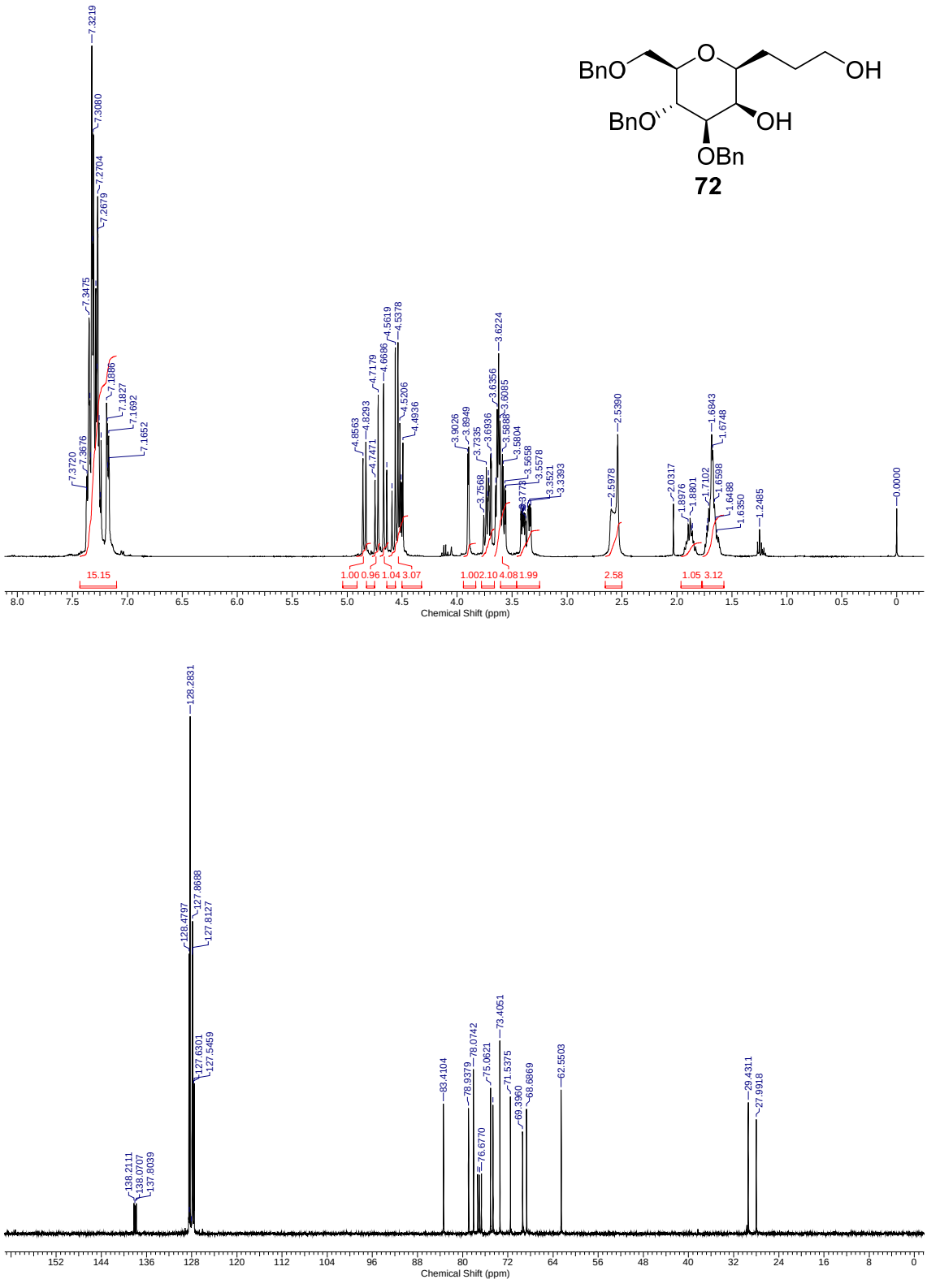

Fig. S69. ^{1}H NMR (400 MHz, $CDCl_3$) and $^{13}C\{H\}$ NMR (100.6 MHz, $CDCl_3$) of compound **72**.

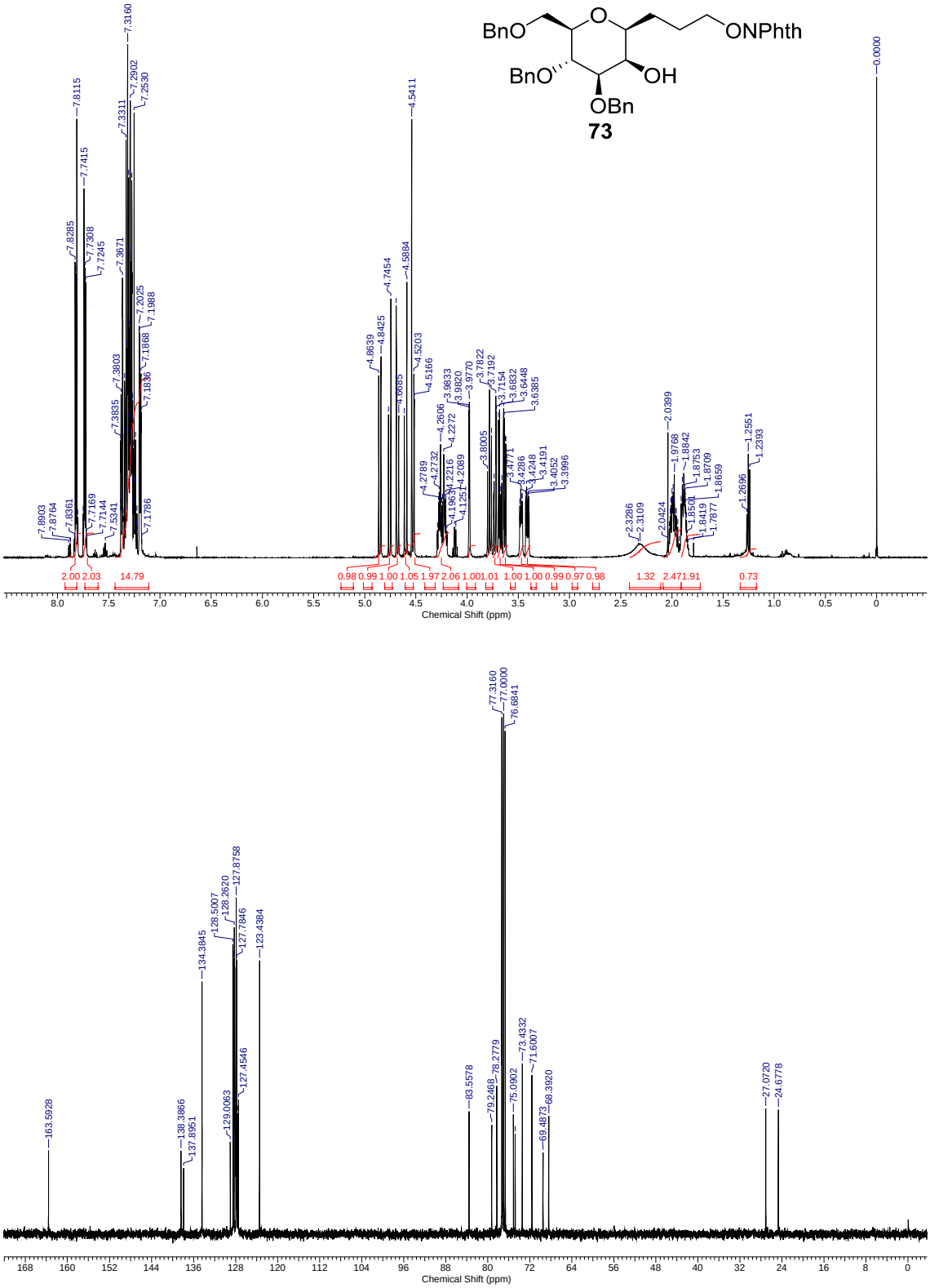

Fig. S70. ^{1}H NMR (500 MHz, $CDCl_3$) and $^{13}C\{H\}$ NMR (100.6 MHz, $CDCl_3$) of compound **73**.

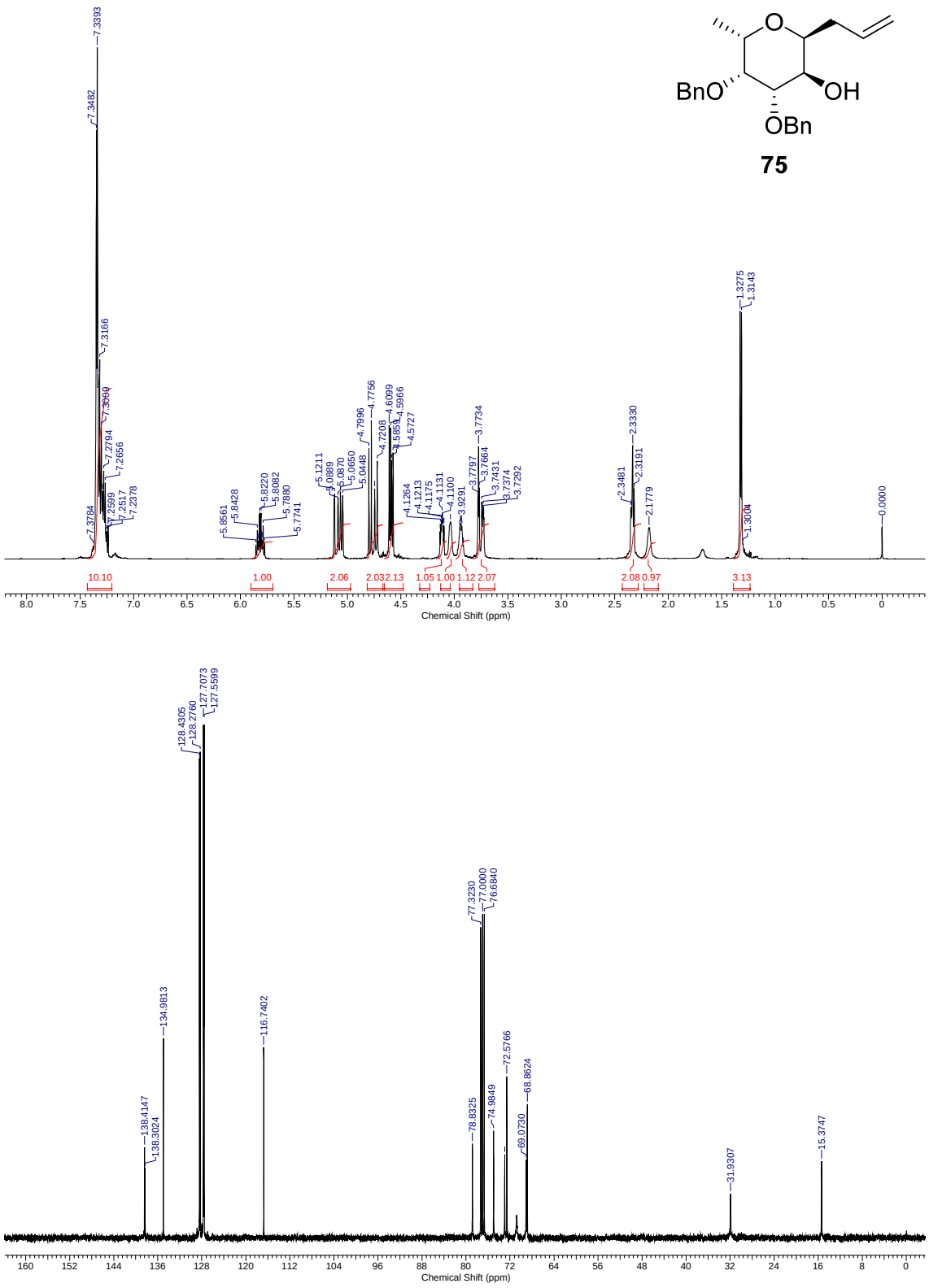

Fig. S71. ^{1}H NMR (500 MHz, $CDCl_3$) and ^{13}C{H} NMR (100.6 MHz, $CDCl_3$) of compound **75**.

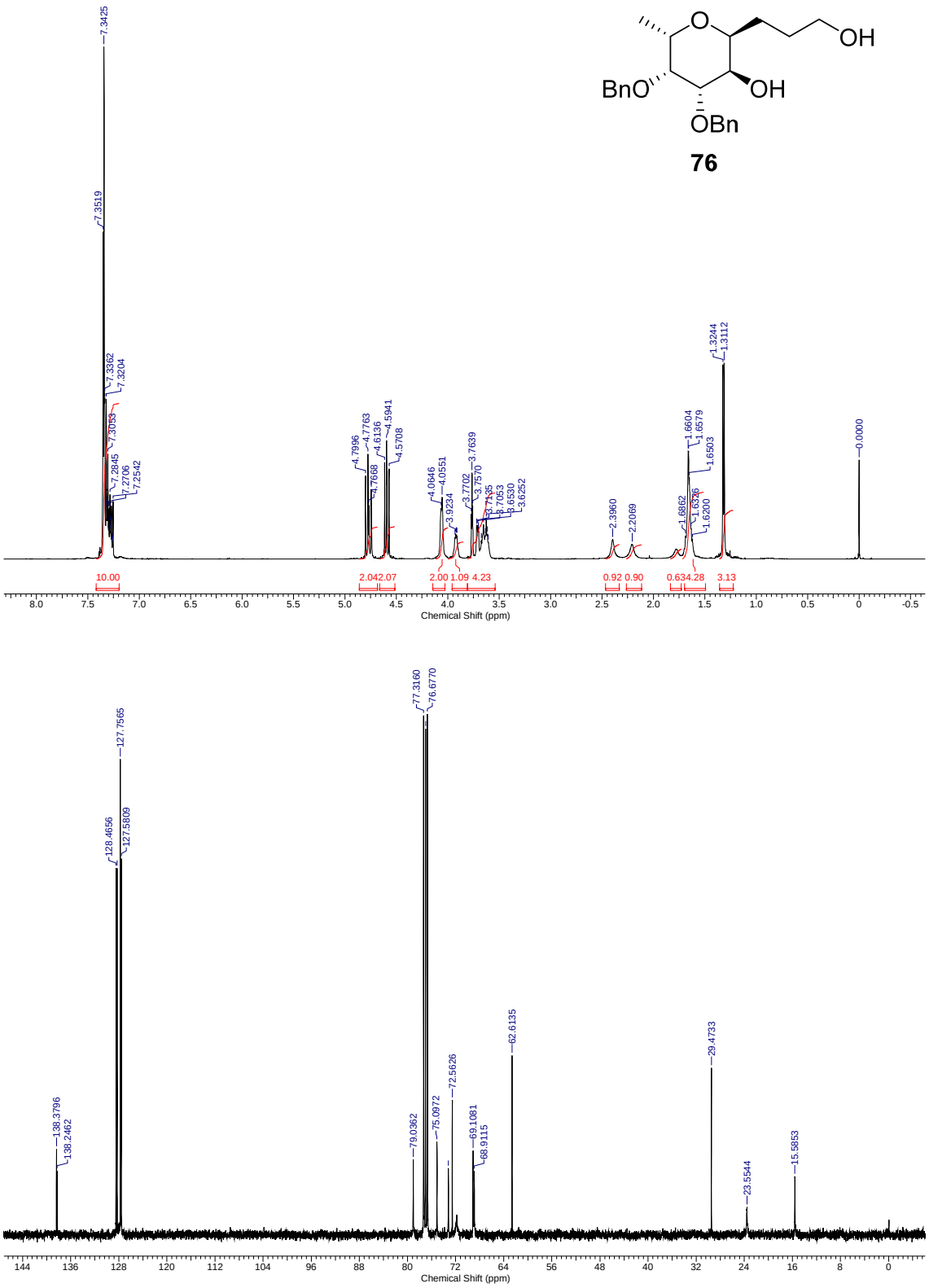

Fig. S72. ^{1}H NMR (500 MHz, $CDCl_3$) and $^{13}C\{H\}$ NMR (100.6 MHz, $CDCl_3$) of compound **76**.

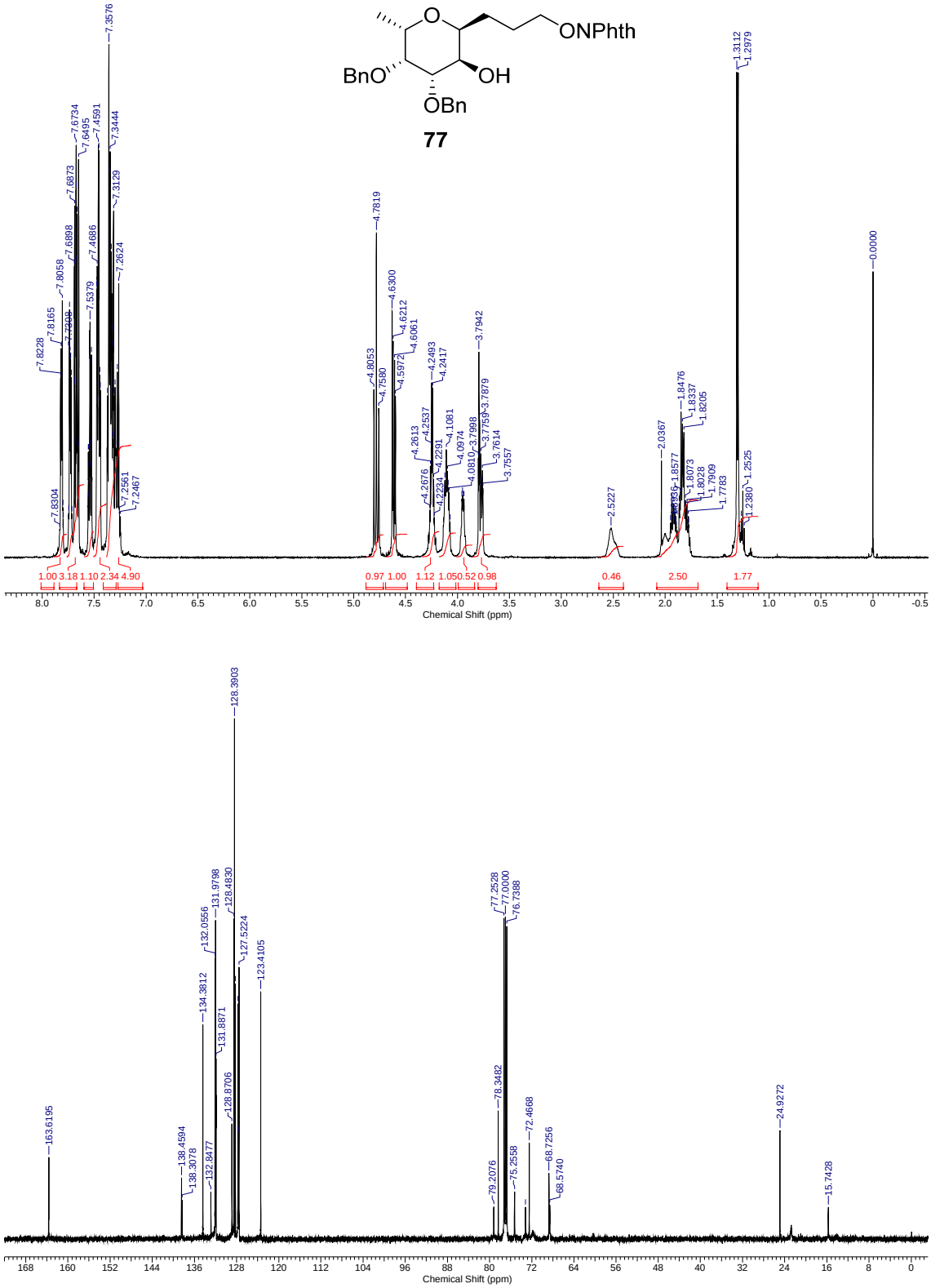

Fig. S73. ^{1}H NMR (500 MHz, $CDCl_3$) and $^{13}C\{H\}$ NMR (125.7 MHz, $CDCl_3$) of compound **77**.

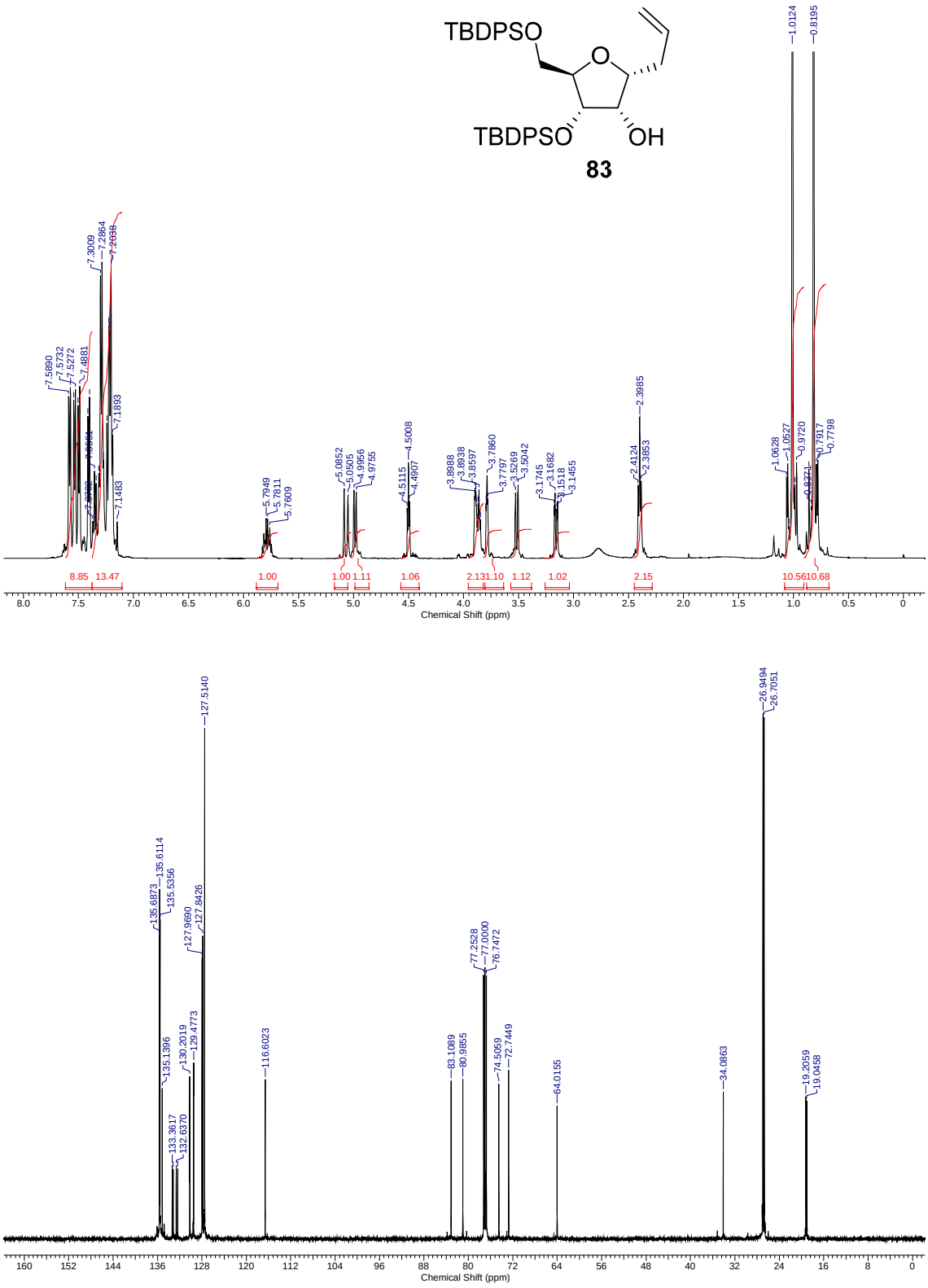

Fig. S74. ^{1}H NMR (500 MHz, $CDCl_3$) and $^{13}C\{H\}$ NMR (125.7 MHz, $CDCl_3$) of compound **83**.

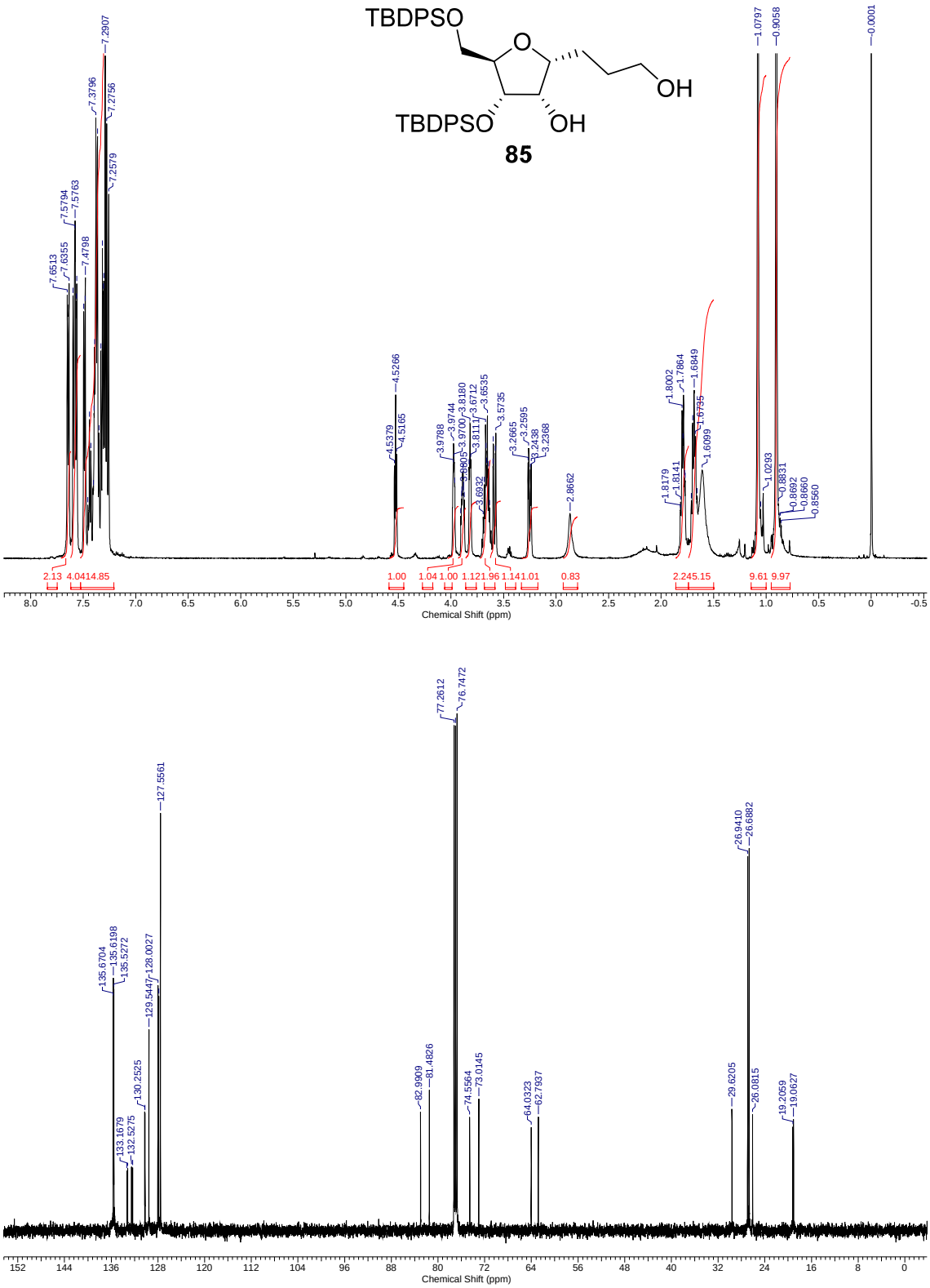

Fig. S75. ^{1}H NMR (500 MHz, $CDCl_3$) and ^{13}C{H} NMR (125.7 MHz, $CDCl_3$) of compound **85**.

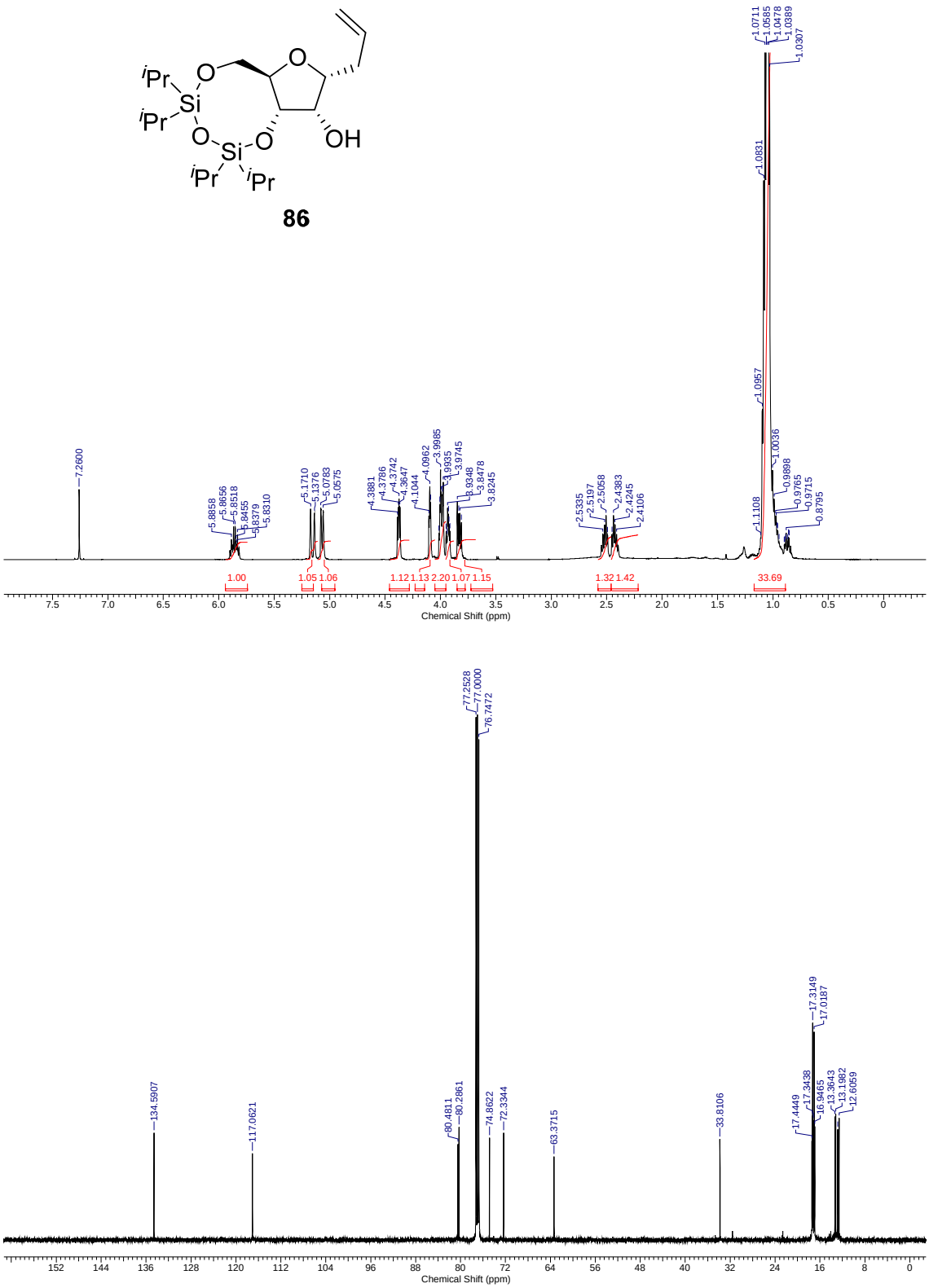

Fig. S76. ^{1}H NMR (500 MHz, $CDCl_3$) and $^{13}C\{H\}$ NMR (125.7 MHz, $CDCl_3$) of compound **86**.

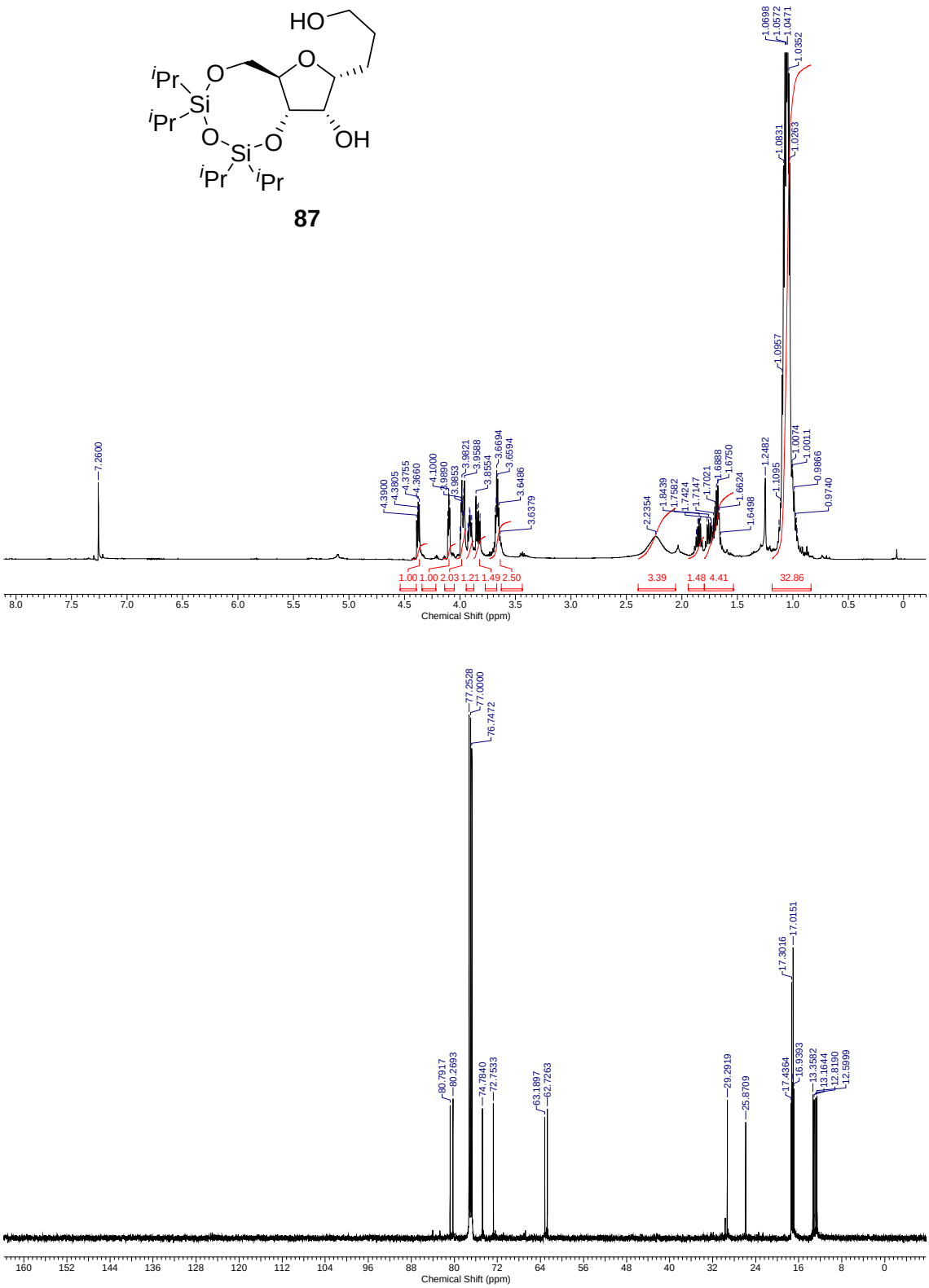

Fig. S77. ^{1}H NMR (500 MHz, $CDCl_3$) and $^{13}C\{H\}$ NMR (125.7 MHz, $CDCl_3$) of compound **87**.

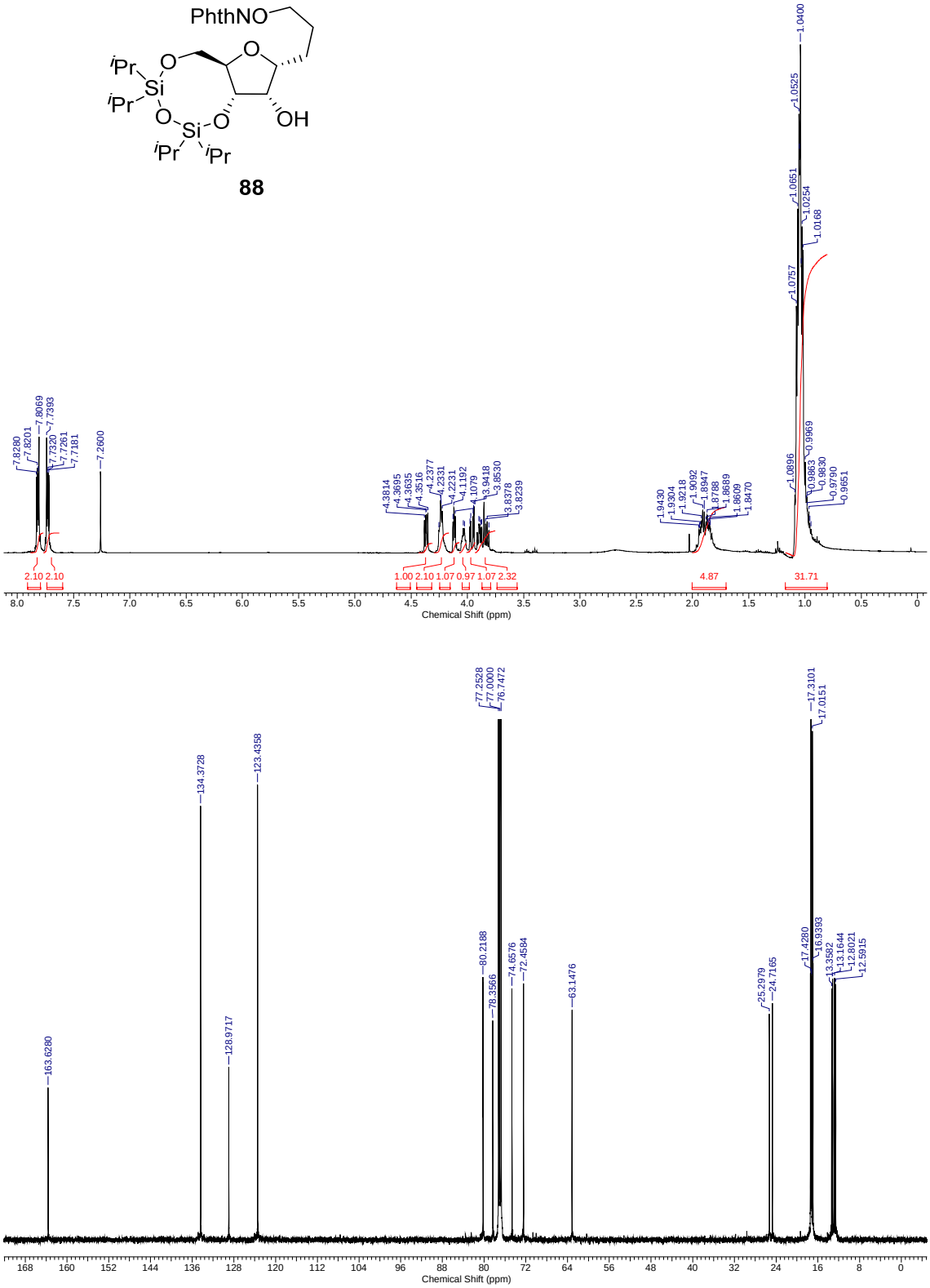

Fig. S78. ^{1}H NMR (400 MHz, $CDCl_3$) and $^{13}C\{H\}$ NMR (125.7 MHz, $CDCl_3$) of compound **88**.

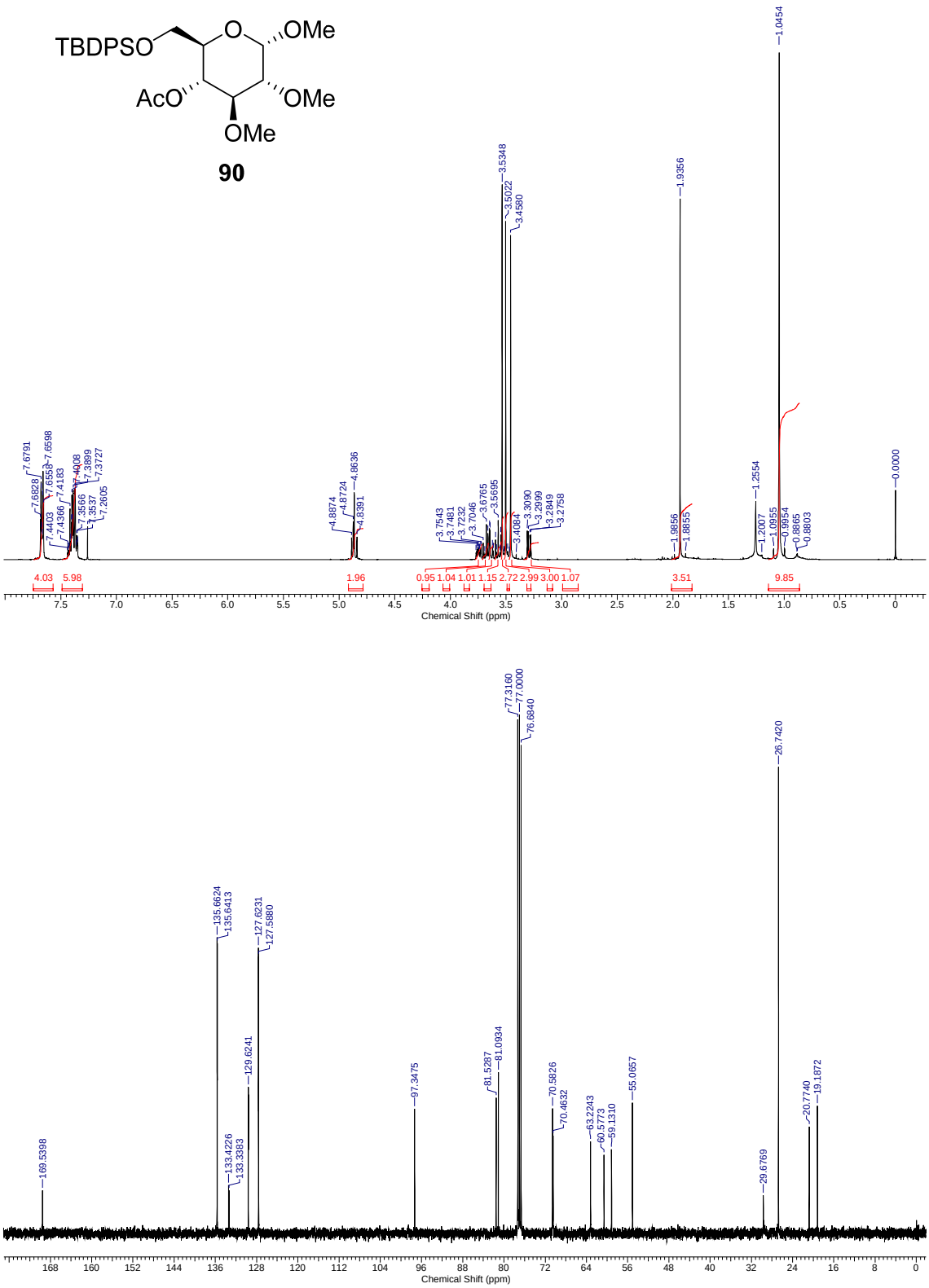

Fig. S79. ^{1}H NMR (400 MHz, $CDCl_3$) and $^{13}C\{H\}$ NMR (100.6 MHz, $CDCl_3$) of compound **90**.

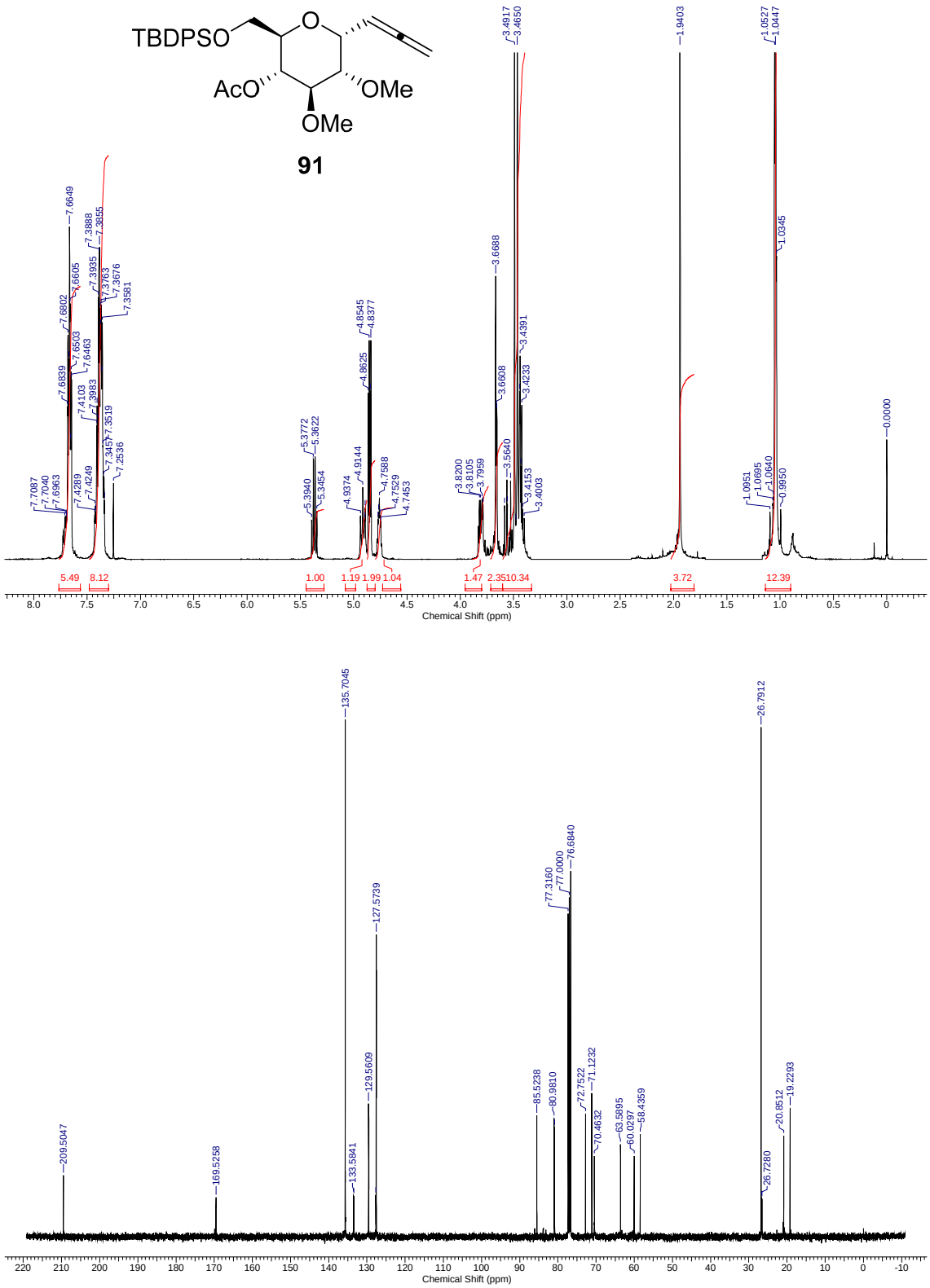

Fig. S80. ^{1}H NMR (400 MHz, $CDCl_3$) and $^{13}C\{H\}$ NMR (100.6 MHz, $CDCl_3$) of compound **91**.

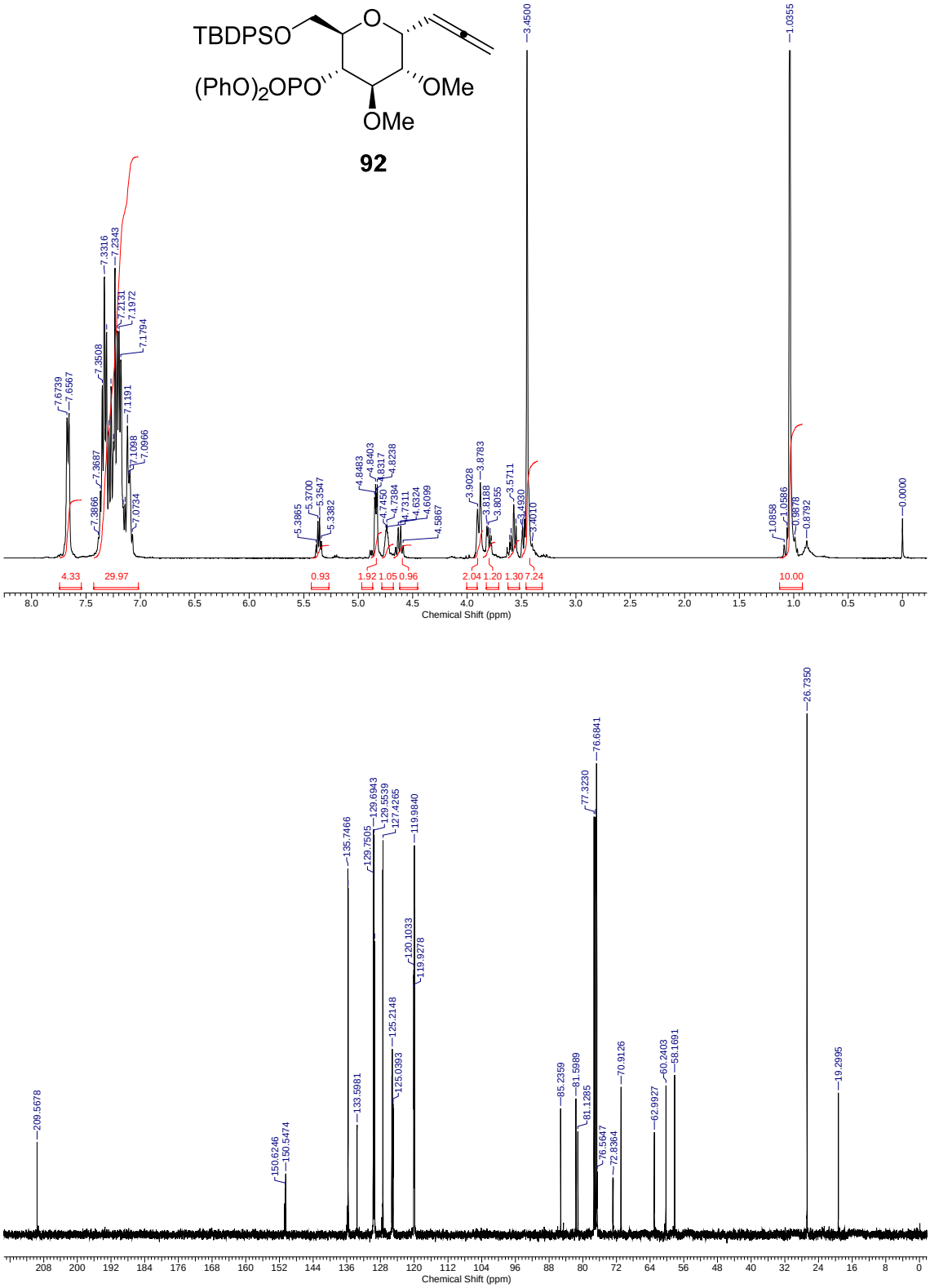

Fig. S81. ^{1}H NMR (500 MHz, $CDCl_3$) and $^{13}C\{H\}$ NMR (100.6 MHz, $CDCl_3$) of compound **92**.

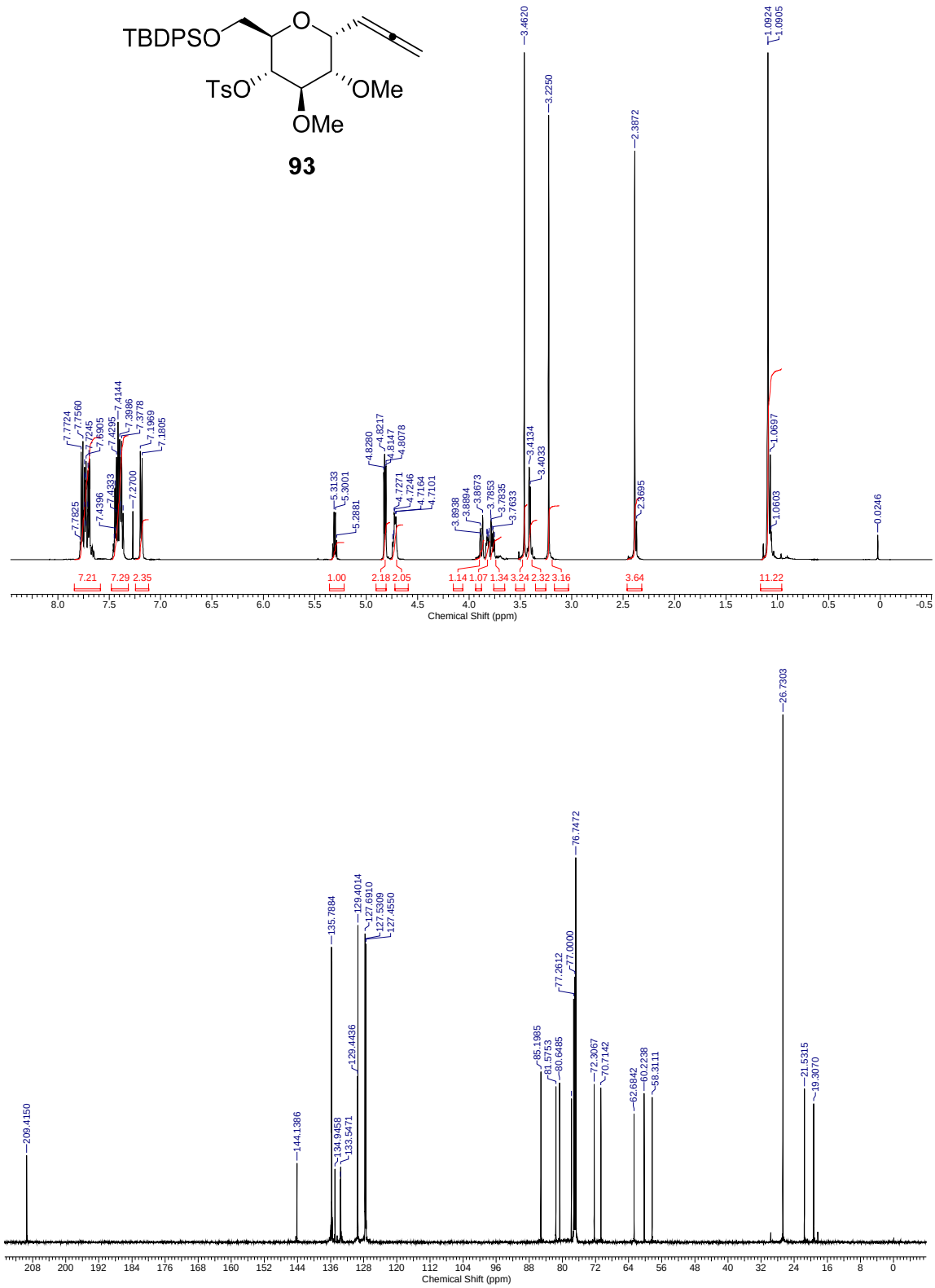

Fig. S82. ^{1}H NMR (500 MHz, $CDCl_3$) and $^{13}C\{H\}$ NMR (125.7 MHz, $CDCl_3$) of compound **93**.

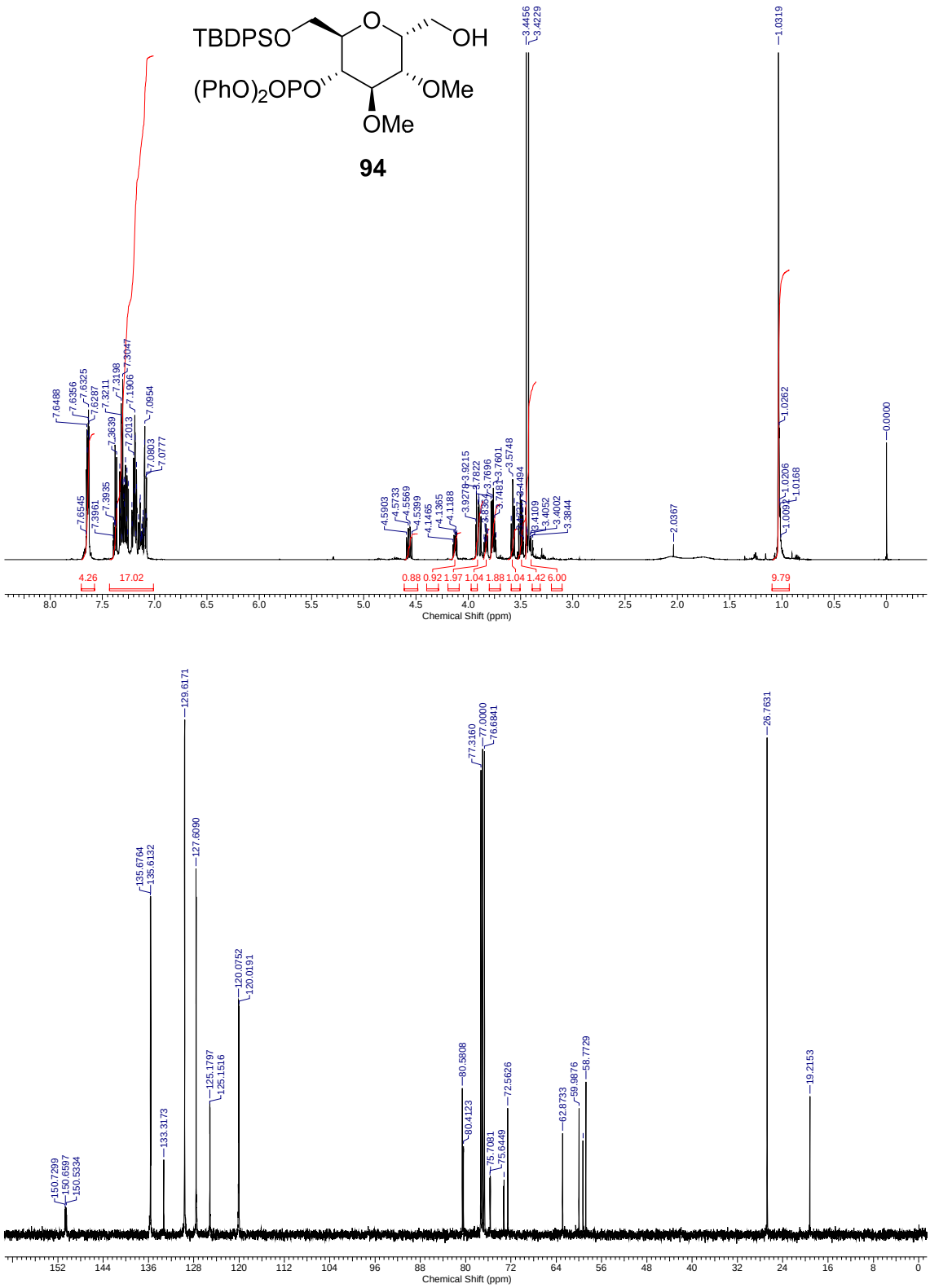

Fig. S83. ^{1}H NMR (500 MHz, $CDCl_3$) and $^{13}C\{H\}$ NMR (100.6 MHz, $CDCl_3$) of compound **94**.

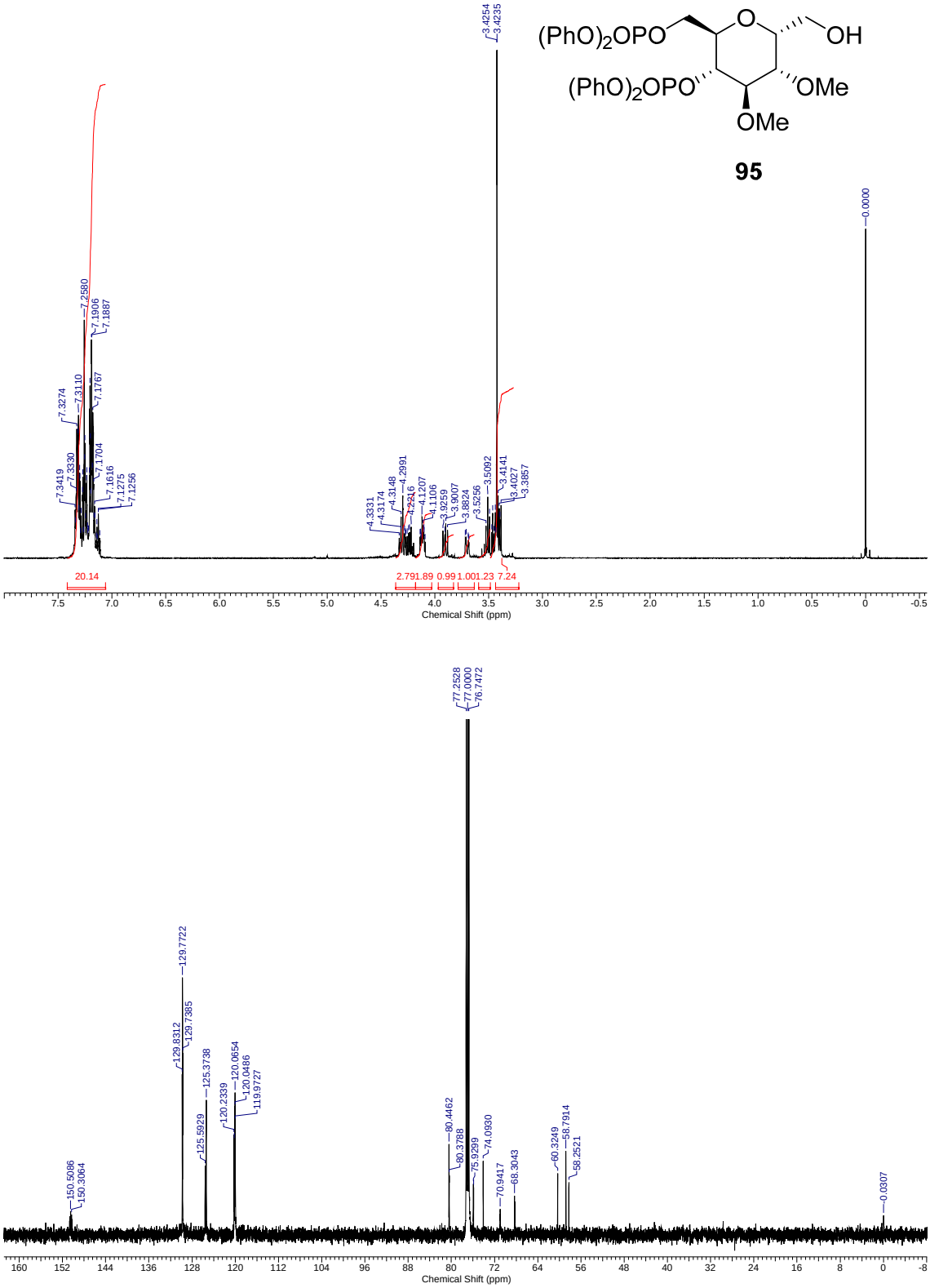

Fig. S84. ^{1}H NMR (500 MHz, $CDCl_3$) and $^{13}C\{H\}$ NMR (125.7 MHz, $CDCl_3$) of compound **95**.

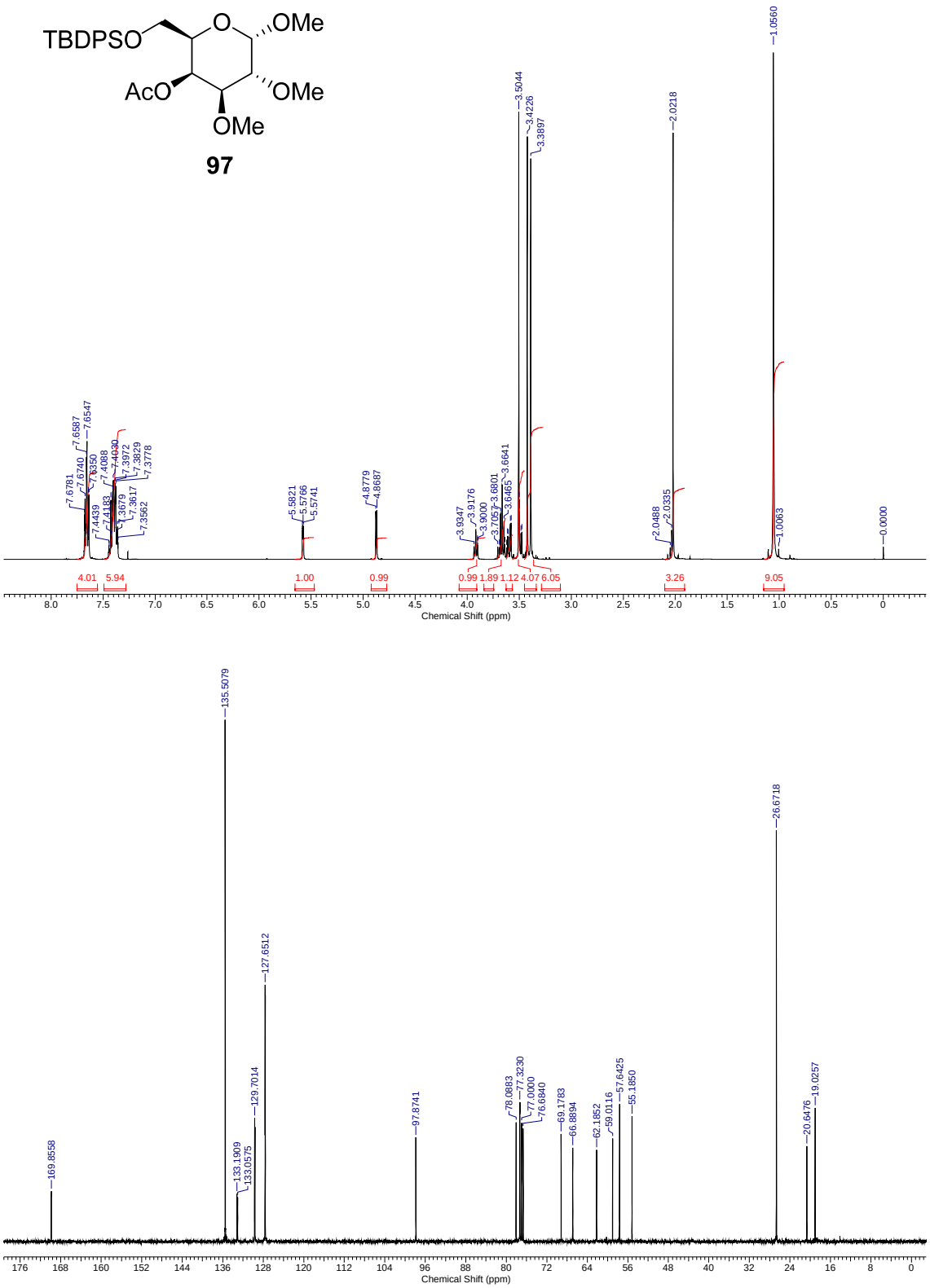

Fig. S85. ^{1}H NMR (400 MHz, $CDCl_3$) and $^{13}C\{H\}$ NMR (100.6 MHz, $CDCl_3$) of compound **97**.

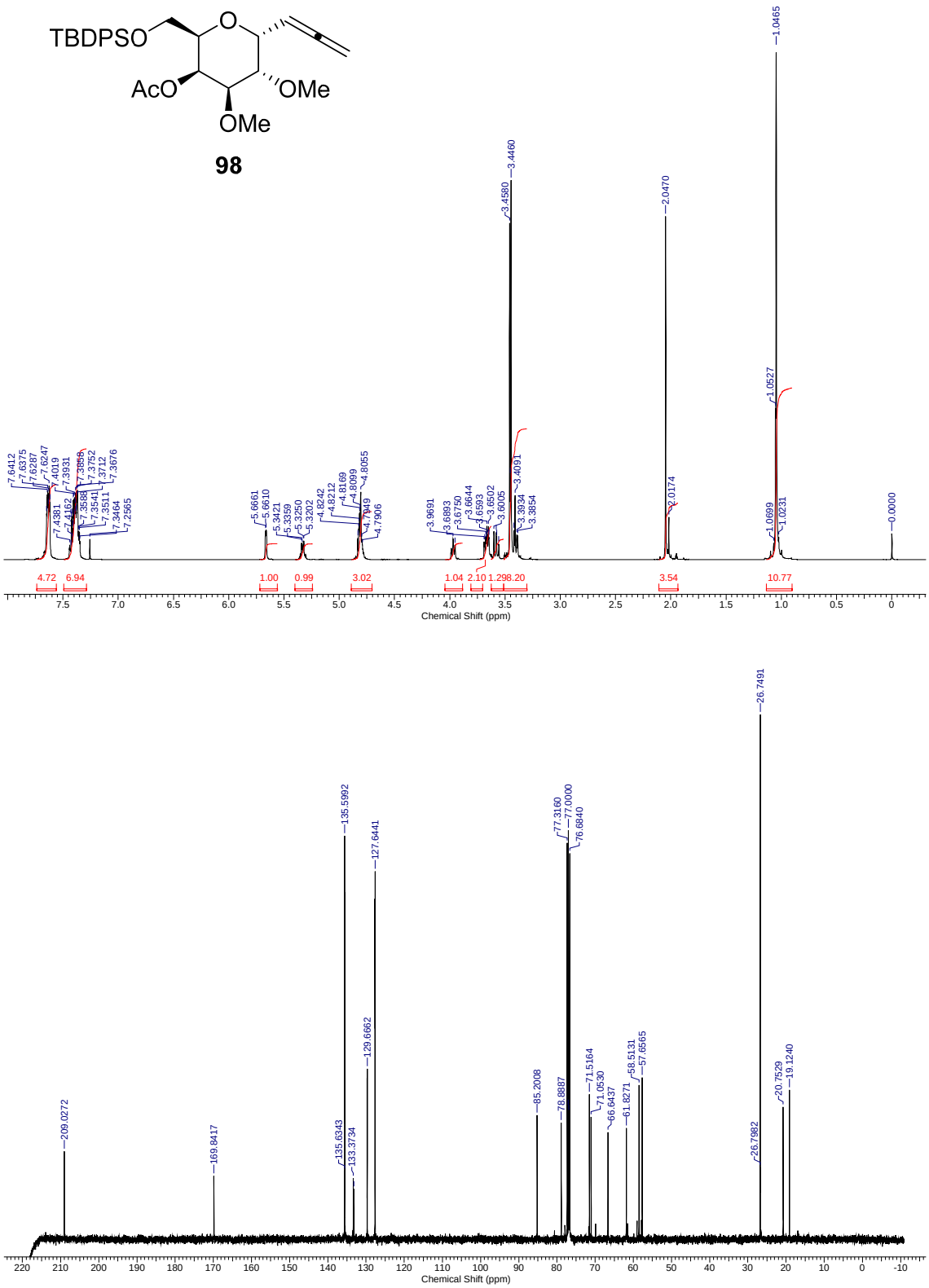

Fig. S86. ^{1}H NMR (400 MHz, $CDCl_3$) and $^{13}C\{H\}$ NMR (100.6 MHz, $CDCl_3$) of compound **98**.

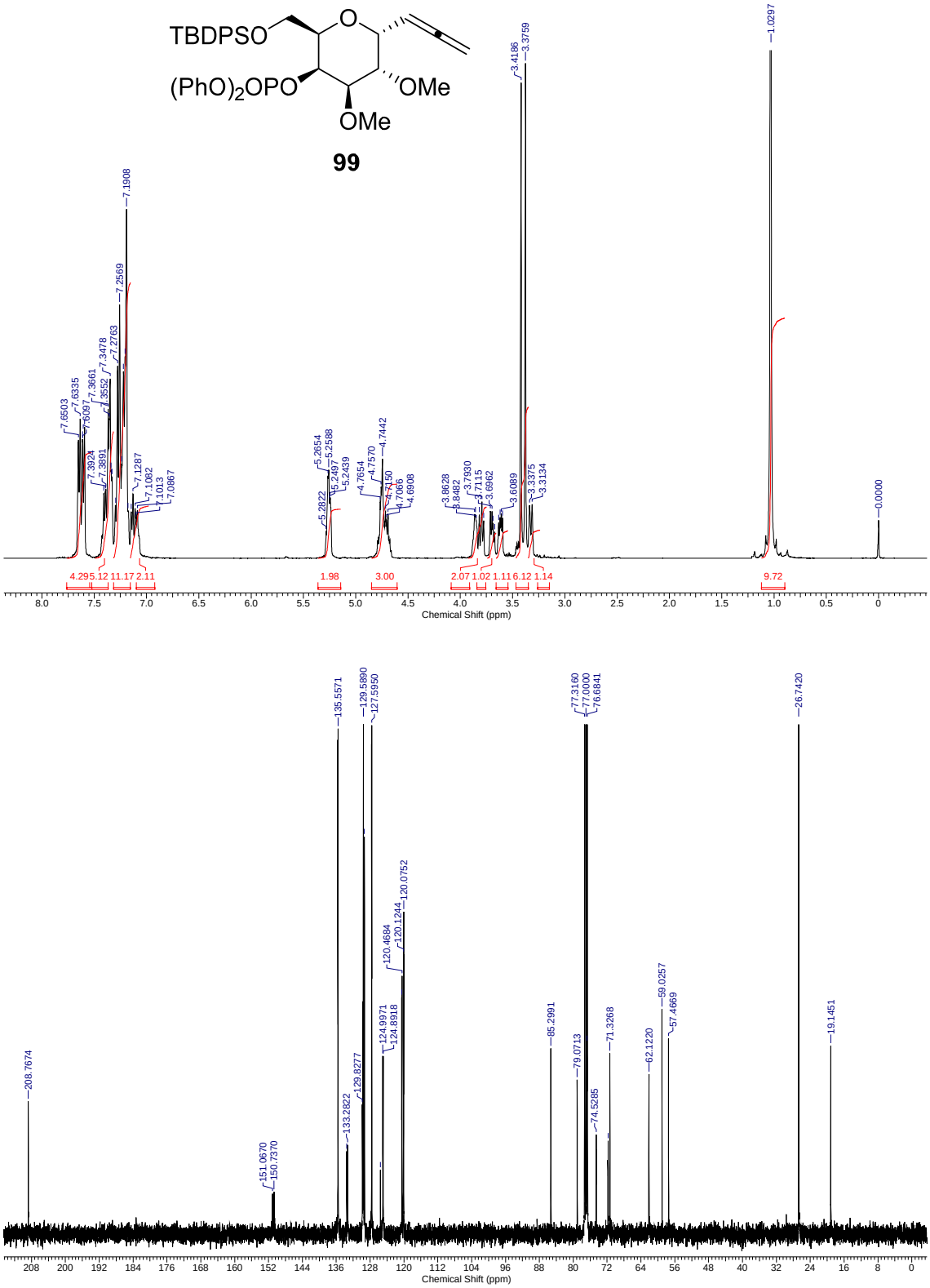

Fig. S87. ^{1}H NMR (400 MHz, $CDCl_3$) and $^{13}C\{H\}$ NMR (100.6 MHz, $CDCl_3$) of compound **99**.

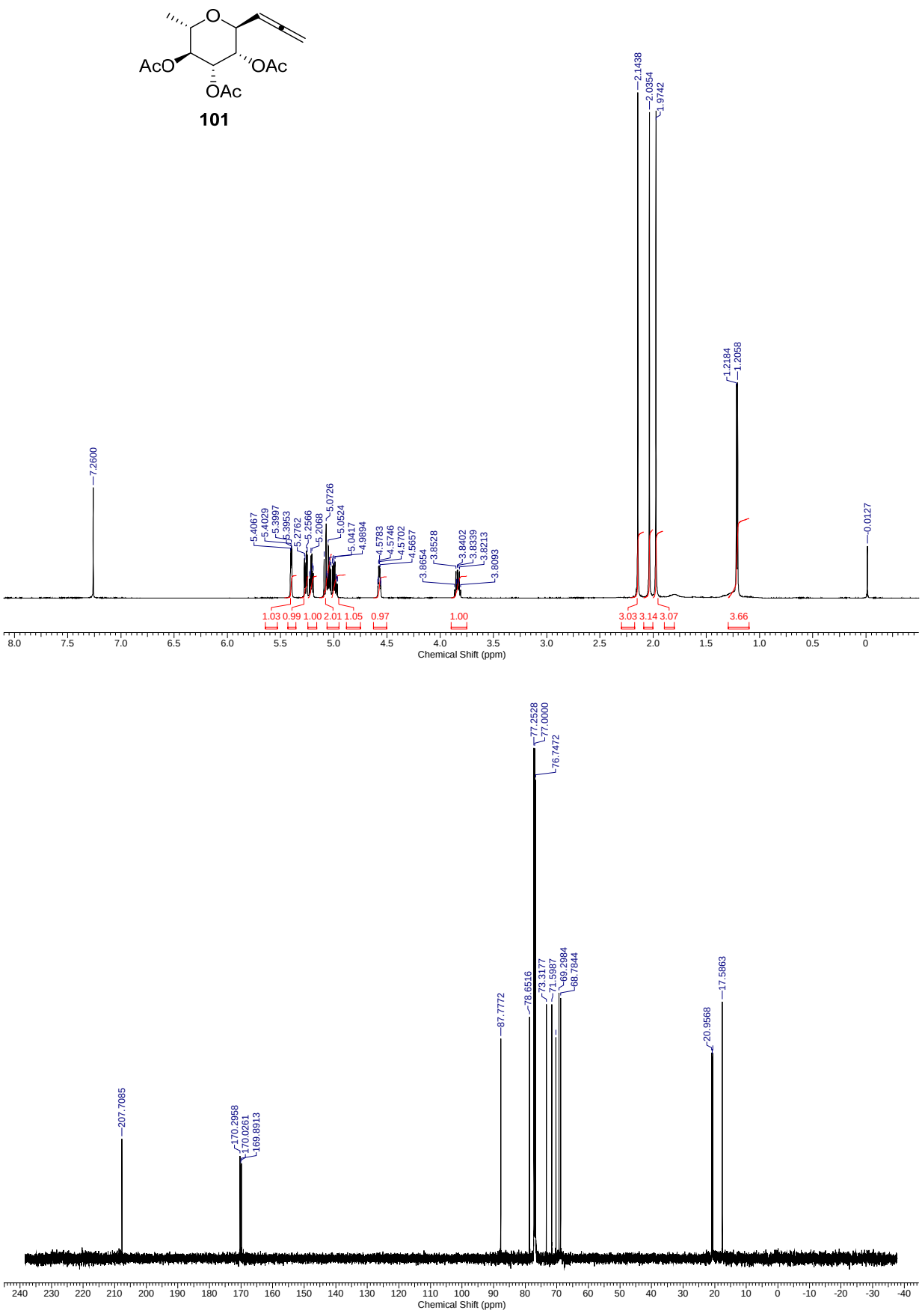

Fig. S88. ^{1}H NMR (500 MHz, $CDCl_3$) and ^{13}C{H} NMR (125.7 MHz, $CDCl_3$) of compound **101**.

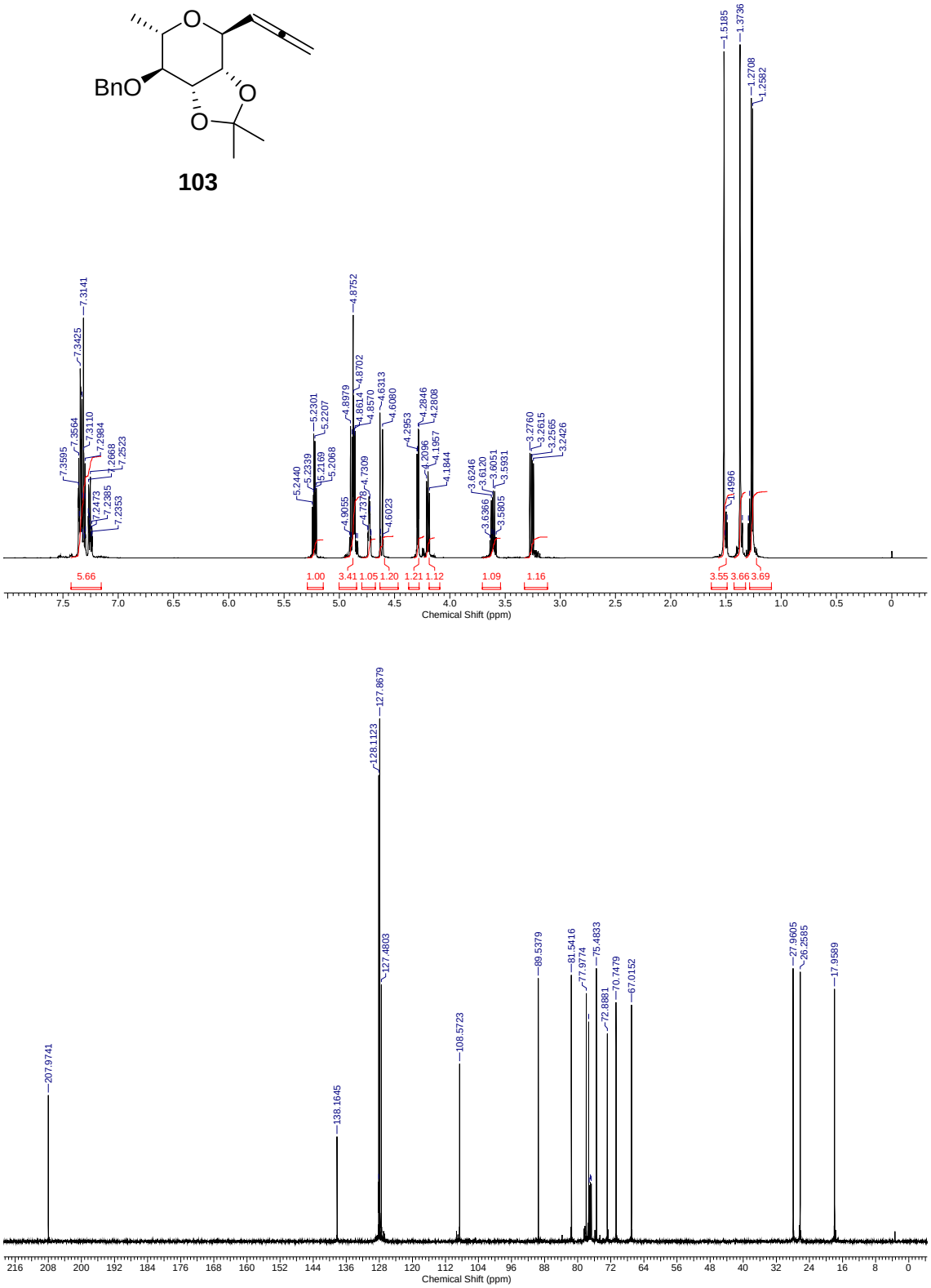

Fig. S89. ^{1}H NMR (500 MHz, $CDCl_3$) and $^{13}C\{H\}$ NMR (125.7 MHz, $CDCl_3$) of compound **103**.

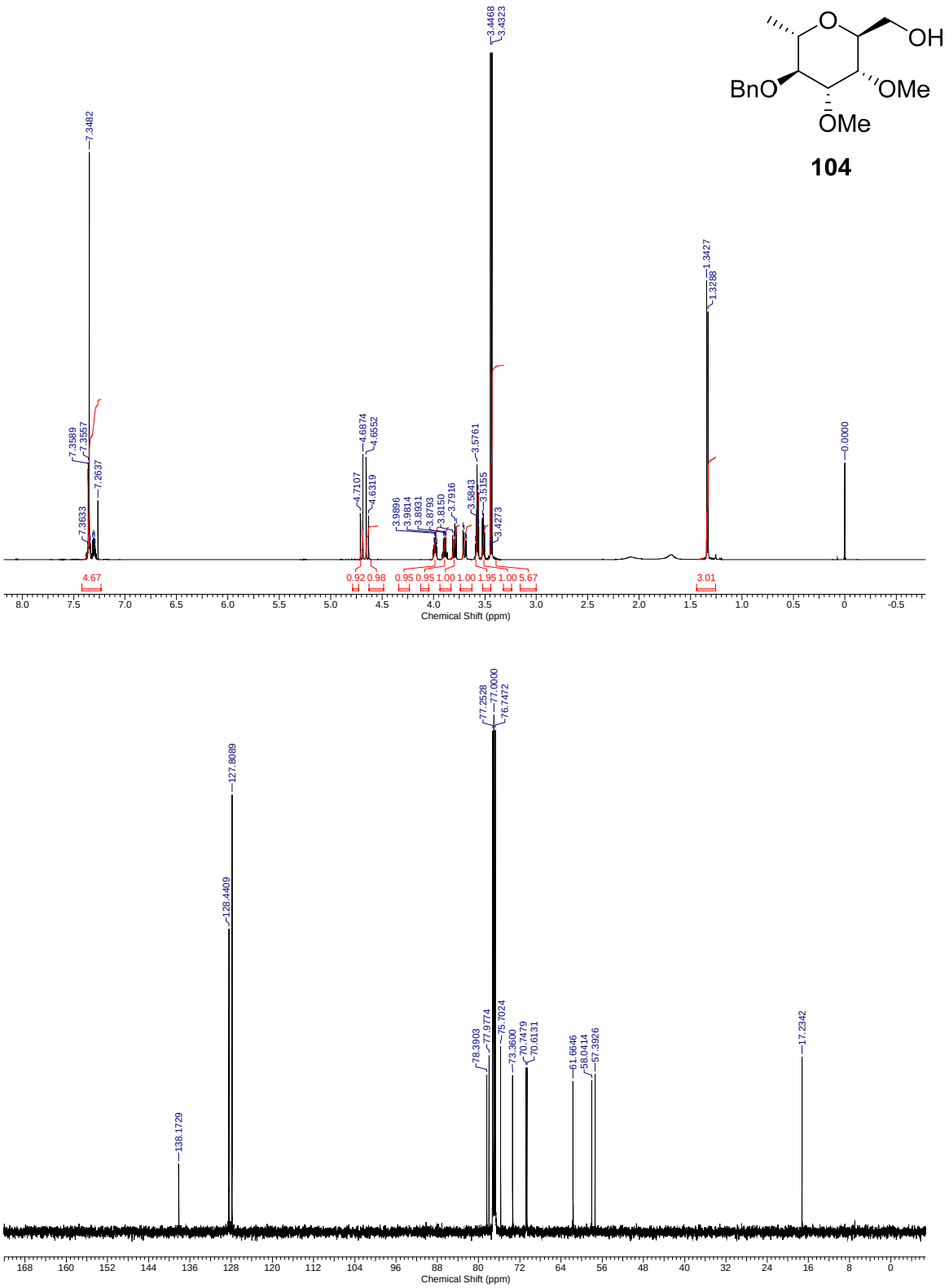

Fig. S90. ^{1}H NMR (500 MHz, $CDCl_3$) and $^{13}C\{H\}$ NMR (125.7 MHz, $CDCl_3$) of compound **104**.

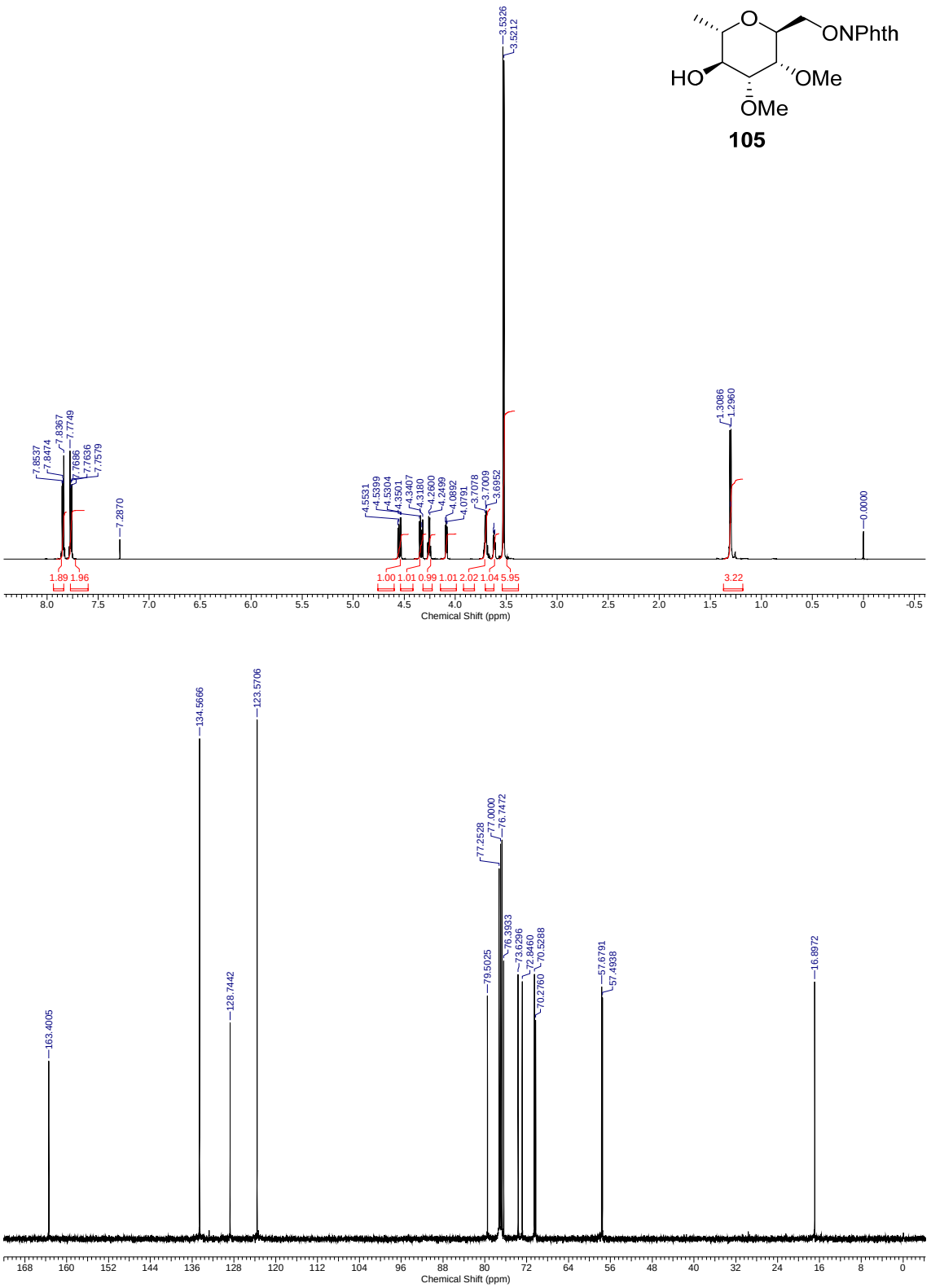

Fig. S91. ^{1}H NMR (500 MHz, $CDCl_3$) and $^{13}C\{H\}$ NMR (125.7 MHz, $CDCl_3$) of compound **105**.

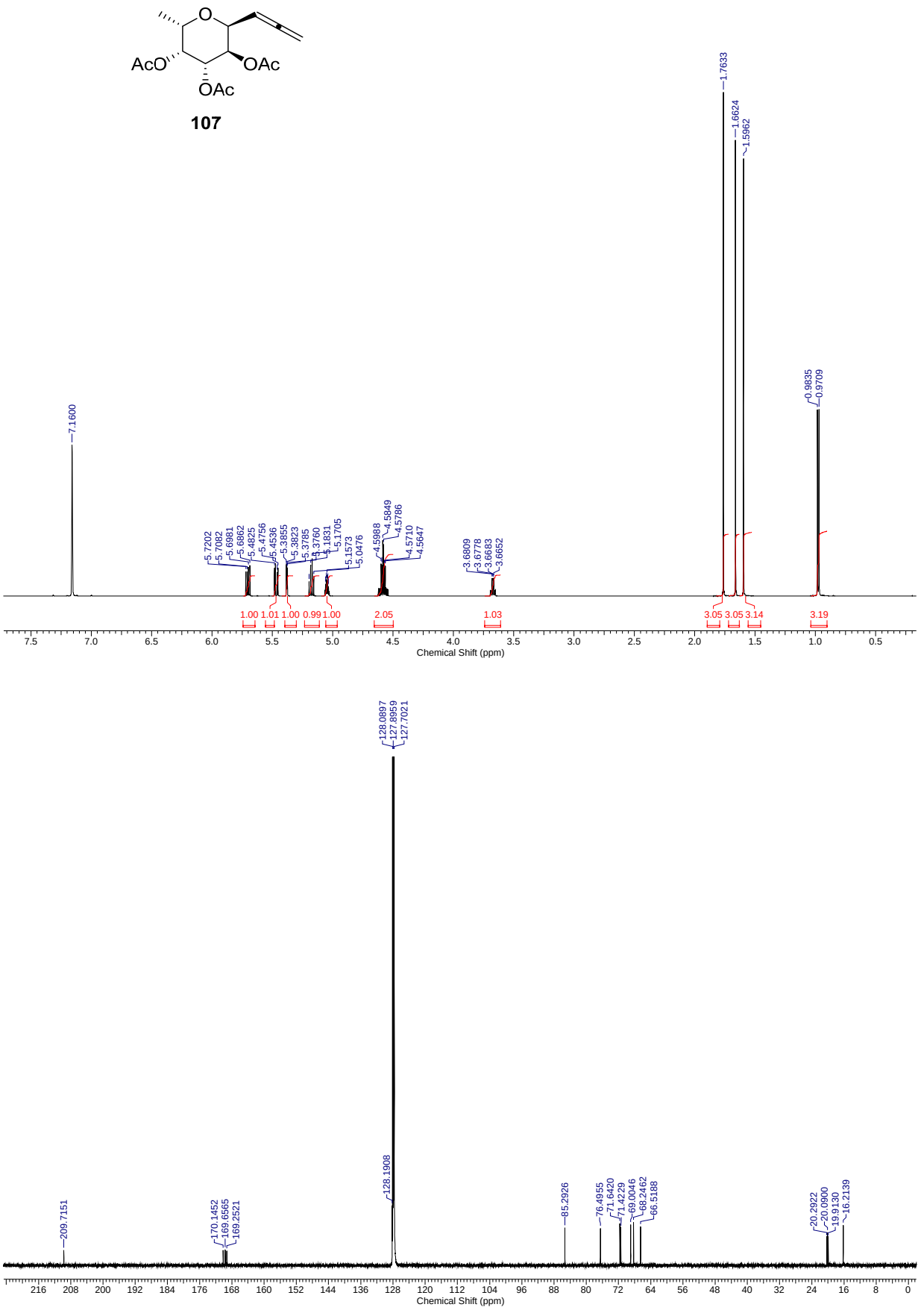

Fig. S92. ^{1}H NMR (500 MHz, C_6D_6) and ^{13}C{H} NMR (125.7 MHz, C_6D_6) of compound **107**.

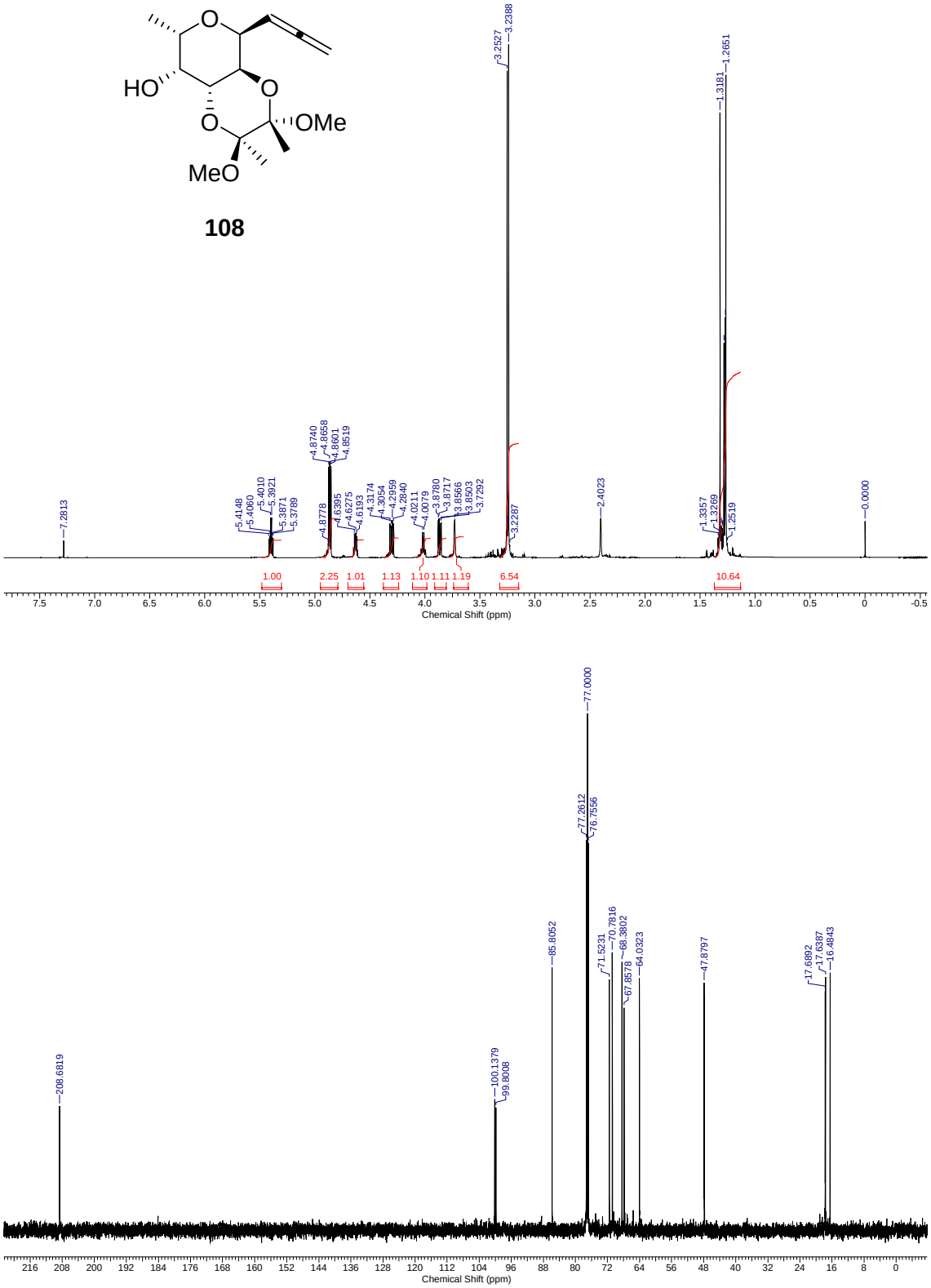

Fig. S93. ^{1}H NMR (500 MHz, $CDCl_3$) and $^{13}C\{H\}$ NMR (125.7 MHz, $CDCl_3$) of compound **108**.

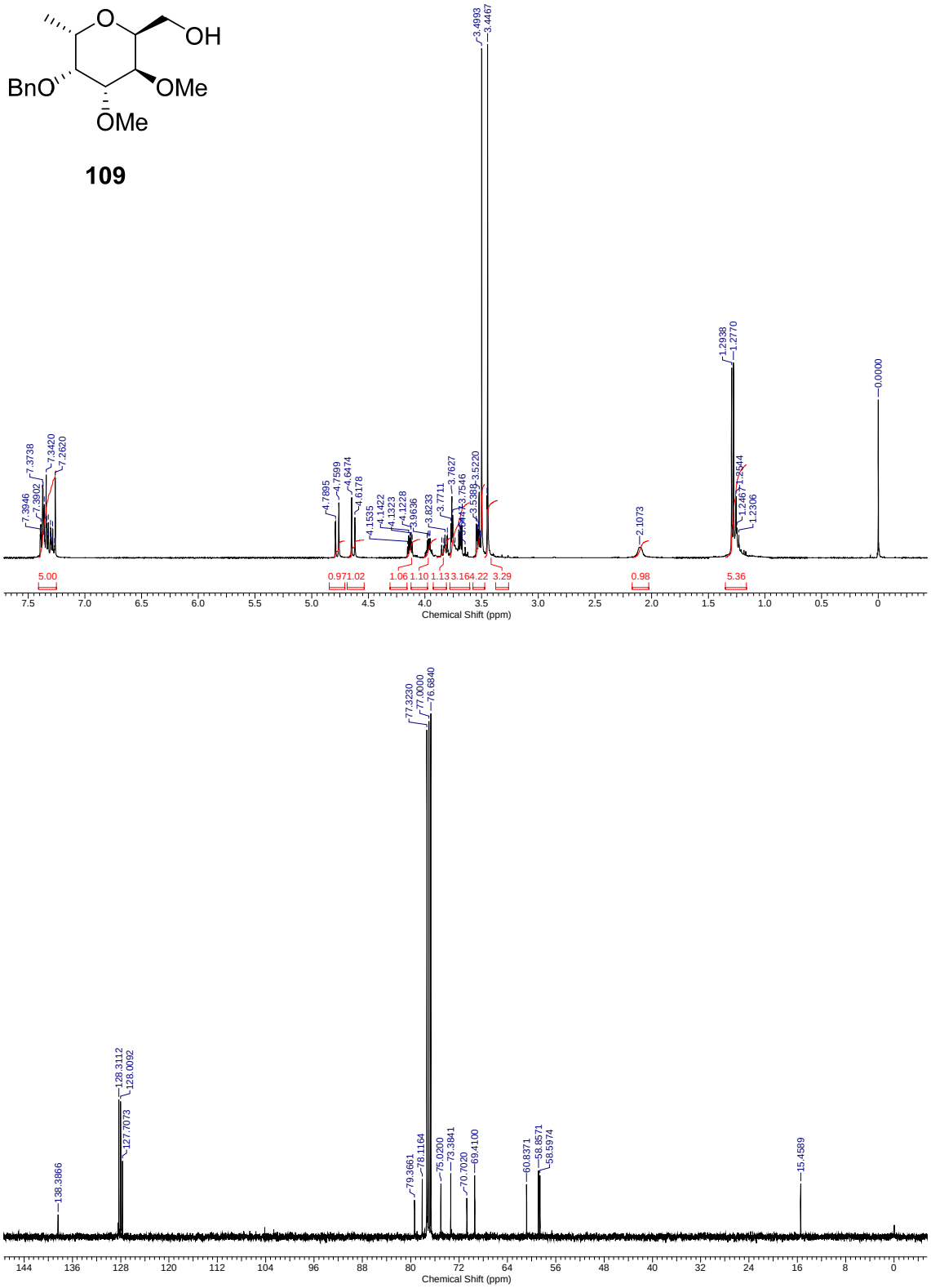

Fig. S94. ^{1}H NMR (400 MHz, $CDCl_3$) and $^{13}C\{H\}$ NMR (100.6 MHz, $CDCl_3$) of compound **109**.